UNIVERSITY OF CALIFORNIA, SAN DIEGO

Effects of trace metals on diatom export products from the euphotic zone and significance for biogeochemical cycles

A dissertation submitted in partial satisfaction of the
requirements for the degree
Doctor of Philosophy

in

Oceanography

by

Daniel J Richter

Committee in charge:

Professor Christopher D. Charles, Chair
Professor Katherine Barbeau
Researcher Mark Hildebrand
Professor Marc A. Meyers
Professor Richard D. Norris

2013

The dissertation of Daniel J Richter is approved, and it is acceptable in quality and form for publication on microfilm and electronically:

_____

_____

_____

_____

_____

Chair

University of California, San Diego

2013

DEDICATION

To all the diatoms who succumbed in the making of this thesis, and to you, the reader. You may be the last. . .

EPIGRAPH

Dinner! —Mom

TABLE OF CONTENTS

LIST OF FIGURES

LIST OF TABLES

ACKNOWLEDGEMENTS

This highly interdisciplinary thesis could not have been possible without contributions of time, expertise, and equipment from many scientists in many fields. Expertise on diatoms, their growth, and the basics of their physiology were supplied by Mark Hildebrand, as well as many people in his lab. Of particular note are Benoit Tesson, Roshan Shrestha, and Aubrey Davis, who have all helped provide useful insights and direction, as well as explaining where in the lab to find things. All culture growth, monitoring of growth, and preparations for both the polyphosphate and dissolved silica assays took place in Mark's lab.

While the growth took place in the Hildebrand Lab, preparations for the trace-metal clean growth of diatoms took place in the Barbeau Lab. Bottles, filters, reagents, and materials for the cleaning of these materials were all supplied by the Barbeau Lab. Though the ship time for the Chilean Cruise was funded through UC Ship Funds, and my travel was funded by the SIO Graduate Office, the materials were provided and the risks of sending materials overseas assumed by the Barbeau Lab. While I collected the Chilean samples myself using Barbeau Lab equipment, it was the members of the Barbeau lab who collected the CA Current samples. A great deal of credit is due to Kathy in helping me prepare for the Chilean cruse. Much of the data that is reported in Chapter 4 I would not even have known to collect, much less known how to collect it cleanly without her guidance.

Similarly, members of the Barbeau Lab have proved invaluable throughout this thesis. Kelly Roe introduced me to the basic lab techniques for trace metal chemistry, and to culturing phytoplankton under trace-metal clean conditions. Randelle Bundy ran all of the Cu and Fe speciation data in Chapter 4, and must necessarily be a co-author on any publication that results from that work. Andrew King provided valuable insights into how to prepare phytoplankton samples for ICP-MS analysis, and Chris Dupont helped get me started with the MINEQL software, and important considerations when using it.

Most of the data in Chapter 2 are from analyses performed on an ICP-MS. This is an extremely complicated instrument, whose difficulty of operation is exceeded only by the difficulty of interpreting its results and preparing samples to

run on it. In the actual running of the instrument, I am indebted to the time, patience, and help of Bruce Deck, Sean Duncan, Joel Fodrie, Liyan Tian, and Pat Castillo. To Liyan I owe thanks for her patience in teaching me some of the more basic points of clean lab courtesy, protocols, and maintenance. I also owe Pat a great debt of gratitude for allowing me to take up space in and make use of his clean lab, materials, and acids for the preparation of my samples. He was also invaluable in figuring out how to prepare ICP-MS runs so that I would be able to extract usable data from the results.

The images that appear in Chapter 3 were taken in the Azam Lab. Ty Samo deserves credit for helping train me on the microscope, as well as providing insights into what I was seeing and why.

Tristan Carland deserves credit for teaching me the basics of both the R statistical computing environment, and getting me started in LaTeX for the writing of this thesis.

I also had help in the culturing of diatoms from two undergraduates: Heather Kroll and Audrey Zak. Thank you to you both for your time, intelligence, and curiosity!

Finally, a big thanks to my adviser, Chris Charles. The parameters of this project were often outside his comfort zone, yet he always supported me in the pursuit of my goals, and found money for analyses where and when money was required. His skeptical approach to science has also taught me an important, if sometimes painful, lesson about what it takes to be a scientist. I hope that it is in evidence in the proceeding pages.

The implementation of science requires a great deal of time, resources, and expertise to support. However, science must by done by a scientist, and here I would like to acknowledge the many organizations and people who have supported this scientist. I have been funded by the UC Regents Fellowship, the NSF Graduate Research Fellowships Program, Teaching Assistant appointments, the NSF GK-12 Fellowship, and the SIO graduate office. While this provided my financial support, I have been personally supported by a great number of wonderful students, administrators, faculty, and staff at SIO and UCSD, as well as a great number

unaffiliated with the University. Though many are deserving of mention, I will here limit acknowledgment to Taylor, my wife. You have been a great companion though both the good times and the hard times, and I will always remember how much we laughed through all of it.

Thank you.

VITA

2005	B. S. in Environmental Geoscience *magna cum laude*, University of Notre Dame, South Bend, IN
2005	UC Regents Fellowship
2006-2009	NSF Graduate Research Fellowships Program Fellow
2009-2010	Graduate Teaching Assistant, University of California, San Diego
2010-2012	NSF GK-12 Program Fellow
2010	M. S. in Earth Sciences, University of California, San Diego
2013	Ph. D. in Oceanography, Scripps Institution of Oceanography at the University of California, San Diego

ABSTRACT OF THE DISSERTATION

Effects of trace metals on diatom export products from the euphotic zone and significance for biogeochemical cycles

by

Daniel J Richter

Doctor of Philosophy in Oceanography

University of California, San Diego, 2013

Professor Christopher D. Charles, Chair

This thesis has been motivated by questions pertaining to the cycling of bioactive elements through the ocean on geological time scales. By definition, such questions cannot be addressed without understanding the organisms that mediate their fate, as well as the geological deposits in which they are deposited. I have further focused on metals, which have their own unique chemistry both in seawater and within the cell. This thesis is thus a highly interdisciplinary exercise.

In chapter 2 I use a novel trace-metal clean and pH-controlled culturing technique to culture the coastal diatom *Thalassiosira pseudonana* under variable trace metal regimes. These experiments yield the first evidence for Cd incorporation into the diatom frusutle, for variability in frustular Cu incorporation, and

add nuance to previous observations of frustule-bound Zn. I evaluate existing paradigms for macronutrient and micronutrient cycling throughout the ocean in light of these data, and evaluate the potential for frustule-bound Cu, Zn, and Cd as paleoproxies.

In chapter 3 I investigate the variability of polyphosphate in 4 species of diatom with the growth cycle and with variable Cu availability. I use a method that reports extractable polyphosphate (*e*-poly P) that does not include whole-cell P, but does include P bound in polyphosphate granules missed by some other methods. I find wide variability in *e*-poly P over the course of the growth cycle, over the range of $[Cu^{2+}]$ examined, and interspecific differences between the diatoms considered.

In chapter 4 I report polyphosphate, Cu and Fe speciation, *in situ* phytoplankton community composition, macronutrient, and physical data from two cruises of opportunity in the Humboldt and California Currents. I use a sampling technique that enables quantification of all these parameters from a single 50 L sample of sea water processed using trace-metal clean techniques. I report some of the first particulate polyphosphate measurements from the ocean, I find no evidence for any of these parameters determining *e*-poly P, and I suggest that community growth cycle is the dominant determinant of poly P *in situ*.

Chapter 1

Introduction to the thesis

This doctoral dissertation has been motivated by questions about how bioactive elements cycle through the ocean on geologic time scales. My approach to such questions has focused on how variable metal concentrations, including Fe, Cu, Zn, and Cd, affect phytoplankton export products from the photic zone, especially opal and polyphosphate. I have employed a highly interdisciplinary approach that blends biological, geological, and chemical techniques to address these questions. Phytoplankton, which are limited to the upper surface of the ocean by light penetration, mediate the fate of elements throughout the water column by the uptake of nutrients at the surface and redistribution of these elements to depth via sinking and remineralization. When sinking phytoplankton deliver materials to the ocean floor, these materials and the elements they contain may be preserved as geological deposits, effectively removing them from circulation. Therefore, to understand the cycling of elements through the ocean, one must begin with phytoplankton.

1.1 Biological considerations: diatoms and their ecological significance

Diatoms are a natural study organism in seeking to answer questions of nutrient cycling in the ocean due to their dominance in key areas of the ocean and their unique physiology. Overall, diatoms are responsible for an estimated

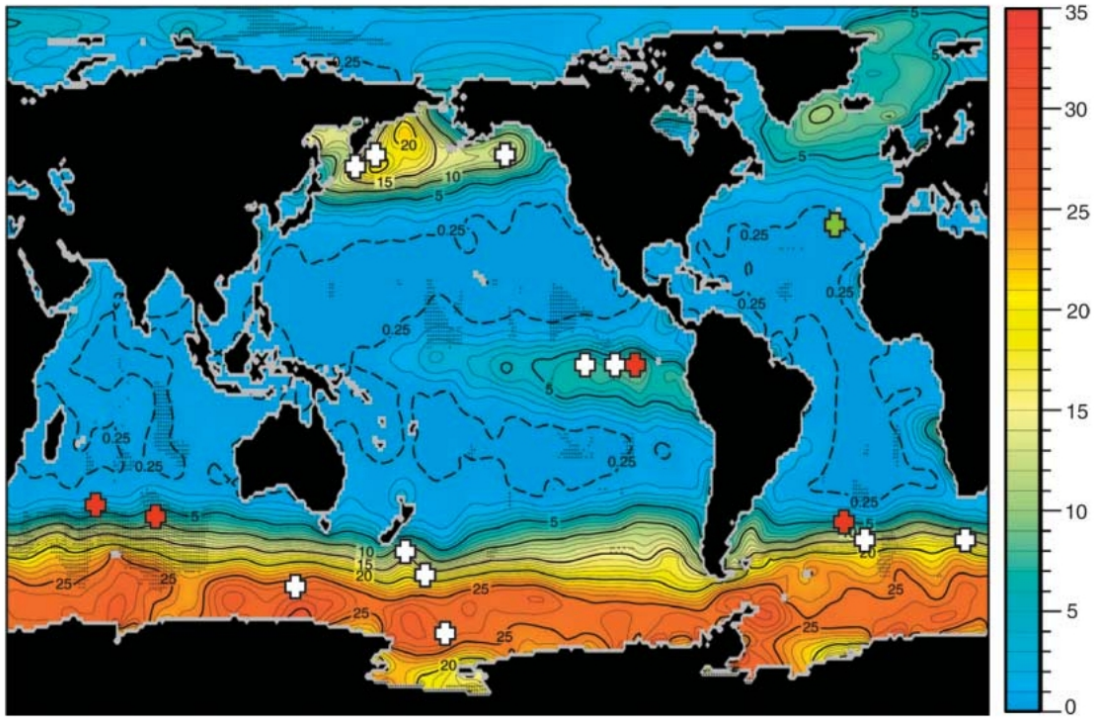

Figure 1.1: HNLC regions and meso-scale iron addition experiments as of 2007. Warmer colors indicate higher concentrations of Nitrate in µmol/L, and largely define the HNLCs. Figure from Boyd et al., (2007).

43% of primary productivity in the oceans, and 75% of primary productivity in so-called High-Nutrient Low Chlorophyll (HNLC) regions of the ocean including the Southern Ocean, the Equatorial Pacific, the North Pacific, and some coastal areas (Nelson and Tréguer, 1995) (Figure 1.1). Such dominance makes understanding the interactions between diatoms and the elements of interest a necessary precondition to understanding the marine biogeochemical cycles of these elements.

Diatoms derive their name, which means 'cut in half' (Armbrust, 2009), from their most distinctive feature: an intricately patterned and species-specific silica frustule. The frustule has two main parts: an epitheca, and a hypotheca that nestles inside it, akin to a petri dish (Figure 1.2). These two parts are in turn composed of valves (epivalve and hypovalve, respectively) on the top and bottom of the cell, and thinner girdle elements on the sides that link the two halves together (Round et al., 1990). The diatom frustule is protected from dissolution by a

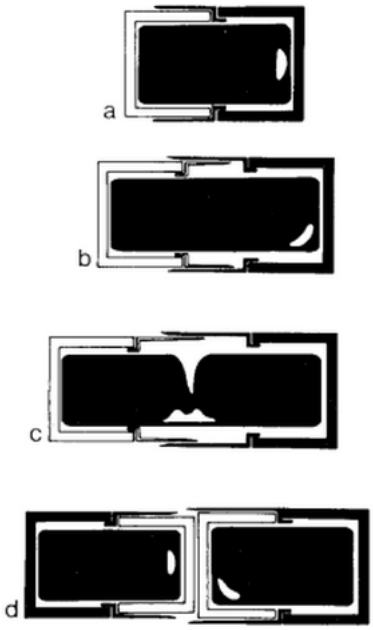

Figure 1.2: Schematic showing the epitheca (in black) and the hypotheca (in white) enclosing the protoplasm of a diatom cell (black) with nucleus (white) from Round et al., (1990). The progression from a to d shows the uniaxial growth of the cell, completion of the thecae by mitosis and cytokinesis, and finally daughter cells beginning to separate with new hypovalves formed beneath the girdle of the parent cell.

proteinaceous cell-wall layer (Bidle and Azam, 1999), and is thus more analogous to a skeleton than a shell (Round et al., 1990).

Having a relatively dense, mineralized frustule makes diatoms efficient vehicles for delivering biomass to the ocean floor via enhanced sinking rates. This characteristic earns diatoms a place as one of a select few 'ballast species' (Buesseler, 1998; Armstrong et al., 2001). Because of the enhanced sinking rates, such ballast species play a disproportionate role in delivering materials from the photic zone and to the ocean floor.

HNLC regions of the ocean are of interest because of their wide and dynamic range of export possibilities through time and space. These regions are characterized by an abundance of nutrients delivered to the surface ocean by upwelling, but low productivity due to the lack of an essential metal, iron (Martin et al., 1990;

Boyd et al., 2007). Whereas nutrient-poor, oligotrophic areas of the ocean are always characterized by a lack of nutrients and low productivity, HNLC regions may not always exhibit the same degree of Fe-limitation. For example, greater equator to pole temperature differentials during ice ages would increase wind speeds, and consequently the delivery of iron-rich dust to HNLC regions (Martin et al., 1990). The enhanced delivery of dust and the iron it contains to HNLC regions is one of several mechanisms hypothesized to account for the carbon sequestration that marks the transition from interglacial to glacial periods (Kohfeld et al., 2005).

Diatoms are intimately associated with HNLC regions. With rare exceptions, diatoms have an obligate requirement for silicic acid (Del Amo and Brzezinski, 1999). As a result of upwelling, this nutrient is abundant in HNLC and coastal regions, but scarce in oligotrophic waters (Figure 1.3). Furthermore, diatoms show an unparalleled ability to rapidly utilize nutrients when Fe-limitation is lifted (Cullen, 2006; Boyd et al., 2007). The combination means that diatoms play an important role in mediating export from the photic zone in HNLC regions, and the unique physiology of diatoms will determine the residual nutrient concentrations in surface waters that are exported from HNLC regions to other parts of the globe in overturning thermohaline circulation (Talley, 1999; Matsumoto, 2002; Matsumoto and Sarmiento, 2008). Thus, a substantial portion of carbon sequestration accompanying any regime change between interglacial and glacial periods would likely occur in these HNLC regions, and it would be largely mediated by sinking diatoms.

1.2 Geological considerations: export products of interest

A geological consequence of diatom dominance in HNLC regions is the presence of siliceous oozes in sediments underlying these regions. For instance, Southern Ocean sediments, beneath the largest HNLC region, are composed almost entirely of diatom frustules and account for 17-37% of present day opal accumulation (Cortese and Gersonde, 2004) (Figure 1.3). This amounts to a huge sink for silicic acid from the oceans, as well as any frustule-associated elements. As a testament

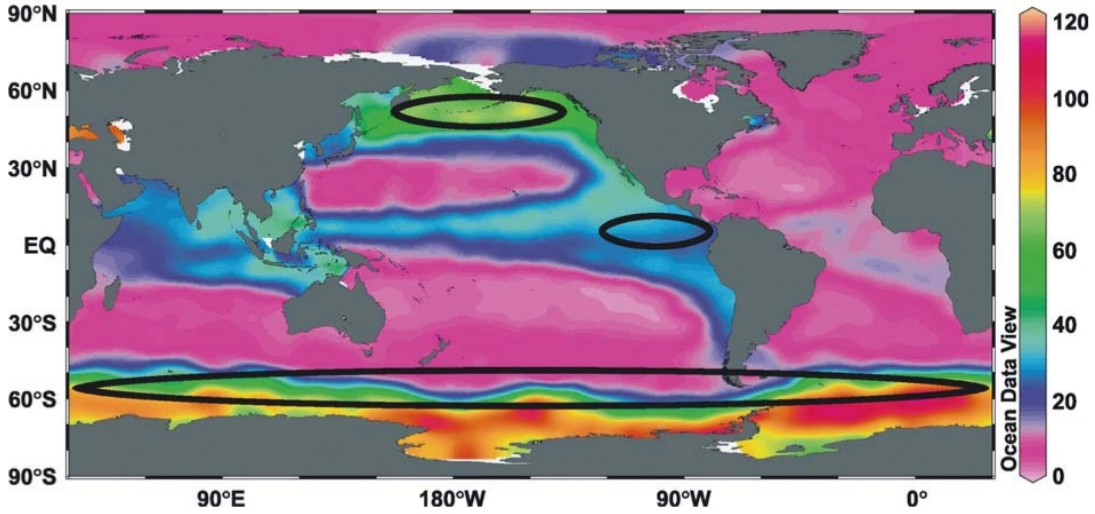

Figure 1.3: Color map showing the concentration of dissolved silica at 250 m depth in µM with ellipses highlighting regions of modern-day opal accumulation in sediments. Figure modified from Cortese and Gersonde, (2004).

to the power of diatom-driven export from the photic zone, prior to the expansion of diatoms ∼100 million years ago (Armbrust, 2009), silicic acid was common in the marine environment, whereas today it is scarce and limits diatom production as well as the distribution of other species that secrete biosilica (Maldonado et al., 1999).

Diatom biosilica, though intricately patterned on the nanoscale, is not structured on the atomic scale, and is thus amorphous. Biogenic opal's chemical formula is $SiO_2{*}nH_2O$, and it forms by the polymerization of silica monomers to form stable nuclei, the growth of the nuclei into spherical particles, and the aggregation of these particles to form structural motifs (Perry, 2003). As polymerization continues, negative charge builds up on the surface of the particle. This negative charge must be neutralized either by organic components, such as ammonium ions, or by cations (Perry, 2003). Unlike substitution of uranium into the calcite of corals, which substitutes for calcium in a well defined and well-patterned crystal structure (Sturchio et al., 1998), the disorder inherent in opal on the atomic scale enables cations to be included not only by substitution (as, for example, aluminum may substitute for Si; Gehlen et al., 2002), but also by inclusion.

Such inclusion enabled by disorder on the atomic scale is one method by which the elements of interest in this thesis could be stored and exported in diatom opal. Another possibility is that they are an essential part of the organic apparatus that is used to create the high-fidelity pattern replication observed in diatom frustules. For instance, both Mn and Fe have been found in association with diatom frustules, but only at very specific points in the frustule, suggestive of a role for these metals in metaloproteins involved in frustule formation (de Jonge et al., 2010) (Figure 1.4). Moreover, sequential leaching with HF of diatom frustules collected from sediments shows that once the outer 20% of opal is removed, the Zn:Si and Al:Si measured in a sample is stable (Hendry et al., 2008). Likewise, N isotopes of diatom-bound organic matter also appear to be physically protected (Sigman et al., 1999). This indicates that elements bound within diatom frustules are resistant to diagenesis and leaching. Therefore, diatomaceous oozes, in addition to being repositories of Si from the ocean, may also be significant sinks for some metals. Copper is one such metal, as elevated Cu concentrations have been noted overlying diatomaceous oozes in the Southern Ocean (Boyle, 1977; Monteiro and Orren, 1985).

Sedimentary apatite deposits are another geological deposit considered in this thesis. As much as 80%, and possibly more, of all phosphorus burial in the ocean occurs as dispersed, fine-grained apatite ($CaPO_4$) deposits within both coastal and deep-sea sediments (Ruttenberg and Berner, 1993; Filippelli and Delaney, 1996; Benitez-Nelson, 2000). The origin of such deposits had long been unclear, but recently polyphosphate deposited in sediments was shown to act as an efficient nucleation site for apatite (Diaz et al., 2008) (Figure 1.5). This efficiency has been attributed to the co-location of polyphosphate with calcium (phosphate and calcium being the major components of apatite) in an organelle known as the acidocalcisome (Diaz et al., 2008; Docampo et al., 2005). Furthermore, the size of authigenic apatite grains were comparable to those of polyphosphate bodies in the acidocalcisomes of diatoms overlying polyphosphate and apatite-rich sediments. Diatoms cannot account for all of the authigenic apatite distribution in sediments, but as dominant ballast species, they are likely to play an important role.

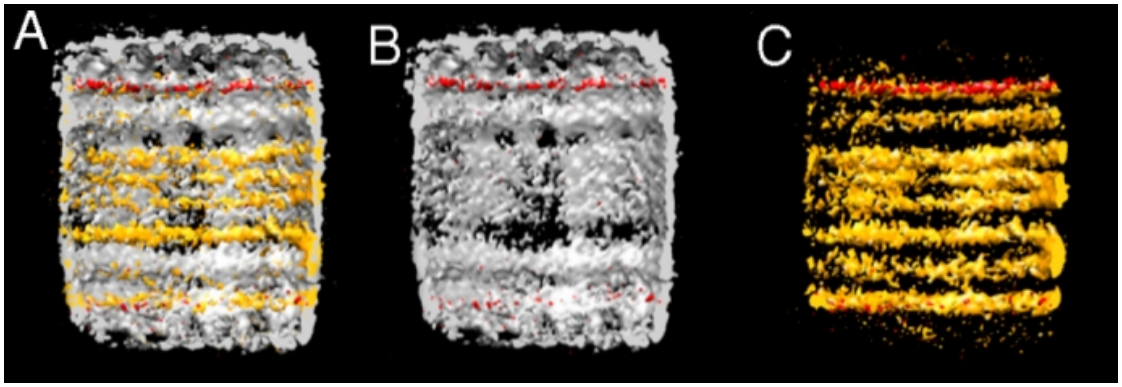

Figure 1.4: Images of the diatom *Cyclotella meneghiniana* generated using quantitative 3D elemental tomography showing the 3D structure. Highlighted elements include Si (gray), Fe (orange) and Mn (red). Image A shows all three elements, B shows only Si and Mn, and C shows only Fe and Mn. Mn and Fe are contained within the frustule, Mn is associated with a ridge of Si inside the cell marking where the valve face joins the girdle bands, and the strong Fe band collocated with weak silicification indicates the boundary between the epitheca and hypotheca (de Jonge et al., 2010).

Polyphosphate is ubiquitous in cells, but its role in the cell has long been ignored (Brown and Kornberg, 2004). Recent studies have implicated polyphosphate in a variety of cellular functions including oxidative, osmotic, heat, and nutritional stress responses, quorum sensing, biofilm formation, motility, virulence, stringent response, sporulation, Fe storage and delivery, photosynthesis regulation, Ca-mediated cell signaling, heavy metal sequestration, cytoplasmic pH regulation, germination, seed embryo development, symbiosis modulation, and mycorrhizal colonization in species including bacteria, non-vascular plants, protists, vascular plants, and plant-microbial interactions (Seufferheld and Curzi, 2010). Such diverse functionality across such a diversity of life renders polyphosphate's role in the cell resistant to simple classification, and variable methods and study organisms limit the universal application of lessons learned.

The size off the authigenic apatite sink is of some importance. Phosphorus is considered by some the ultimate limiting nutrient in the ocean, meaning that on time scales of thousands to tens of thousands of years, the amount of phosphorus in the ocean limits primary productivity (Tyrrell, 1999). Removing P more efficiently, say by increasing the delivery rate of polyphosphate to sediments, could lower the

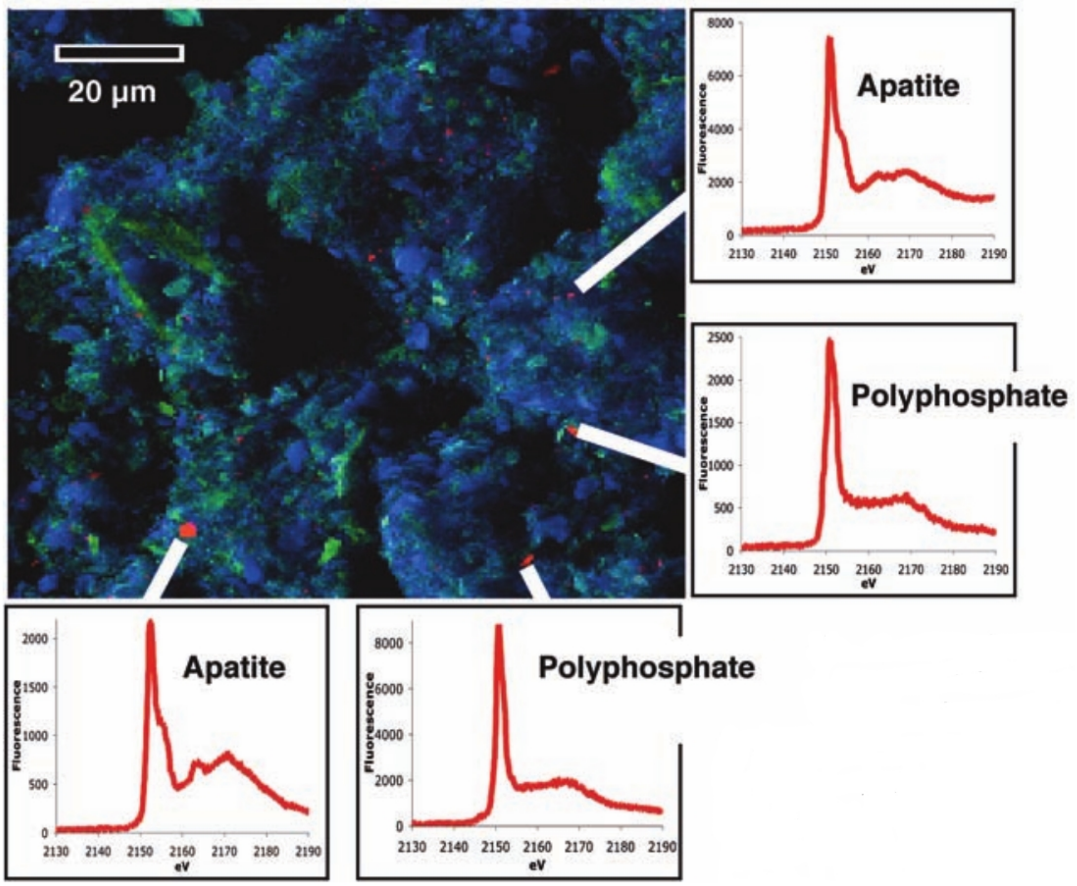

Figure 1.5: X-ray fluorescence image and fluorescence spectra of sediments in the Effingham Inlet. Red spots indicate P rich regions. For four of these spots, the fluorescence spectra are also shown, with 2 indicating polyphosphate and 2 indicating apatite. In the background are aluminum (blue) and magnesium (green). Image from Diaz et al., 2008.

biological carrying capacity of the oceans, thus limiting its ability to sequester carbon.

1.3 Chemical considerations: metals in the marine environment

As evidenced by the dominance of diatoms in the boom-bust cycles of Fe-limited waters of HNLC regions (Cullen, 2006; Boyd et al., 2007), trace metals play an important part in determining community composition in the marine environment, and nutrient export from the photic zone. In addition to Fe, metals considered here include Cu, Zn, and Cd. All these other metals have a role in the cell (Morel and Reinfelder, 1994; Barón et al., 1995; Lane and Morel, 2000), and all are toxic at high concentrations (Brand et al., 1986; Sunda and Huntsman, 1996). Because of their role as micronutrients, their biogeochemical cycles are of interest in and of themselves, but their importance is magnified by tight correlations observed between these metals and other nutrients.

For instance, Zn has been observed to co-vary with Si in the marine environment, and Cd has been shown to have a tight relationship with P (Bruland, 1980) (Figure 1.6). Attempts have been made to exploit such relationships for use as paleoproxies. Cadmium in foraminifera tests has been used to infer ancient surface concentrations of phosphate (Boyle, 1992; Boyle et al., 1995; Rickaby and Elderfield, 1999), and Zn in diatoms frustules has been used to link surface $[Zn^{2+}]$ to upwelling and circulation as well as mixed layer salinity (Ellwood and Hunter, 2000b; Hendry et al., 2008). As previously mentioned, Cu concentrations are elevated above diatomaceous oozes (Boyle, 1977; Monteiro and Orren, 1985). While Cu is known to be incorporated into the frustule by the living diatom (de Jonge et al., 2010) (Figure 1.4), preferential Cu scavenging by diatoms frustules is another process that could explain this relationship (Balistrieri and Murray, 1984; Monteiro and Orren, 1985).

Metals have also been implicated in the allocation of P to polyphosphate within the cell. As in opal, polymerizing polyphosphate accumulates excess nega-

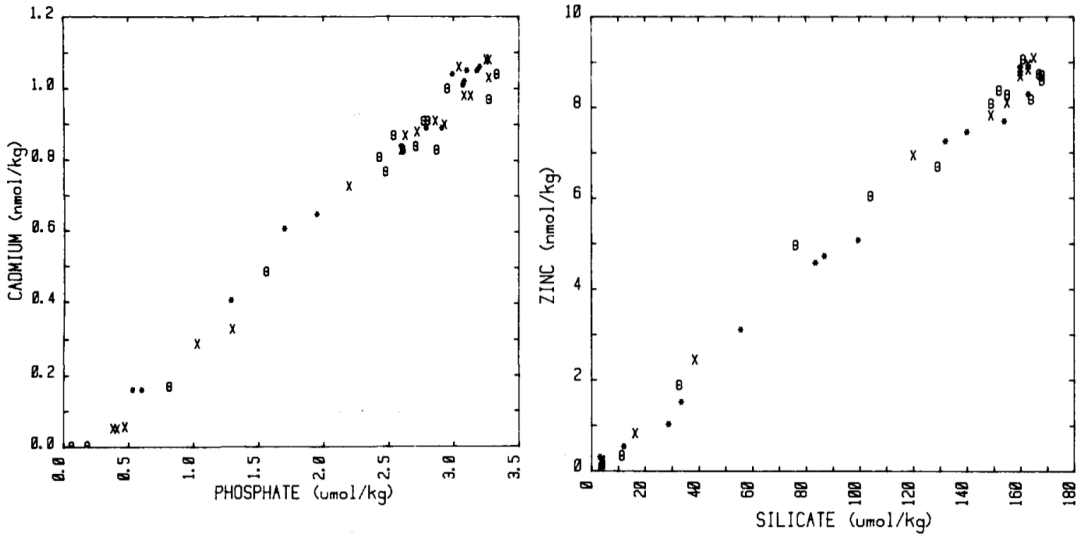

Figure 1.6: Plots comparing phosphate (µmol/kg) to total cadmium (nmol/kg) (left) and silicate (µmol/kg) to total zinc (nmol/kg) (right) on three separate cruises at the same sampling site in the North Pacific Ocean from (Bruland, 1980). Each cruise is represented by either an open circle, a closed circle, or an 'x'. The straight lines indicate strong correlation between these two elements.

tive charge that must be balanced for polymerization to continue (Seufferheld and Curzi, 2010). This is routinely accomplished by calcium in an organelle known as the acidocalcisome (Docampo et al., 2005; Seufferheld et al., 2008). Metals would also have a positive charge in the acidic conditions of this organelle and have been shown to accumulate in polyphosphate bodies when in excess, perhaps as a form of cellular detoxification (Jensen et al., 1982; Jensen et al., 1982a; Walsh & Hunter, 1992).

1.4 Challenges of working with metals

Working with trace metals presents substantial challenges. Their concentrations in the ocean are vanishingly small, on the order of parts per billion (Bruland, 1980) (Figure 1.6). These low concentrations are effectively lowered further by the complexation of metals with ligands. While ligands in the ocean are heterogeneous and their origins unclear, possible ligands for the metals considered here include chloride ions, thiols, humics, photochemical break-down products, as well

as ligands purposely synthesized and excreted by phytoplankton to bind metals (Moffett and Brand, 1996; Saito et al., 2003; Bundy et al., 2012).

In culture experiments, it is necessary to replicate both the low concentrations of metals, as well as their speciation. Replicating low concentrations requires time-consuming cleaning procedures and specialized equipment to ensure metals do not contaminate cultures or samples. As an example, autoclaves, which are standard for biological culture studies, cannot be used at any point in the process. Instead, microwave sterilization is used (Keller et al., 1988). The speciation is controlled by adding well-characterized metal chelators, such as Ethylenediaminetetraacetic acid (EDTA) (Price et al., 1988). Once added, software is used to calculate the resultant concentrations (Westall et al., 1976).

However, such software is of limited utility if culture conditions change between inoculation and collection. One notable change that can affect metal speciation and the availability of silicic acid, the Si-species taken up by diatoms (Del Amo and Brzezinski, 1999), is pH (Figure 1.7). As phytoplankton take up CO_2 from the media for photosynthesis, the pH of the media may rise more than a full pH unit over the course of growth (Chapter 2). While this problem has been solved for the needs of most culture experiments by bubbling filtered air into cultures or using stir bars to increase gas exchange, these solutions are are not directly applicable to trace metal studies. Glassware is never sufficiently clean for trace metal chemistry, and plastics not thoroughly acid-cleaned can be a source of contamination for Zn in particular. Using Teflon stir bars in plastic bottles with uneven surfaces at the bottom flakes the plastic. This exposes plastic surfaces from either the stir bar or the container that were not acid cleaned, and introduces tiny particles into the media that cannot be easily and cleanly separated from the sample, and which could cause damage to instruments used for final analysis. Accordingly, none of the previous trace metal culture studies pertinent to this thesis report having controlled pH in their experiments (Sunda and Huntsman, 1992; Ellwood and Hunter, 2000a; Jaccard et al., 2009b).

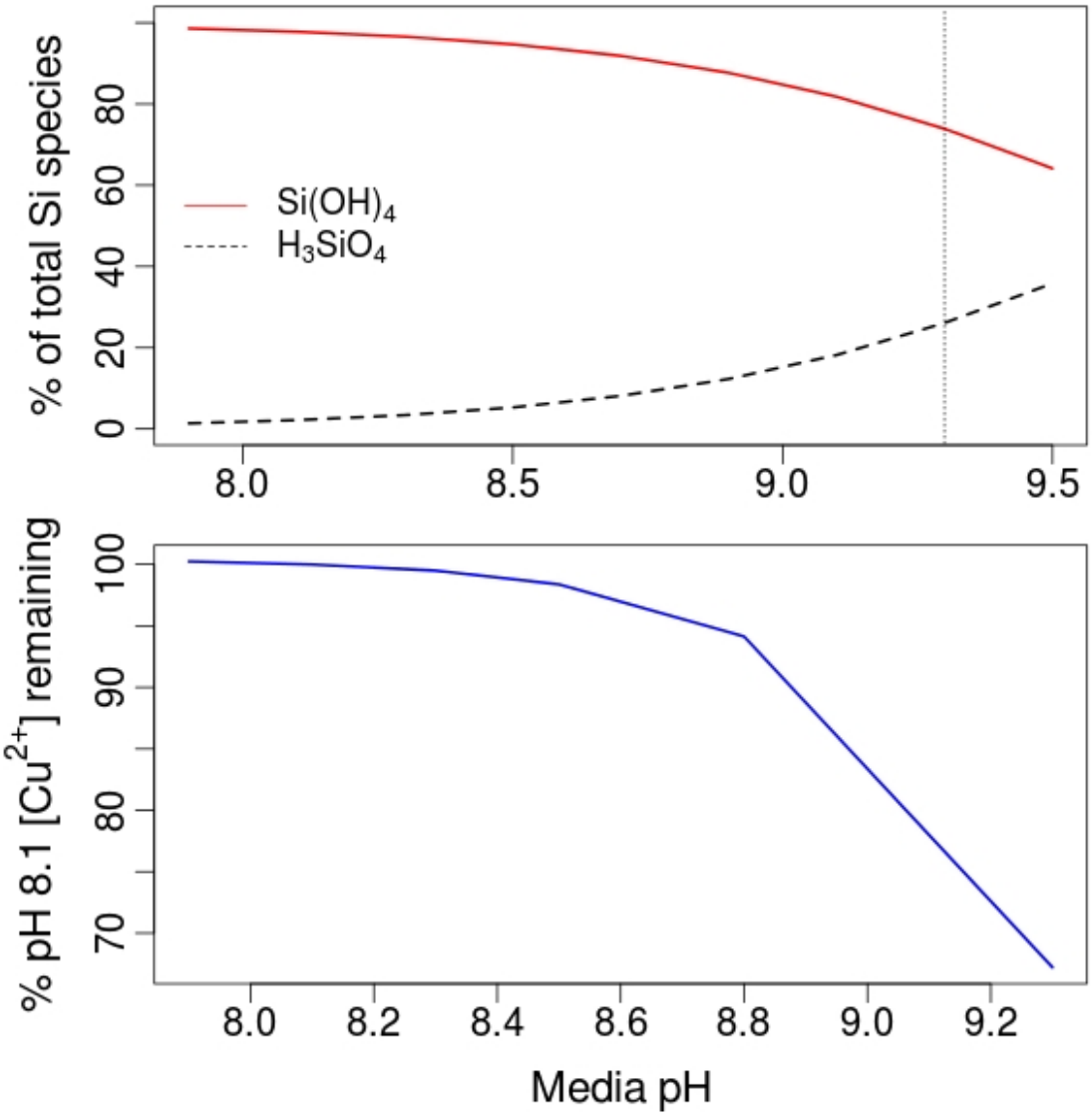

Figure 1.7: Plots showing pH vs. % of total dissolved silicate species as $Si(OH)_4$ (solid red line), which is the preferred species taken up by diatoms (Del Amo and Brzezinski, 1999), and H_3SiO_4 (dashed black line) on the top plot, and % of Cu^{2+} remaining relative to the amount available at pH = 8.1 in the Aquil medium used for culture in Chapter 2 on the bottom plot. All calculations were made using the MINEQL software (Westall et al., 1976) varying only pH. The dotted line is drawn at pH = 9.3, the highest pH obtained by diatoms grown in the absence of pH control (Chapter 2). At pH 9.3 $[Si(OH)_4]$ = 74% and $[H_3SiO_4]$ = 26% of all dissolved silicate species. At pH 9.3, only 67% of $[Cu^{2+}]$ remains, with comparable remaining $[Cd^{2+}]$ and $[Zn^{2+}]$.

1.5 Summary and Thesis Outline

My general interest in the cycling of bioactive elements on geological time scales distilled into a focus on upwelling regimes and the diatoms that dominate primary productivity in them. Though diatom export products constitute a major portion of sediments underlying these regions (Cortese and Gersonde, 2004), we do not understand fundamental aspects of diatom physiology that may affect the variability of both the opal and polyphosphate in these sediments. Constraining the boundaries of such variability is an important precondition towards the ultimate goal of understanding the cycling of these elements through time. Though not the only variable that might affect diatoms' production of opal and polyphosphate, the challenges inherent in trace metal work has led to a paucity of published data on the subject. Furthermore, the methods for the trace metal clean culture of diatoms still exhibit poor control over variables such as pH and pCO_2 that introduce considerable uncertainty into results.

Similarly, the versatility of polyphosphate in a diverse array of organisms has contributed to a general lack of focus in the literature, with few contributions dedicated to understanding this molecule in marine organisms and in the marine environment. However, the importance of phytoplankton-derived polyphosphate in the recently elucidated pathway for authigenic apatite formation in sediments (Diaz et al., 2008), and the importance of such minerals as a sink for the ultimate limiting nutrient in the ocean (Benitez-Nelson, 2000; Tyrrell, 1999) has underlined the importance of understanding marine polyphosphate cycling. While studies focused on polyphosphate in marine organisms have increased, there are no standardized methods for its quantification, and some methods underrepresent granular polyphosphate, the most likely candidate for nucleating authigenic apatite in sediments (Eixler et al., 2005). In this thesis, I accepted the challenges presented by working with trace metals, and in a highly interdisciplinary approach I blend tools and techniques from biology, geology, and chemistry to address fundamental questions about the cycling of nutrients and trace metals in the ocean.

In the second chapter I employ a novel, trace-metal clean technique to control pH that eliminates much of the variability in $[Si(OH)_4]$, trace metal speciation,

and pCO_2 that would have increased the uncertainty of previously published results. This technique was used to culture the diatom *Thalassiosira pseudonana* at variable availabilities of Cu, Zn, and Cd. Cells grown using this technique were then processed to analyze the elemental composition of an HNO_3-soluble 'intracellular' fraction, and an HF-soluble 'frustule' fraction on an ICP-MS. The results contrast sharply with previous work done on the same diatom species, highlighting the importance of further constraining the mechanisms responsible for Zn incorporation into diatom frustules before frustule-bound Zn can be robustly applied as a paleoproxy. This approach also yielded evidence of variable Cu and Cd incorporation into diatom frustules, and enabled the comparison of multiple elements measured simultaneously on the same instrument from a diatom population. These results yield interesting insights into the role of metals in frustule formation, into the comparative importance of *in vivo* incorporation vs scavenging in explaining the elevated Cu signal above diatomaceous oozes, the relative ease with which metals are incorporated into the frustule, and the potential and limitations for analyzing metal contents in diatom frustules recovered from marine sediments.

In the third chapter I shift my focus to the variability of polyphosphate with the growth cycle and, considering polyphosphate's role in metal uptake and detoxification, variable $[Cu^{2+}]$. I chose copper because it is the only metal considered in chapter 2 whose naturally occurring concentration in the surface ocean can be toxic to some species of phytoplankton (Mann et al., 2002), and so is the metal most likely to cause variability in intracellular polyphosphate allocation in natural waters. I employ an extraction technique that does not report whole-cell P, but would include P bound in granular polyphosphate, and which can be run several times for multiple samples quickly and at low expense. Focusing on one metal and employing this technique enabled me to investigate 4 diatoms instead of one, and thus begin to assess whether the polyphosphate response varies between pennate and centric diatoms, and between diatoms adapted to estuarine, coastal, and oceanic conditions. This approach yielded some of the first observations of polyphosphate variation with the growth cycle, and with variable $[Cu^{2+}]$. I also consider how N:P ratios vary in Cu-treated cells, since a change in polyphosphate

might reasonably be expected to change the N:P ratio of sinking organic matter.

In chapter 4 I attempt to identify the variables governing polyphosphate allocation in natural phytoplankton assemblages. Previous results indicate polyphosphate varies as a function of nutrient availability and as a general stress response, and the data in previous chapter indicate polyphosphate varies between species, with $[Cu^{2+}]$, and with the growth cycle. I therefore report nutrient data, data on Fe-limitation (which would induce a stress response), community composition, and copper speciation. I perform these analyses on samples collected on two cruises of opportunity in two eastern boundary currents: the California and Humboldt Currents. Though no obvious correlations between polyphosphate and other parameters emerged, this finding is interesting in and of itself. I conclude based on the magnitude of variability in polyphosphate observed in chapter 3 that the growth state of the phytoplankton community being sampled may well be the dominant factor determining community polyphosphat allocation.

Chapter 2

Partitioning of Cu, Zn, and Cd between the intracellular and frustule fractions of the diatom *Thalassiosira pseudonana* and relevance to biogeochemical cycles

2.1 Abstract

Here I report findings that the diatom *Thalassiosira pseudonana* incorporates Cu, Zn, and Cd into its frustule as a function of the ambient and intracellular metal concentration. Unlike previous studies, I maintained a relatively stable culture pH that would prevent metal and silicate speciation from varying by more than 4% during batch culture. This was accomplished at low cost with filtered ambient air and a simple bubbler, meaning the technique could be easily incorporated into future trace metal culture work. The resulting culture conditions are a better approximation of real-world conditions, especially for Zn, which at higher pH and lower pCO_2 would be heavily recruited for carbonic anhydrase. I find comparing trends of metal to P (Me:P) ratios in the frustule to be a useful metric

in addition to the metal to Si (Me:Si) ratios reported in earlier works. Differences exist between frustule Zn:P and Zn:Si trends, indicating comparing both metrics may yield useful information. I also report relative incorporation efficiency, showing that Zn is more efficiently incorporated into the frustule than Cu, and less efficiently incorporated than Cd at oceanic [Cd^{2+}], though absolute Cd:$Si_{Frustule}$ ratios are one to two orders of magnitude lower than Zn:$Si_{Frustule}$. I also find that increasing [Cu^{2+}] results in greater Zn incorporation into the frustule without raising intracellular Zn concentrations, and that under no conditions tested is Cu more abundant in the frustule than Zn. The observations reported here provide useful insights into the role diatoms may play in the cycling of these metals in the modern ocean, though they do not alter the general framework of current models. Finally, I evaluate the potential for these metals to serve as paleoproxies, and conclude that Cd is unlikely to serve as a useful proxy due to limited variability and low incorporation. Cu may prove useful in limited situations and with further development. Zn is a useful proxy as shown in earlier works, but the Zn:$Si_{Frustule}$ does not vary with Zn alone. Multiple factors may influence this ratio including Mn, $Si(OH)_4$, Cu, or pH to give the same Zn:$Si_{Frustule}$ for multiple [Zn^{2+}]. Given the poor understanding of the physiology governing Zn incorporation, this ratio should be only cautiously employed for paleoceanographic applications.

2.2 Introduction

Despite the importance of diatoms (Nelson and Tréguer, 1995; Boyd et al., 2007; Buesseler, 1998; Armstrong et al., 2001) and their frustules (Cortese and Gersonde, 2004; Monteiro and Orren, 1985; Matsumoto and Sarmiento, 2008) for understanding nutrient cycling in the modern ocean, and despite the demonstrated ability of trace metals to limit phytoplankton growth by their absence or overabundance (e.g. Brand et al., 1986; Mann et al., 2002; Martin et al., 1990), there has been relatively little investigation into how trace metals affect diatom frustule formation and composition. This is due in no small part to the difficulty of trace-metal clean culture and analysis of diatoms and their frustules. Unlike culture

experiments of foraminifera (e.g. Spero et al., 1997), where the isotopes of interest are derived from water and a sea water constituent, HCO_3^-, measured in mM concentrations, trace metals are found at nanomolar to picomolar ranges in sea water (Table 2.1). From this limited pool, only 'free' metals are bioavailable (Sunda, 1988; Bruland, 1991). Whereas the elements of interest in foraminifera become lattice-forming constituents of the mineral structure, trace metals (excepting Al and Ge; e.g. Gehlen et al., 2002; Davis & Hildebrand, 2008) are incorporated at a level millions of times lower than silicon. At such low levels of incorporation, contamination at every stage is a concern, as is simply obtaining enough material for analysis. The mismatch between Si levels and Zn levels has also necessitated separate measurements of these two elements on different instruments, introducing an additional source of error into results (Jaccard et al., 2009b; Ellwood and Hunter, 2000a).

A further and as yet unresolved complication is the increase in pH from 8.1 to ∼9.3 that commonly occurs in batch cultures as diatoms take up CO_2 during photosynthesis. The concentrations of both free metals and silicic acid, the species of silicon favored by diatoms (Del Amo and Brzezinski, 1999), decrease by ∼32% and 26%, respectively, as pH increases. This introduces significant deviations from initial conditions and compromises the environmental relevance of culture studies (Figure 1.7; Westall et al., 1976). Elevated pH would also be expected to affect the physiology of phytoplankton, as one response to decreased CO_2 availability at high pH would be upregulation of carbonic anhydrase, an enzyme with Zn as a co-factor (Morel and Reinfelder, 1994; Lane and Morel, 2000). Due to the relatively high incorporation of Zn into the frustule (Ellwood and Hunter, 2000a; Jaccard et al., 2009b; de Jonge et al., 2010), and its apparent involvement in cellular Si metabolism (Thamatrakoln and Hildebrand, 2008; Rueter Jr and Morel, 1981; Sunda and Huntsman, 1992), interactions of this metal with diatoms has attracted appreciable attention in the literature. However, none of the studies investigating the role of Zn in the frustule or in cellular Si dynamics report controlling pH in their experiments.

Part of the focus on frustule-bound Zn derives from its tight correlation

with Si in the modern ocean (Bruland, 1980). This in turn has led to research focused on defining variable Zn incorporation into the frustule (Jaccard et al., 2009b; Ellwood and Hunter, 2000a), and to research aimed at exploiting this variability to derive information on surface ocean conditions through time (Jaccard et al., 2009a; Ellwood and Hunter, 2000b; Hendry et al., 2008). While this focus on Zn is justified, interactions between diatom frustules and the trace metals Cd and Cu are also of interest. Like Zn:Si, Cd and P have demonstrate a tight correlation in the modern ocean (Bruland, 1980; Elderfield and Rickaby, 2000), but no work has yet reported finding Cd incorporated into diatom frustules. Elevated copper concentrations have been found above diatomaceous oozes (Boyle, 1977; Monteiro and Orren, 1985), and has also been found to be incorporated into the frustule by living diatoms (de Jonge et al., 2010). This has led to unanswered questions of how much of the Cu source from diatomaceous oozes is due to Cu incorporated by living diatoms and how much may be attributed to Cu sorbed or complexed by sinking diatoms (Monteiro and Orren, 1985). Thus, understanding the incorporation of Zn, Cu, and Cd into the frustule by living diatoms is important for understanding the cycling of these metals in the ocean. Additionally, if incorporation of Cu and Cd into diatom frustules were found to occur, and to be variable, this variability could, like Zn, be exploited for paleoceanographic reconstructions.

In this work I report findings on patterns of trace-metal incorporation into diatom frustules. Using the diatom *Thalassiosira pseudonana*, I sought to improve techniques for the trace metal clean culture and analysis of diatom frustules, and to evaluate the present understanding of global nutrient cycles in light of data collected. I investigated the elemental ratios of Cu, Zn, and Cd relative to both Si and P in the nitric acid-soluble 'intracellular' fraction, and in the HF-soluble 'frustule' fraction. Using ICP-MS analysis, I report results from the first pH-controlled and trace-metal clean culture experiments focused on these metals. These experiments show incorporation of all three metals into diatom frustules, and are the first to compare the relative incorporation rates of these metals into the organic matter vs the frustule relative to Si, P, and each other. I find evidence that incorporation of all three elements into the frustule varies with ambient metal availability, that

Me:P ratios may be used alongside Me:Si ratios in diatom frustules while yielding different information, differing frustule incorporation efficiencies between these metals, and a dependence of frustule-bound Zn on ambient [Cu^{2+}]. I offer new insights into the marine cycling of Cd and Cu in light of these data, and I comment on the prospects for using frustule-bound Zn, Cd, and Cu as paleoproxies.

2.3 Materials and Methods

All data reported in this paper were collected from *in vitro* samples of the coastal diatom *Thalassiosira pseudonana* (CCMP 1335 obtained from the Hildebrand Lab) grown under trace-metal clean conditions. A flow chart of the steps described below is included in Figure 2.1.

2.3.1 Experimental Preparation and Considerations

Extensive acid-cleaning of all equipment used in culturing and processing diatom cultures was required. Diatoms were grown in polycarbonate (PC) bottles cleaned as follows:

1. One day soak in Citranox soap, followed by 6 rinses with DI water.
2. Two day soak in 10% trace-metal grade HCl, followed by 6 rinses with Milli-Q water.
3. Two day soak in 1% trace-metal grade HCl, followed by 6 rinses with Milli-Q water.
4. Two day soak in Milli-Q water.

Following the Citranox soak, all cleaning steps took place in a class 100 clean room.

The cleaned bottles were filled with Aquil media (Price et al., 1988) containing 100 µM EDTA prepared from reagent-grade salts, nutrients, trace metals, and vitamins. Salts were dissolved in Milli-Q water, pH adjusted to 8.1 ± 0.1, then the media was allowed to pass through a column with Chelex resin located in a class 100 clean room to remove contaminant metals via ion-exchange. Vitamin stocks and Chelexed nutrient stocks were added in a sterilized laminar-flow

Table 2.1: Metal additions in M added to Cd, Cu, and Zn-treated diatoms in a 1:1 ratio with EDTA. The observed oceanic high and low concentrations for each metal are also reported (Cu from Coale and Bruland, 1988; Zn from Bruland, 1989; Cd from Lane et al., 2008). Free metal concentrations were calculated using MINEQL (Westall et al., 1976).

Metal	Cu_T	Cu^{2+}	Zn_T	Zn^{2+}	Cd_T	Cd^{2+}
Ocean Low	5.4E-10	1.4E-14	4.0E-11	3.0E-13	2.0E-12	1.8E-14
Ocean High	5.3E-9	1.0E-11	9.1E-9	3.1E-10	1.0E-9	9.4E-12
			This study:			
Spike 1	1.0E-8	8.0E-15	8.5E-10	2.4E-13	9.4E-11	1.5E-14
Spike 2	3.0E-8	2.4E-14	7.6E-9	2.1E-12	8.5E-10	1.4E-13
Spike 3	1.0E-7	8.0E-14	6.9E-8	1.9E-11	7.6E-9	1.2E-12
Spike 4	3.0E-7	2.4E-13	6.2E-7	1.7E-10	6.9E-8	1.1E-11
Spike 5	1.0E-6	8.0E-13	1.9E-6	5.3E-10	2.1E-7	3.3E-11
Spike 6	3.0E-6	2.4E-12	5.6E-6	1.6E-09	6.2E-7	9.8E-11
Spike 7	1.0E-5	8.0E-12	1.7E-5	4.8E-09	1.9E-6	3.0E-10
Spike 8	5.0E-5	4.0E-11	5.0E-5	1.4E-08	5.6E-6	8.9E-10
Spike 9	n/a		n/a		5.0E-5	7.9E-9

hood, and the media was microwave sterilized (Keller et al., 1988). After cooling the media to room temperature, 0.2 µm-filtered trace-metal mix was added in a sterilized laminar flow hood.

A total of 25 cultures were grown under variable trace metal conditions in 3 experiments: variable Cu (8 cultures), variable Zn (8 cultures), and variable Cd (9 cultures). Trace-metal additions were added in a 1:1 ratio with EDTA to control metal speciation (Table 2.1). Trace-metal additions were designed so that the free concentration of each metal, calculated using MINEQL (Westall et al., 1976), would encompass the range of values found in the modern ocean (Table 2.1). Trace-metal additions were allowed to equilibrate with the media overnight before diatom inoculation. While trace-metal clean, this procedure was not sterile due to the inability to sterilize the apparatus (parts of which would not fit in a microwave

for sterilization) without also contaminating it with trace metals. However, as diatoms dominated throughout the experiment, this should not have significantly affected results.

Diatom stock cultures were maintained in clean, sterile 60 ml PC bottles in Aquil media. Prior to inoculation in the experimental bottles, diatoms were grown to the necessary densities and by two intermediate inoculations in acid-cleaned, microwave-sterilized 60 ml and 500 ml PC bottles, respectively. For the Zn-treatment, diatoms were limited for Zn by growing them for 9-12 days in Zn-free Aquil media until their cellular density was limited relative to a control, Zn-replete culture.

Prior to acid cleaning, holes were drilled into the caps of the 1L bottles to accommodate an acid-cleaned 5-ml serological pipette. Under a laminar-flow hood, the pipette was placed through the hole such that it would deliver air to the bottom of the bottle without touching the bottom when the cap was completely screwed down. Parafilm was wrapped around the outside of the cap to seal the point of contact with the serological pipette to prevent dust and bacterial contamination during growth. The top of the serological pipette was fitted with acid-cleaned Tygon tubing attached to a 0.1 µm vacuum-line filter. Thus, when the cap was screwed down, the only point of entry to the culture was through the 0.1 µm filter (Figure 2.2a).

2.3.2 Diatom Growth

Since free metal, silicic acid, and pCO_2 concentrations are sensitive to changes in pH, ambient air was bubbled into eight 1L PC experimental bottles through two 0.1 µm vacuum-line filters to keep pH < 8.5. MINEQL calculations reveal that media free Cu, Zn, and Cd concentrations vary less than 2% and silicic acid concentrations vary less than 4% between pH 8.1 and 8.5. Without bubbling, however, uptake of CO_2 by diatom cultures routinely raised media pH to $\sim$9.3, at which point growth was inhibited. At this pH, free metal and silicic acid concentrations are calculated to drop to 68% and 76% of their pH 8.1 concentrations, respectively, and pCO_2 would be reduced to 3% of its pH 8.1 value (Westall et al.,

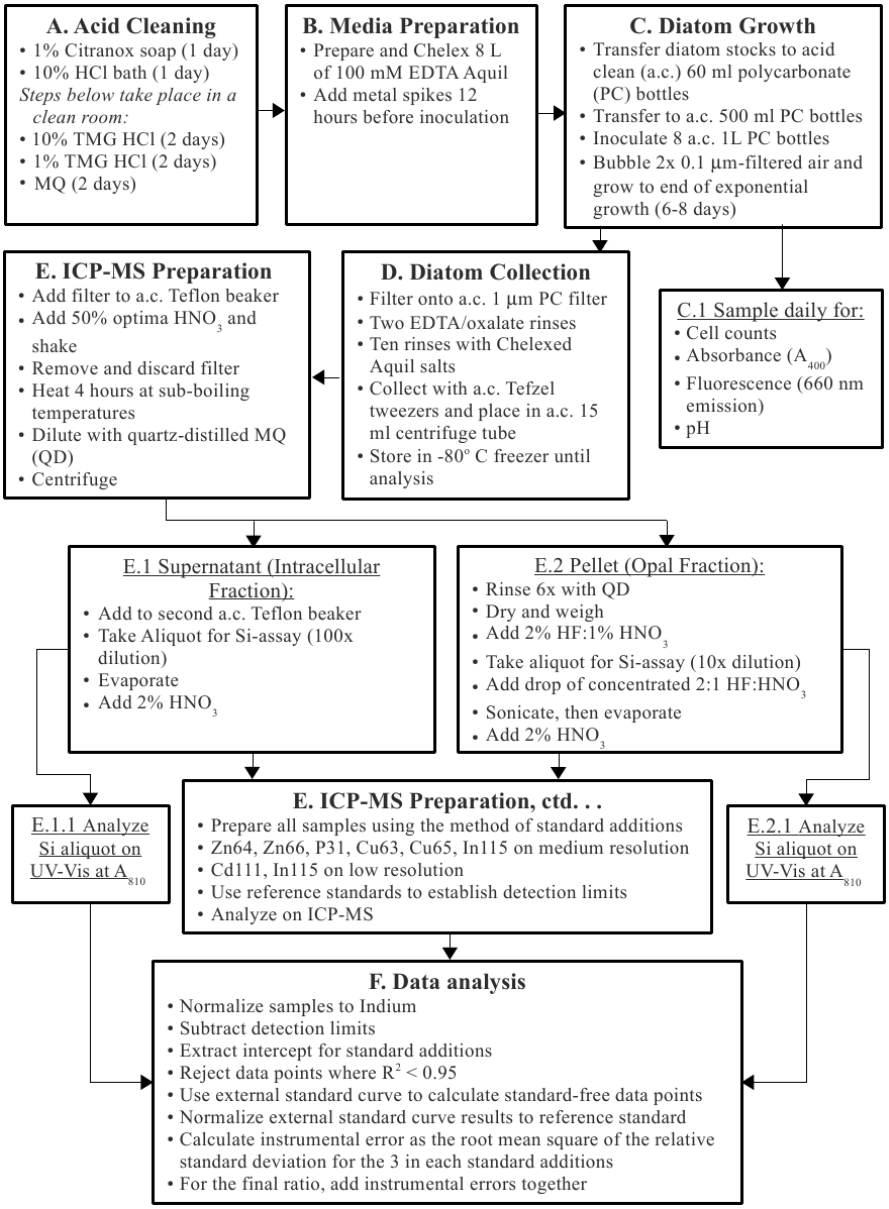

Figure 2.1: Flow chart of sample processing steps

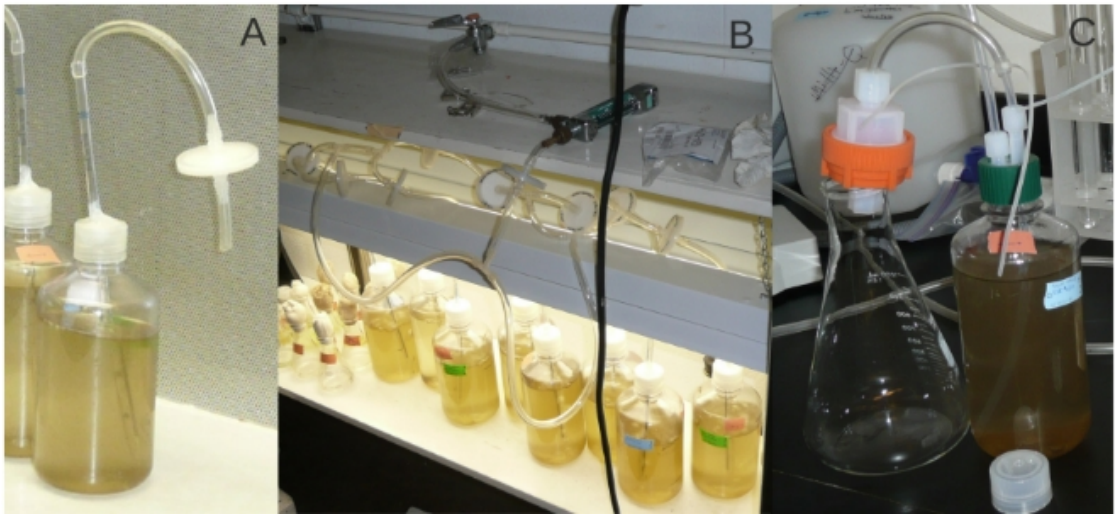

Figure 2.2: Culture equipment use for diatom growth. (A) Apparatus for keeping cultures clean during bubbling and sampling, (B) trace-metal clean bubbling, and (C) filtration using positive pressure. In A, a diatom culture is in the laminar-flow hood with TM-clean serological pipette that also served as a bubbler, parafilm wrapped around point where bubbler meets the cap to prevent metal or biological contamination, and 0.1 µm filter in place. B shows 8 cultures connected to air source. Note that one 0.1 µm filter is in line just down stream of the air-flow regulator, and each 1L culture has its own 0.1 µm filter that remains attached until sampling in a laminar-flow hood. C shows the set-up for filtration in a class 100 clean room. Air is directed through two 0.1 µm filters (not shown) into the culture, which then forces the media through a 1 µm pore-sized filter in a Teflon filter housing.

1976). Airflow was regulated using a needle-valve regulator. Air was delivered to the bubbler/serological pipette using $\frac{1}{4}$-inch acid-washed Tygon tubing connected with polypropylene (PP) connectors (Figure 2.2b). It was found that bubbling evaporated 300-400 mls of water during the course of an experiment. To maintain volume and ionic strength, MQ water was added to Zn and Cd cultures with an acid-cleaned serological pipette such that total volume was not allowed to vary by more than 10%. However, this was not done for the Cu-treatment.

Cell growth and media pH were monitored daily. Diatoms were grown on a 14:10 light dark cycle at 21 ± 1 ℃. Lighting was provided by 3 cool white fluorescent bulbs and one plant growth fluorescent bulb at ∼4300 lux. All cultures were sampled at the same time of day ± 1 hr. This was ∼3 hours into the light cycle for Cu and Cd, and ∼7 hours for Zn-treated cultures. Cultures were transferred from the culture room to a laminar flow hood with 0.1 µm filters in place and tops screwed tight. In a laminar-flow hood, the Tygon tubing with the 0.1 µm filter was removed from the serological pipette, the cap unscrewed, and ∼ 6 mls of media were sampled using the acid-cleaned serological pipette that also served as a bubbler. Three ml was used to measure fluorescence and absorbance on a Molecular Devices Spectramax M2, while at a minimum the samples with the highest and lowest fluorescence were also counted on a hemocytometer. The remaining three ml was used to measure media pH on a Thermo Orion PerpHecT LogR meter, model 320. Maximum growth rate was calculated as

$$(2.1)\ r = \ln(F_2/F_1)/(T_2\text{-}T_1)$$

Where F is fluorescence, and T is time in days. Days were selected by eye when the fluorescence plotted on a semi log-plot formed a straight line (Andersen, 2005). Though exponential growth typically ended around day 4 of growth, cell numbers were still increasing. To maximize the material available for analysis, growth was allowed to continue until cell counts plateaued, 6-8 days after inoculation in stationary phase.

2.3.3 Diatom Rinsing and Collection

Diatoms were collected at the end of exponential growth using positive pressure with air filtered through two 0.1 µm vacuum-line filters to filter cultures through a Savillex in-line filter holder in a class 100 clean room onto acid-washed, 47 mm diameter, 1 µm pore-size PC filters (Whatman) (Figure 2.2c). Filtered cells were rinsed with an oxalate-EDTA mixture adjusted to pH 7 for two 5-minute rinses followed by ten 1.5 ml rinses with a Chelexed Aquil salts (i.e. without nutrients, vitamins, or trace metal mix) solution while the filter was still in-line (Tang and Morel, 2006). This process scavenges surface-sorbed metals by a ligand-promoted process, and has been shown to be effective for removing iron-oxide species as well as Cu, Zn, and Cd. Filters were then folded in half using Tefzel tweezers and placed in an acid-cleaned polypropylene centrifuge tube and frozen at -80℃.

2.3.4 Diatom Cleaning for HR-ICP-MS Analysis

The procedure for diatom cleaning and ICP-MS preparation was largely adapted and modified from Ellwood & Hunter (2000a). Frozen filters with algal cells were taken into a class 100 clean room and placed in 15 ml Teflon beakers. Two mls of optima grade 50% HNO_3 were added, the beaker shaken vigorously to remove diatoms from the filter, then acid-cleaned Tefzel tweezers were used to remove the filter. Another 1 ml of 50% optima HNO_3 was used to rinse diatoms from the filter, which was then discarded. The tightly capped beaker was then heated to sub-boiling temperatures for 4 hours, allowed to cool, then brought to a final volume of ∼8 mls using quartz-distilled Milli-Q water and centrifuged at 3000 g for 10 min at 20℃ to separate the silica frustules from the acid-soluble, 'intracellular' fraction.

The supernatant (intracellular fraction) was pipetted off and placed in a second Teflon beaker. An aliquot was taken for Si analysis using the molybdenum-blue method on a Beckman Coulter DU 730 Life Science UV/Vis Spectrophotometer (Strickland and Parsons, 1965), and the rest was evaporated under an upside down Teflon beaker with continuously circulating air supplied through two 0.1 μm filters in line. 2% HNO_3 was then added, and the sample was divided into triplicate for

ICP-MS analysis using the method of standard additions. A 1 ppb indium (In) spike was used as an internal standard for all ICP-MS analyses.

The remaining frustule fraction was rinsed 6 times with quartz-distilled Milli-Q water and heated to dryness under a heat-lamp in the upside-down Teflon beaker. Once dry, the opal (frustule fraction) was digested by adding 2% (v/v) optima-grade HF in a 2:1 HF:HNO_3 solution. This ratio is standard for the dissolution of mineral samples and prevents the volatilization of some metals (Dolezal, J., Povondra, P., Šulcek, 1968). Once added, samples were sonicated for 2 hours in 1/2 hour increments using a Fisher Scientific FS60D sonicator. Dilute HF in excess was chosen because when reacted with silica at low temperatures, this favors the formation of the soluble species SiF_6 over the volatile SiF_4 (Hendry et al., 2008). In some samples, a white organic precipitate would sometimes form. This precipitate would disappear with heating (taking care not to exceed boiling temperatures), or with addition of optima-grade H_2O_2 and further sonication. Once the sample was completely dissolved, an aliquot was removed for Si-analysis.

Concentrated optima-grade HF was then added to the solution, the beaker sonicated for 1 hour, and then heated to dryness. The strong HF and heating promoted the formation of the volatile SiF_4 thus removing the potential for Si-matrix effects during analysis (Hendry et al., 2008; Davis and Hildebrand, 2008). An aliquot of concentrated optima nitric acid was added, the beaker sonicated 1 hour, then evaporated to dryness. The procedure was repeated once more, and served to promote the dissolution and removal of any fluorite formed during the dissolution procedure. 2% HNO_3 was then added and the sample divided into thirds for analysis by the method of standard additions.

2.3.5 ICP Method, set-up, error assessment, controlling matrix effects, and data processing

A multi-element standard was prepared gravimetrically from single-element standards. A 3-point external standard curve was prepared by serial dilutions of the multi-element standard to account for any matrix effects (Cullen, 2001). A reference standard prepared from single-element reference standards was run

every 6 measurements to account for drift. The detection limits for each run were calculated as 3 times the standard deviation of this reference standard. All samples were run with In as an internal standard, and data were normalized to In values before processing.

Samples were run on a Thermo Scientific Element 2 ICP-MS. Cd was analyzed on low resolution, while all other elements were analyzed on medium resolution. All ICP-MS measurements were made using the method of standard additions. Data points with R^2 values < 0.95 were excluded and the external calibration curve was used to calculate the elemental concentration measured in the lowest point in the standard additions curve, which had no standard added. Where two isotopes were available for comparison, I report the isotope with the highest average R^2 values for a sample set (Table 2.2).

Since all data points presented represent a ratio between two elements, the error for the two elements being compared were simply added together. The error for an individual element was calculated using the root mean square of the instrumental relative standard deviation (RSD) for the 3 points analyzed by standard additions. The procedure is the same for reporting Me:Si ratios, as the Si data were also measured in triplicate. In samples where the external standard curve was used instead of standard additions, the instrumental RSD values corresponding to the sample without standard added were added together for both elements being compared. Note that lacking an accepted reference standard for this type of work, errors represent only instrument precision, and not accuracy of the values.

As all solutions added into the final sample vials were weighed (sample, indium spike, standard (where appropriate), and 2% HNO_3), all data outputs were corrected for variable weight added, then normalized to In. Detection limits were subtracted from all data points. Final values in ppb were extracted from 3-point standard additions curves, or normalized to the nominal values in the reference standard for data calculated using the external standard curve.

Table 2.2: Isotopes used for final analysis. The isotope with the highest average R^2 values or with the fewest R^2 values < 0.95 in the standard additions curves was selected for use in final analysis.

Cu-treated		Zn-treated		Cd-treated	
Intracellular	frustule	Intracellular	frustule	Intracellular	frustule
Cu65	Cu65	Cu63	Cu65	Cu63	Cu63
Zn66	Zn66	Zn64	Zn66	Zn66	Zn66
				Cd111	Cd111

2.4 Results

2.4.1 Diatom growth

At the lowest Zn concentration, maximum diatom growth rate was $> 2\sigma$ lower than the average of the other Zn-treated samples. Otherwise, maximal growth rates were not significantly affected over the range of metal concentrations investigated (Appendix A). This growth limitation at the lowest Zn concentrations indicated that cells were indeed limited by Zn prior to inoculation, and that there was not significant Zn contamination during the culturing phase of experimentation. Though there was a 1-2 hour delay between sampling and pH measurement, which may have elevated pH, culture pH measurements were below 8.5 for all cultures except two (6.9E-8 M Cd_T on day 3, and 5E-5 M Cd_T on day 5; Appendix A). This kept relative speciation of free metals and silicic acid from varying by more than 4% of their values calculated at pH = 8.1 (Westall et al., 1976). Final cell densities in the Cu treatment were slightly higher than either the Zn or Cd treatments, but this may be attributed to evaporation during culture.

2.4.2 ICP-MS results

ICP-MS data reported here were measured on 4 separate days. Indium counts from these 4 days indicated good consistency between runs and stability within runs (Table 2.3). Detection limits were calculated on each individual day,

Table 2.3: ICP-MS consistency between runs. (LR) = low resolution, (MR) = medium resolution, cps = counts per second, RSD = relative standard deviation. Though In(LR) reads below 1E6 cps on 10/18/10, Cd was not included in the media for samples run on this day, so no elements were evaluated using low resolution.

Run date	In(LR) cps	RSD	In(MR) cps	RSD	samples run
10/18/10	9.8E+5	2.37%	5.4E+4	2.67%	Intracellular and frustule Cu treatment, cultures 2,4,6,8
01/12/12	3.3E+7	3.56%	2.1E+4	3.46%	Cu treatment, intracellular 1,3,5,7; frustule 1
01/24/12	2.5E+7	5.20%	1.8E+4	7.30%	Cu treatment frustule 3,5,7;
01/25/12	.0E+7	5.14%	2.1E+4	5.50%	Zn treatment frustule 8, all Cd-treatment

and subtracted from the data before standard additions analysis. Detection limits on each individual day were fairly consistent, with a maximum relative standard deviation of the detection limits across the 4 days of 64% for P, and a minimum of 27% for Cu65. Only one sample had an element below detection limits (P for 3E-6 M Cu_T added in the Cu-treatment), and so P data for this sample were excluded from the results.

Data calculated via external standard curve, standard additions, the R^2 values associated with each standard addition calculation, associated 1σ errors, and the combined data set used for final analysis are reported in Appendix B. As all reported data represent a ratio between measurements of 2 elements, a standard additions $R^2 < 0.95$ for one element compromises the data point. Therefore, where one element had an $R^2 < 0.95$, the values calculated from the external standard curve for both elements being compared were used; i.e no ratio represents a mixing of data calculated via standard additions and external standard curve.

Three frustule samples were excluded from analysis: 3E-6 Cu_T added was obviously contaminated (Cu values were 2 orders of magnitude higher than any other data point for a comparable amount of frustule dissolved), as was the standard-free sample in the standard additions curve for 5E-6M Zn_T with respect to copper. 1E-6 M Cd_T was spilled prior to analysis, with insufficient sample remaining for analysis.

Table 2.4: R^2 and p-values for linear fits to element data in the intracellular and frustule fraction relative to Si on a log-log plot (Appendix C). Bold numbers indicate instances where Me:Si yielded more robust statistics for the variable metal than Me:P. The split significance between Cu:P and Cu:Si of the p-value and R^2 values for the organic Cu treatment is accounted for by the fact that only 4 data points were available in the Cu:Si treatment.

			Intracellular			
	Cu-treated		Zn-treated		Cd-treated	
	p-value	R^2	p-value	R^2	p-value	R^2
Cu	0.0014	**0.9959**	0.4358	-0.0452	0.3893	-0.0201
Zn	0.6902	-0.3560	0.0037	0.7425	0.7756	-0.1287
Cd					0.0001	0.8743
			Opal			
	Cu-treated		Zn-treated		Cd-treated	
	p-value	R^2	p-value	R^2	p-value	R^2
Cu	0.0400	0.5238	0.6374	-0.1207	0.8874	-0.1624
Zn	0.0514	0.4780	**0.0459**	**0.4311**	0.9672	-0.1663
Cd					0.0096	0.6504

2.4.3 Consistency between the three different experiments

Average maximal growth rates between the three experimental treatments were comparable (Appendix A), indicating consistency in the growth conditions for the three experiments. Comparing elemental ratios at comparable $[Cu^{2+}]$ and $[Zn^{2+}]$ in the three experiments showed good agreement. For instance, Cd did not appear to affect Cu or Zn either intracellularly or in the frustule. Taking the standard deviation of elemental ratios in these samples, I found that the lowest two Cu treatments (50% and 150% as much Cu added as in the Cd treatments), as well as the 3rd data point in the Zn treatment (86% as much Zn as in Cd, but limited for Zn) fell within 2 standard deviations of the Cd mean for Cu:P and Zn:P. All Cd samples had stated Aquil concentrations for $[Zn^{2+}]$ and $[Cu^{2+}]$ (Price et al., 1988).

Table 2.5: R^2 and p-values for linear fits to element data in the intracellular and frustule fraction relative to both P on a log-log plot (Appendix D). Bold numbers indicate instances where Me:P yielded more robust statistics for the variable metal than Me:Si. Me:P ratios yielded higher R^2 and lower p-values than Si for all data sets except the frustule fraction of the variable Zn treatment. The split significance between Cu:P and Cu:Si of the p-value and R^2 values for the organic Cu treatment is accounted for by the fact that only 4 data points were available in the Cu:Si treatment

			Intracellular			
	Cu-treated		Zn-treated		Cd-treated	
	p-value	R^2	p-value	R^2	p-value	R^2
Cu	**0.0002**	0.9000	0.2202	0.1109	0.6236	-0.1014
Zn	0.2174	0.1138	**0.0013**	**0.8166**	0.8105	-0.1328
Cd					**1.6E − 9**	**0.9950**
			Opal			
	Cu-treated		Zn-treated		Cd-treated	
	p-value	R^2	p-value	R^2	p-value	R^2
Cu	**0.0098**	**0.8035**	0.8784	-0.1617	0.5932	-0.1079
Zn	**0.0155**	**0.7549**	0.0675	0.3614	0.7548	-0.1462
Cd					**0.0049**	**0.7179**

Table 2.6: Me:Si Spearman correlation coefficients and p-values.

		Cu-treatment		Zn-treatment	Cd-treatment
	Cu_{cell} v. $Cu_{Frustule}$	Cu_{cell} v. $Zn_{Frustule}$	Zn_{cell} v. $Zn_{Frustule}$	Zn_{cell} v. $Zn_{Frustule}$	Cd_{cell} v. $Cd_{Frustule}$
Rho (ρ)	0.8000	1.0000	0.0000	0.8571	0.7143
P-value	0.333	0.083	1.000	0.011	0.058

Table 2.7: Me:P Spearman correlation coefficients and p-values.

		Cu-treatment		Zn-treatment	Cd-treatment
	Cu_{cell} v. $Cu_{Frustule}$	Cu_{cell} v. $Zn_{Frustule}$	Zn_{cell} v. $Zn_{Frustule}$	Zn_{cell} v. $Zn_{Frustule}$	Cd_{cell} v. $Cd_{Frustule}$
Rho (ρ)	1.0000	0.8857	0.6667	0.6429	0.9524
P-value	0.003	0.033	0.083	0.096	0.001

Table 2.8: Whole cell % element allocated to the frustule. This table lists the percentage of whole-cell Cu, Zn, Cd, and P that was allocated to the frustule for each of the 3 metal treatments. Percentages listed here for Zn are generally lower than found in Jaccard et al. (2009b), and that study found higher % incorporation of Zn at higher [Zn^{2+}] whereas these data show the highest % incorporation at low [Zn^{2+}].

Variable metal	Free metal (M)	% P in frustule	% Cu in frustule	% Zn in frustule	% Cd in frustule
Cu	8.0E-15	0.08%	1.48%	5.01%	
	8.0E-14	0.10%	0.68%	11.73%	
	8.0E-13	0.02%	0.16%	2.15%	
	8.0E-12	0.03%	0.13%	12.28%	
	2.4E-14	0.09%	0.27%	3.76%	
	2.4E-13	0.02%		5.66%	
	2.4E-12		0.06%	2.57%	
	4.0E-11	0.004%	0.12%	3.79%	
Zn	2.4E-13	0.01%	0.09%	2.65%	
	2.1E-12	0.02%	0.11%	1.29%	
	1.9E-11	0.01%	0.00%	0.13%	
	1.7E-10	0.04%	0.36%	0.61%	
	5.3E-10	0.02%	0.17%	0.42%	
	1.6E-9	0.01%	0.36%	0.56%	
	4.8E-9	0.02%	0.03%	0.83%	
	1.4E-8	0.01%	0.58%	0.63%	
Cd	1.5E-14	0.17%	0.62%	1.73%	7.12%
	1.4E-13	0.08%	0.34%	0.62%	3.92%
	1.2E-12	0.14%	0.26%	0.55%	0.82%
	1.1E-11	0.14%			
	3.3E-11	0.14%	0.41%	0.64%	0.07%
	9.8E-11	0.23%	0.50%	0.76%	0.12%
	8.9E-10	0.07%	0.22%	0.40%	0.10%
	7.9E-9	0.15%	0.54%	0.94%	0.31%

Table 2.9: Relative frustule incorporation efficiency (E) relative to Zn. Calculated using equation (2.2). Note that in no instance does E for Cu exceed a value of 1, indicating that in no instance is Cu more efficiently incorporated into the frustule than Zn. By contrast, Cd exhibits highly variable incorporation efficiency, with a trend towards lower efficiency at higher $[Cd^{2+}]$.

Variable metal	Free metal (M)	Cu63	Cu65	Cd111
Cu	8.0E-15	0.33	0.34	
	8.0E-14	0.12	0.18	
	8.0E-13	0.06	0.11	
	8.0E-12	0.02	0.03	
	2.41E-14	0.07	0.11	
	2.41E-13			
	2.41E-12	0.00	0.01	
	4.01E-11	0.02	0.03	
Zn	2.4E-13	0.01	0.03	
	2.1E-12	0.09	0.14	
	1.9E-11	0.00	0.26	
	1.7E-10	0.27	0.30	
	5.3E-10	0.13	0.19	
	1.6E-09			
	4.8E-09	0.01	0.08	
	1.4E-08	0.24	0.18	
Cd	1.5E-14	0.46	0.46	4.16
	1.4E-13	0.24	0.17	2.87
	1.2E-12	0.37	0.42	1.18
	1.1E-11	0.15	0.14	0.04
	3.3E-11	0.40	0.31	0.07
	9.8E-11	0.87	0.41	0.20
	3.0E-10			
	8.9E-10	0.35	0.20	0.16
	7.9E-09	0.50	0.37	0.01

Table 2.10: Relative frustule incorporation efficiency (E) relative to P. Note that with only rare exceptions highlighted in bold, metals are incorporated into the frustule with a higher efficiency than P. Note that despite this, there is only one observed instance in which any metal is more abundant than P in the frustule; for Zn in at the highest Cu-addition (Appendix B).

Variable metal	Free metal (M)	Cu63	Cu65	Zn64	Zn66	Cd111
Cu	8.0E-15	11.52	11.92	29.27	35.12	
	8.0E-14	4.80	7.05	66.01	39.92	
	8.0E-13	5.34	8.55	74.56	104.13	
	8.0E-12	2.73	3.99	129.27	132.21	
	2.41E-14	3.14	4.71	42.08	42.71	
	2.41E-13					
	2.41E-12					
	4.01E-11	32.89	35.89	555.48	470.18	
Zn	2.4E-13	3.76	8.78	453.29	559.60	
	2.1E-12	2.74	4.23	36.58	29.55	
	1.9E-11	**0.14**	9.73	18.79	26.40	
	1.7E-10	3.47	3.93	12.36	13.03	
	5.3E-10	3.39	4.68	18.28	25.08	
	1.6E-09			38.45	35.58	
	4.8E-09	**0.47**	3.17	28.42	40.44	
	1.4E-08	44.54	39.34	77.52	103.64	
Cd	1.5E-14	11.06	5.08	26.68	26.36	90.19
	1.4E-13	3.31	2.41	10.32	13.82	39.69
	1.2E-12	1.96	2.22	6.17	5.25	6.19
	1.1E-11	17.43	16.46	86.21	117.15	5.11
	3.3E-11	8.34	4.62	29.60	20.74	1.26
	9.8E-11	11.48	5.44	62.63	13.17	2.65
	3.0E-10					
	8.9E-10	10.64	3.77	32.60	25.55	**0.66**
	7.9E-09	12.22	8.92	29.09	24.34	**0.35**

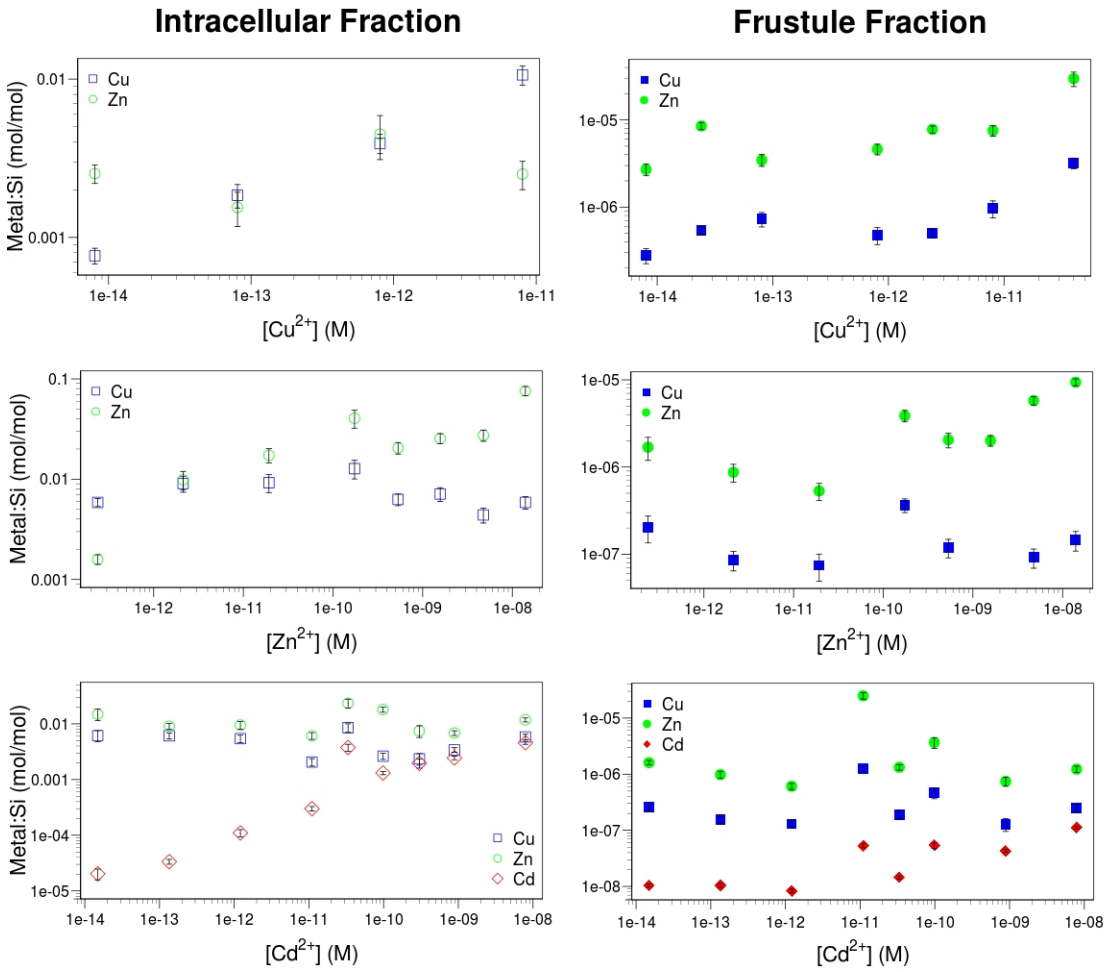

Figure 2.3: Ambient metal concentrations in the variable Cu (top), Zn (middle), and Cd (bottom) treatments vs Me:Si ratios for the intracellular (left column, open symbols) and frustule (right column, solid symbols) fractions on a log-log plot. Single element plots with better scaling along with the linear fits can be seen in Appendix C. Intracellular Cu treatment has only 4 data points because no Si values were taken for 4 data points of the 10/18/10 ICP-MS run (Table 2.3). Note that while Cu exceeds Zn in the intracellular fraction, in no instance is this the case in the frustule fraction. In the Zn-treatment, the points at the lowest $[Zn^{2+}]$ of the frustule fraction deviate from the pattern observed in the organic fraction, and from previous studies. In the Cd treatment, both Cu/Zn and Cd/Zn decrease from the organic to the frustule fraction.

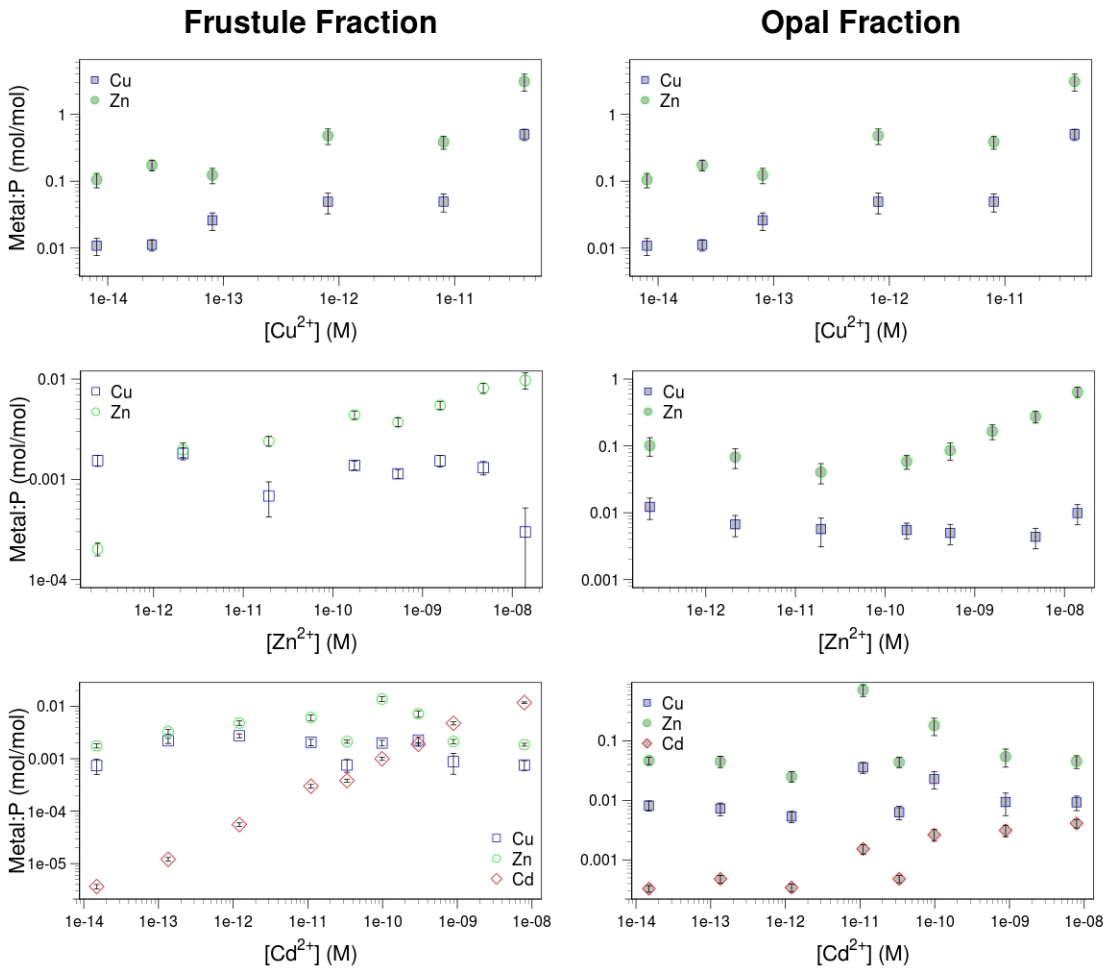

Figure 2.4: Ambient metal concentrations in the variable Cu (top), Zn (middle) and Cd (bottom) treatments vs the Me:P ratios for the intracellular (left column, open symbols) and frustule (right column, shaded symbols) fractions on log-log plots. Single element plots along with the linear fits are in Appendix D. Note the more linear nature of the curve for Zn:P$_{Frustule(Zn)}$ relative to Zn:Si$_{Frustule(Zn)}$ in Figure 2.3. Also note that the higher Cd:Zn and Cd:Cu in the cell(Cd) treatment relative to Figure 2.3 is an artifact of using data calculated with the external standard curve for these points, since $R^2 > 0.95$ for standard additions of P (Appendices C, D).

2.4.4 Metal:Si vs Metal:P results, intracellular and frustule fractions

I use the subscripts 'Cell(Me)' to denote the intracellular, nitric acid-labile fraction, and 'Frustule(Me)' to denote the elemental ratio in the HF-soluble frustule fraction, where 'Me' may be Cu, Zn, or Cd depending on which of the 3 experiments the sample is included in: variable Zn, variable Cu, or variable Cd. For example, the Zn:P ratio of the intracellular fraction in the Cu treatment is denoted 'Zn:$P_{Cell(Cu)}$'.

Data for Cu, Zn, and Cd were compared to both Si and P, and plotted against increasing free metal availability on a log-log plot (Figures 2.3 and 2.4). All data points in these two figures were included in the linear fits whose R^2 and p-values are reported in Tables 2.4 and 2.5. Of the metals considered here, previous studies had reported only Zn:$P_{Cell(Zn)}$ and Zn:$Si_{Frustule(Zn)}$

Though a linear fit is not optimal for some of these data sets, it does offer a common baseline prediction enabling basic statistical evaluation of the prediction. Fitting a linear curve yielded relatively high R^2 values and p-values < 0.01 for all intracellular fraction measurements of both the variable Me:Si and Me:P ratios (Tables 2.4 and 2.5). In the frustule fraction, $p < 0.05$ for all Me:P ratios except Zn, though $p < 0.05$ when compared to Si. Intriguingly, Zn:$P_{Frustule(Cu)}$ shows a statistically significant ($p < 0.05$) positive trend in the linear fit despite no such correlation between variable [Cu^{2+}] and intracellular Zn.

2.4.5 Comparing intracellular and frustule-bound metal concentrations

I used Spearman correlation to assess the dependency of frustule Me:P concentrations upon intracellular Me:P (Tables 2.6 and 2.7). In the variable Cu treatment, intracellular Cu displays statistically significant correlation with both Cu and Zn, but only considering the ratio to P, not Si. Similarly, the correlation between intracellular and frustule Zn is only significant when compared to Si, and for Cd it is only significant compared to P.

The % of each metal included in the organic vs the frustule fraction is reported in Table 2.8. In most cases, metals are 100-1000 times more abundant in the organic matter than the frustule. The highest metal incorporation into the frustule occurred at the lowest [Cu^{2+}], [Zn^{2+}], and [Cd^{2+}]. Our values for % cellular Zn in the frustule are low relative to values reported by Jaccard et al., 2009b, who reported 1-27% of the cell's Zn reserve was frustule-associated. Furthermore, Jaccard et al., 2009b found higher Zn incorporation at higher [Zn^{2+}] instead of lower [Zn^{2+}]. The highest observed metal incorporation occurs in the Cu-treatment for Zn, where as much as ∼12% of the cellular Zn was associated with the frustule.

2.4.6 Comparing relative incorporation rates

Relative frustule incorporation efficiency was calculated as:

$$(2.2)\ \mathrm{E} = (\mathrm{A/B})_{Frustule}/(\mathrm{A/B})_{cell}$$

where A and B are any two elements measured. In this formulation, $E > 1$ signifies a more efficient incorporation of A into the frustule from the intracellular fraction relative to B, whereas $E < 1$ signifies B is more efficiently incorporated than A. Relative frustule incorporation efficiency was assessed relative to P and to Zn, and the results are in Tables 2.9 and 2.10.

Comparing these values between treatments, I found that in no case was Cu more efficiently incorporated than Zn, and its incorporation efficiency relative to Zn, but not to P, decreases as [Cu^{2+}] increased. Cd exceeds Zn incorporation efficiency at low [Cd^{2+}], but this decreased substantially at high [Cd^{2+}]. All elements appeared to be incorporated into the frustule more efficiently than P, though P remained more abundant in the frustule except relative to Zn at the highest [Cu^{2+}] tested (Table 2.8; Appendix B). Similarly, though Cd was incorporated more efficiently than Zn at low [Cd^{2+}], it is still roughly 2 orders of magnitude less abundant in the frustule (Figures 2.3 and 2.4).

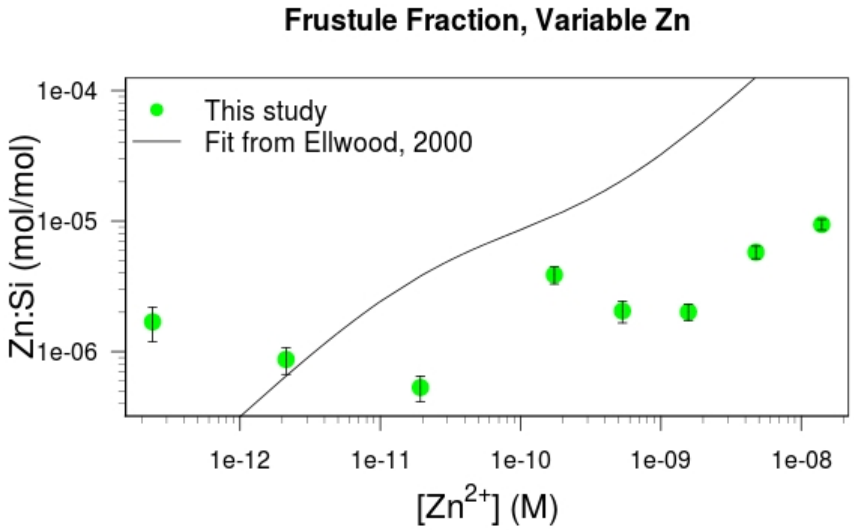

Figure 2.5: Comparing data between studies. The line plotted is from equation 1 of Ellwood and Hunter (2000a). Our data at the lowest $[Zn^{2+}]$ do not fit the trend of previous work, nor do they agree with the intracellular fraction for the same samples. I attribute this difference to lower carbonic anhydrase requirements due to better pH control, and a role for Zn in frustule formation that is prioritized below carbon acquisition. The remaining points all fall below the fit, indicating either less Zn incorporation or higher silicification. I attribute this difference to different culturing conditions, including 2.5x more available Si and 4x more Mn in this study, as well as better pH control.

2.5 Discussion

2.5.1 Comparisons with previous works

Due to the difficulty of both culturing and analyzing diatoms under trace-metal clean conditions, few studies are available for comparison, especially with regard to the frustule fraction. Differences in culturing conditions further limit the utility of direct comparisons, yet comparing the general trends is nonetheless informative.

2.5.2 Zinc

Our data display a curve in Zn:$Si_{Frustule(Zn)}$ similar to that reported by Ellwood and Hunter (2000a) and Jaccard et al. (2009b) and in Zn:$P_{Cell(Zn)}$ reported by Sunda and Huntsman (1992) and Ellwood and Hunter (2000a). Plotting the data side-by side, however, frustule data from this study display a lower Zn:$Si_{Frustule(Zn)}$ than reported by previous studies except the lowest two [Zn^{2+}] (Figure 2.5). Furthermore, the trend of the two data points at the lowest [Zn^{2+}] in the Zn:$Si_{Frustule(Zn)}$ are high relative to both data reported in previous studies, and relative to what would have been predicted based on the Zn:$Si_{Cell(Zn)}$ for the same samples. While this immediately raises suspicions of contamination for these points, I can find no other basis for removing these data points.

The generally lower ratio observed in this data set is likely attributable to the different conditions of the growth media. Since Ellwood and Hunter (2000a) used the same species of diatom, this offers the more direct comparison. The most obvious differences in growth conditions that could have altered Zn:$Si_{Frustule(Zn)}$ ratios are [Mn], [$Si(OH)_4$] , and pH. Jaccard et al. (2009b) found that elevated Mn significantly decreases the Zn/Si ratio, and Ellwood and Hunter (2000a) used a [Mn_T] nearly 4 times lower than in Aquil media. Similarly, more [$Si(OH)_4$] was available to diatoms in this study (100 µM) than in Ellwood (40 µM), which might have allowed greater silicification of the diatom frustules, thus lowering Me:Si ratios. The lack of pH control in previous experiments may also have skewed results, especially since the higher pH I infer was present in their cultures at the

time of collection would cause up-regulation of carbonic anhydrase, an enzyme that uses Zn as a co-factor. Carbonic anhydrase can account for more than half of the intracellular Zn budget (Morel and Reinfelder, 1994), so failing to control for pH could seriously alter results with respect to Zn. This is discussed further in a subsequent section.

2.5.3 Cadmium

While there are no culture experiments that report Cd incorporation into diatom frustules, Hendry and Rickaby (2008) report looking for and largely failing to find Cd in diatom frustules derived from Southern Ocean sediments. This is consistent with our data, as I find Cd incorporation roughly 2 orders of magnitude lower than Zn incorporation at oceanic [Cd^{2+}]. Thus, the amount of sediment they used for analysis was likely too low to detect Cd.

2.5.4 Copper

Martin & Knauer (1973) report finding Cu in diatoms collected by net tow at a ratio of 5.3E-6 mol/mol to 8.5E-6 mol/mol (Boyle, 1977; Martin and Knauer, 1973). de Jonge et al. (2010) also report finding Cu evenly distributed throughout the frustule of a single fresh-water diatom cell grown in culture, but they do not report Cu:Si values. Monteiro and Orren (1985) report Cu elution from siliceous oozes in a ratio of 2.25E-16 g cm^{-2} s^{-1} for a silicate flux of 3 µmol cm^{-2} yr^{-1} as determined in Edmond et al., 1979. The Martin & Knauer (1973) values for Cu are high relative to my findings by approximately an order of magnitude, and they report instances of Cu exceeding Zn in the frustule. Though differences are to be expected between *in vitro* monocultures and *in situ* assemblages, in no instance do I observe Cu incorporation exceeding Zn incorporation into the frustule (Figures 2.3 and 2.4), and the order of magnitude difference might be attributed to issues related to the growth media as previously discussed. Similarly, the the Monteiro and Orren (1985) ratio is also higher than I report here, but this is to be expected as it would also include Cu scavenged as frustules settled through

the water column. They report a Cu/Si of 2.73E-4 (i.e. (1.1E-11 mol kg^{-1} yr^{-1} Cu)/(3E-7 mol kg^{-1} yr^{-1} Si)) from sediments. If we consider that the range of $Cu:Si_{Frustule}$ ratios observed here in *T. pseudonana* is between 7.4E-8 and 3.2E-6 (mol/mol) and assume this ratio is representative of the range for the sinking flux of diatom frustules preserved in Southern Ocean sediment, this would still indicate that diatom-incorporated Cu accounts for a mere 0.03% - 1.2% of Cu eluted from diatomaceous oozes, while the remaining fraction would be scavenged from the water column by sinking frustules (Balistrieri and Murray, 1984).

2.5.5 Metal:Si vs Metal:P

While previous studies report only Me:Si in the frustule, the use of ICP-MS techniques allowed the simultaneous determination of multiple elements. This enabled comparison of Me:P and metal to metal in addition to Me:Si (Appendices C, D, and E). Such comparisons yield similar trends in Me:P and Me:Si (Figures 2.3 and 2.4). The greater statistical significance of the $Zn:Si_{Frustule(Zn)}$ ratio compared to the $Zn:P_{Frustule(Zn)}$ ratio is unexpected given all other Me:P ratios have a better fit than the corresponding Me:Si ratio (Tables 2.4 and 2.5), and given that both Zn and P are measured on the same instrument at the same time for each sample, whereas subsampling for the Si assay introduces additional sources of error. However, this lower p-value may simply be an artifact of fitting a linear curve to what is clearly not a linear relationship. The $Zn:P_{Frustule(Zn)}$ trend is more linear, whereas Zn:Si more closely tracks the stepped function observed in previous works. This may indicate that Zn:P offers a different, more direct signal for ambient metal variability. The frustule fraction of both the Cu and Cd treatment also show differences between Me:P and Me:Si, though they appear less marked than differences observed in the Zn treatment. Regardless, contrasting multiple elemental ratios provides useful insights into the intracellular dynamics of metals.

2.5.6 Comparing incorporation into the frustule vs organic fraction

Increasing available Cu, Zn, and Cd clearly leads to greater intracellular and frustule-associated concentrations of the variable metal relative to P, Si, and other metals (Figures 2.3 and 2.4, Appendices C, D, E). Linear fits to these data show a statistically significant increasing trend in all intracellular fractions ($p < 0.01$) and frustule fractions ($p < 0.05$) (Tables 2.4 and 2.5).

As demonstrated by the high Spearman correlation coefficients in Tables 2.6 and 2.7 ($p < 0.05$), elemental ratios for Cu, Zn, and Cd in the frustule reflect the intracellular concentration. This had already been shown to be the case for Zn in a freshwater diatom (Jaccard et al., 2009b). This shows that though the process of frustule formation is tightly controlled and takes place within the membrane-bound silica deposition vesicle (SDV) (Drum and Pankratz, 1964; Pickett-Heaps et al., 1990), its permeability to metals is a function of intracellular concentrations, even for metals such as Cu and Cd without even a suspected role in frustule formation. While this might have been inferred from previous results showing that variable metal availability results in cellular deformities related to frustule formation (Fisher et al., 1981; Morin et al., 2008), these results show that it is not simply a function of interference in mechanisms responsible for frustule formation, but that these metals are incorporated into the frustule itself. It is unclear whether these metals are incorporated as co-factors in organomolecules involved in the patterning of the frustule, as suggested by Jaccard et al. (2009b), or whether these metals are complexed directly with the frustule. Silicon polymerization in frustule requires cations to neutralize the negative charge that accumulates in polymerizing silicon (Perry, 2003; Schröder et al., 2008) which would explain a direct complexation to frustule as opposed to incorporation as part of an organomolecule.

2.5.7 A role for metals in frustule formation?

Surprisingly, increasing Cu availability also increases Zn incorporation into the frustule, without increasing intracellular Zn. This occurs despite a concomi-

tant increase in the % of total Zn associated with the frustule fraction (Table 2.8), which may simply indicate weaker silicification. If so, it would co-occur with less phosphorus incorporated into the frustule, as both Zn and Cu increase relative to both Si and P. Previous studies have found links between Zn, Cu, and intracellular Si. Thamatrakoln & Hildebrand (2008) find no evidence that Zn is involved in Si uptake into the cell, but leave open the possibility that Zn may play a role in secondary effects on cellular metabolism affecting intracellular Si stores. Rueter & Morel (1981) find elevated Zn increases cellular Si stores, and that Cu interferes with this uptake. Fisher et al., (1981) similarly find that Cu limits Si uptake, and may prevent Si deposition as they observed Cu-treated cells had a similar morphology as Si-starved cells. Consistent with these findings, De La Rocha et al., (2000) find that increased cellular silicon may co-occur with a depressed capacity for silica production. Jaccard et al., (2009b) argue for active incorporation of Zn into diatom frustules as a co-factor in organomolecules involved in frustule deposition based on the tight relationship between Zn_{cell} and Zn_{frust}, the 'saturable' nature of the Zn deposition process, and the observed competition between Mn and Zn incorporation into the frustule. However, a specific frustule-associated organomolecule has not yet been identified and characterized, so for now this should remain just a concept. In light of evidence that carbonic anhydrase has been shown to use polymerized diatom silica as a buffer (Milligan and Morel, 2002), some of this carbonic anhydrase may be incorporated into the frustule. Finally, it may be that Zn usefully complexes directly with the SiO_2 of the opal matrix without needing to invoke an organomolecule.

If Zn is purposefully and usefully incorporated into the frustule, whether as an organomolecule or not, this may explain the divergent trend at low $[Zn^{2+}]$. If Zn is required for normal frustule formation, and if due to good pH control cells had low carbonic anhydrase requirements, this divergent trend at low $[Zn^{2+}]$ may represent prioritization of Zn in the frustule fraction over the organic fraction. By contrast, in previously reported results where pH may have been allowed to reach levels high enough to significantly reduce CO_2 availability, Zn for carbonic anhydrase may have been prioritized above Zn for frustule formation. Further

research is needed to clarify how and if diatoms prioritize Zn-allocation to carbonic anhydrase vs the frustule when limited for Zn.

2.5.8 Zn, Cu, and Cd as paleoproxies

Of primary importance to a paleoproxy is sufficient sensitivity to reliably detect variations in the variable of interest over its natural range through time. $Zn:Si_{Frustule}$ has been used as a paleoproxy with a variation of two orders of magnitude over the range of $[Zn^{2+}]$ found in modern seawater and in freshwater (Ellwood and Hunter, 2000b; Jaccard et al., 2009a; Hendry et al., 2008). My data do not show such wide variability, perhaps due to the effects of good pH control at the lowest $[Zn^{2+}]$, and perhaps due to contamination. However, since cells were limited for Zn in these experiments, and the *in situ* studies on Zn-limitation and co-limitation show complex dynamics without much evidence for widespread Zn-limitation (Sinoir et al., 2012 and references therein), the different $Zn:Si_{Frustule}$ trend observed in our low-Zn cultures may be a result of Zn-limitation that would not occur in the real ocean. If so, the trend observed in previous studies may still present a better guide for interpreting Zn in fossil diatom frustules.

However, the generally lower $Zn:Si_{Frustule(Zn)}$ observed here (Figure 2.5) as well as the increase in $Zn:Si_{Frustule(Cu)}$ with increasing Cu (Figures 2.3, 2.4) demonstrate that Zn is not incorporated into the frustule as a function of $[Zn^{2+}]$ alone. This is clearly far from ideal, as multiple Cu, Zn, Si, Mn, and pH configurations may yield the same $Zn:Si_{Frustule}$. Other untested variables may also be capable of affecting Zn incorporation into the frustule. The more linear Zn:P ratio suggests that this measure may be more robust in any case, and could conceivably mitigate effects from variable $[Si(OH)_4]$. Furthermore, $Cu:Zn_{Frustule}$ is roughly flat for variable Cu (Appendix E), indicating that comparing multiple elemental ratios may offer a means of correcting for the effects of variable ambient Cu:Zn on frustule incorporation. In any case, it is clear that the underlying physiology driving Zn incorporation into diatoms frustules is complicated, and as yet too poorly understood to warrant bold conclusions of past Zn availability in surface waters of the past based on ratios found in sedimentary diatoms. The proxy still holds promise,

but much more research is needed to confidently apply it.

Our data indicate that the Cu:Si and Cd:Si vary by just over 1 order of magnitude over the range of concentrations tested. While much of the variability in Zn:Si occurs over oceanic Zn concentrations, and all the Cu variation occurs across a range found in natural seawater, the largest variations observed for Cd do not occur across free Cd concentrations observed in the ocean. The low Cd:Si and correspondingly higher levels of sediment required will increase the noise from contaminants in any subsequent studies seeking to exploit this incorporation, making the signal harder to resolve.

Cu variations do show potential for use in paleoceanographic applications, though significant obstacles still remain. The variability of the proxy is not as great as for Zn, and like $\mathrm{Zn{:}Si}_{Frustule(Zn)}$ there appears to be a plateau where multiple $[Cu^{2+}]$ may yield the same Cu:Si. The same may be true for Cu:P, though it is less clear. Furthermore, as shown here and in previous studies, Zn and Cu availability and co-variation significantly affects frustule formation, and cellular Si management. Given this co-variation, it is likely that reliable information may only be extracted by mapping both Cu and Zn in the frustule.

More useful information may be obtained from observing variations in Cu isotopic ratios. Work by John et al. (2007) show that Zn isotopic ratios in diatoms contain information about the growth conditions, and can be measured. Cu isotopic ratios may contain similar information, but with Cu incorporated at roughly a tenth the level of Zn on average, comparable analytical challenges are to be expected. Yet, the advent of techniques for multi-element detection in single diatom cells via quantitative 3D elemental tomography (de Jonge et al., 2010) or SXRF (Twining et al., 2004) combined with the micron scale discrimination for sediment sorting enabled by SPLITT techniques (Fuh, 2000; Rings et al., 2004; Moon et al., 2005) provide qualified hope that variable elemental ratios in diatom frustules can be used to tease apart metal and nutrient dynamics through the geologic record. A larger, and still unanswered, question is whether data for *T. pseudonana* are representative of the full range of diatoms diversity preserved in sedimentary archives.

2.5.9 Insights for Cu and particle scavenging

The profile of Cu in seawater has been explained by invoking aeolian and riverine inputs at the surface, nutrient-type draw down from surface waters by primary producers, bacterially mediated remineralization and scavenging of dissolved Cu species by particles at mid-depths and in deep-waters, and a bottom source derived from opal-rich sediments (Boyle, 1977; Bruland, 1980; Monteiro and Orren, 1985). As discussed previously, comparing our data with calculations presented in Monteiro and Orren (1985), my data suggest a mere 0.03% - 1.2% of Cu eluted from bottom water sediments is attributable to Cu incorporated into the frustule by living diatoms, whereas the rest is scavenged. The literature does not report a similar bottom source for Zn, nor is there evidence of a bottom enrichment from oceanographic profiles. Even though Zn is roughly 10 times more abundant in the frustule than Cu, the apparent scavenging signal could erase this advantage if Cu is more efficiently scavenged than Zn. Previous work suggests this is the case. A study by Balistrieri and Murray (1984) indicates that Cu is more efficiently scavenged onto deep ocean sediment (mostly organic) than Zn at ocean pH. Löscher (1999) similarly explain observations of a stronger Cu/Si than Zn/Si correlation in Southern Ocean profiles by more efficient Cu-scavenging than Zn-scavenging. Work by Koning et al. (2007) found that Al rapidly complexed with naked diatom biosilica on a timescale of less than 20 days at an Al:Si of order 1E-4. While they investigated only Al, Cu-silicates might be expected to form as well, or Cu-aluminosilicates. This type of complexation has been found to be limited to the exposed surface of diatom biosilica, and may be etched away by partial dissolution (Hendry et al., 2008). Though no study has compared trace metal sorption efficiencies onto diatom biosilica, the lack of a comparable Zn-bottom source despite its greater biological incorporation into the frustule suggests that Cu is more efficiently scavenged.

2.5.10 Insights for Zn and Si co-variation

The co-variation of Zn and Si in oceanic profiles (Bruland, 1980) and the previously noted ability of diatoms to incorporate Zn into their frustules invites

the conclusion that *in vivo* incorporation drives this co-variation. However, the percentage of total cellular Zn allocated to the frustule observed in this and previous studies is too low to account for this co-variation (Martin and Knauer, 1973; Ellwood and Hunter, 2000a; Jaccard et al., 2009b; de Jonge et al., 2010). Scavenging of some sort must therefore also play a role. Scavenging must also account for the lack of a comparable Cu-max at mid depths, but a larger Cu-bottom source than Zn. Work by Balistrieri (1984) indicates that though Cu is more efficiently scavenged than Zn at surface ocean pH, this ordering flips as pH decreases. World Ocean Circulation Experiment (WOCE) data indicate that oceanic pH at the oxygen minimum may be as low as 7.8 in the Atlantic, and 7.6 in the Pacific, which may be sufficiently depressed to render Zn more efficiently scavenged than Cu (Balistrieri and Murray, 1984; Garcia et al., 2009). As discussed previously, in addition to simple and reversible sorption, metals may also complex irreversibly with naked biosilica to form new minerals that must be etched away. The balance between sorption and complexation must explain the co-variation of Zn and Si at mid-depths, while also explaining a Cu bottom source over diatomaceous oozes without a comparable Zn-bottom source. While modeling the relative sorption and complexation efficiencies for Cu and Zn necessary to account for observed oceanographic trends is beyond the scope of this work, data presented here establish useful boundary conditions on partitioning of Cu and Zn between intracellular and frustule pools within diatom cells, and estimates of the necessary magnitude for scavenging. That Cu may also increase Zn incorporation into the frustule is another consideration that may influence the cycling of these elements in the ocean that would not have been apparent based on culture experiments considering Zn alone.

2.5.11 Insights for Cd and P co-variation

Cd has a tight correlation with P in the ocean (Bruland, 1980; Elderfield and Rickaby, 2000). Though Cd is more efficiently incorporated into the frustule than Zn at concentrations found in the ocean, it is incorporated into the frustule at levels orders of magnitude lower than either Zn or Cu (Figures 2.3 and 2.4). It

is also poorly scavenged by sinking particles (Balistrieri and Murray, 1984). P is inefficiently incorporated into the frustule relative to all metals considered here, with the overwhelming majority in the organic fraction (Table 2.8). This suggests that the overwhelming majority of both Cd and P would remineralize with other organic matter at relatively shallow depths, and not with diatom frustules. The data also show that Cd is more efficiently incorporated into the frustule than P, and thus provides a mechanism for its preferential removal as required by (Elderfield and Rickaby, 2000). However, this explanation is not entirely satisfactory in explaining the tight correlation between the two elements in the ocean, nor in explaining the preferential removal of Cd relative to P towards low latitudes since diatom frustules would not be a significant part of the sinking flux over much of that distance.

Evidence from Walsh & Hunter (1992) show that Cd is concentrated within polyphosphate bodies in the cell, while Diaz et al. (2008) recently noted that diatom-derived polyphosphate efficiently nucleates apatite formation in sediments. Fine-grained, dispersed apatite may account for as much as 80% of P burial in the ocean (Benitez-Nelson, 2000), and consistent with the hypothesis that phytoplankton-derived polyphosphate is the source for these deposits, Cd is commonly the most enriched trace element in phosphorite deposits relative to average shale, though subsequent re-working appears to be prevalent (Nathan et al., 1997). Data summarized and reported in chapter 3 of this thesis indicate that polyphosphate bodies may account for between 5-79% of the extractable phosphorus in phytoplankton cells. The observed close association between Cd and an organelle accounting for a sizable fraction of the cellular P budget suggests that these elements would remineralize at the same time. Consistent with the explanation for Cd:P fractionation in Elderfield and Rickaby (2000), there is evidence that polyphosphate is somewhat refractory in the ocean (Faul and Paytan, 2005; Young and Ingall, 2010; Goldhammer et al., 2010). If the majority of cellular Cd is associated with polyphosphate bodies in the cells of phytoplankton sinking out of the photic zone, and a fraction of those Cd-enriched polyphosphate bodies are delivered to sediments, this provides a second mechanism for the gradual removal

of Cd towards lower latitudes required to fit the observed fractionation factor, and it does not rely entirely on diatoms, as polyphosphate bodies are common to all living things (Brown and Kornberg, 2004).

2.6 Conclusions

In this study I employ a novel technique for the trace metal clean culture of diatoms that is sufficiently clean to limit diatoms for Zn. Simple and cost-effective, this technique also enables clean sampling of the culture throughout growth. Daily sampling of the diatom *T. pseudonana* grown with variable Zn, Cu, and Cd show that this technique was effective at keeping pH < 8.5 by bubbling ambient air into cultures. Maintaining this degree of pH control should keep free metal and orthosilicic acid concentrations from varying by more than 4%, and would also prevent depletion of culture CO_2 during growth. These are all important considerations for any trace metal clean diatom culture, but especially when Zn is the metal of interest, since at low pCO_2 it would be heavily recruited for carbonic anhydrase.

Results from the variable Zn experiment differ from previous works, even works considering the same diatom species, as the $Zn:Si_{Frustule}$ for most data points is substantially lower. Additionally, I find that increasing media $[Cu^{2+}]$ is positively and significantly correlated with elevated $Zn:Si_{Frustule}$. Previous work has also identified [Mn] as a factor determining $Zn:Si_{Frustule}$ (Jaccard et al., 2009b), and the higher $[Si(OH)_4]$ employed here relative to previous studies may also have affected the ratio. While my data do not resolve the relative importance of $[Cu^{2+}]$, $[Zn^{2+}]$, pH, $[Si(OH)_4]$, or [Mn] in determining $Zn:Si_{Frustule}$, it is clear that this ratio is not a function of $[Zn^{2+}]$ alone. In light of this, more work must be done to understand the dynamics of metal incorporation into diatom frustules before $Zn:Si_{Frustule}$ can be robustly applied as a paleoproxy.

Experimental results also provide the first *in vitro* evidence that both Cu and Cd are variably incorporated into the diatom frustule as a function of ambient free metal availability. Utilizing an ICP-MS enabled simultaneous determination of

multiple elements, and reveal that in no instance does Cu exceed Zn in the frustule, Cu and P are less efficiently incorporated into the frustule from the intracellular fraction than Zn, and Me:$P_{Frustule}$ is a useful metric of metal incorporation that complements Me:$Si_{Frustule}$.

While I conclude that Zn:$Si_{Frustule}$ remains a useful paleoproxy, I find minimal variability in Cd:P at ocean [Cd^{2+}] and significantly lower incorporation relative to both Cu and Zn. Cd is therefore unlikely to be useful as a paleoproxy due to both low variability and a probable high signal-to-noise ratio. By contrast, Cu:$P_{Frustule}$ and Cu:$Si_{Frustule}$ may prove useful, but significant obstacles still remain including lower variability than Zn, $\sim$1/10 the concentration of Zn, and the potential for multiple [Cu^{2+}] yielding the same Cu:Si. Determination of Cu isotopes in the frustule is plausible, and may prove more useful overall.

Considering how these findings might enhance our understanding of metal cycling in the modern ocean, I find that they provide useful boundary conditions for modeling the relative importance of biologic incorporation of metals into diatom frustules vs scavenging as they sink through the water column. This is especially true for Cu and Zn, whose mid- and bottom-depth profiles relative to Si cannot be explained by biologic incorporation alone, and I invoke variable and pH-dependent sorption onto sinking organic matter and direct, saturable complexation with diatom biosilica to outline the expected parameters. While preferential Cd incorporation into the frustule relative to P is consistent with the direction of fractionation required to explain global surface Cd:P ratios, I identify Cd incorporation into and sequestration with polyphosphate bodies as a more satisfactory explanation that does not rely on diatom productivity alone.

Chapter 3

Polyphosphate variability in 4 diatom species with the growth cycle and variable [Cu^{2+}]

3.1 Abstract

Ubiquitous in living cells, polyphosphate bodies (PPBs) are known to have varied cellular functions, yet they remain profoundly understudied. In this chapter I report variations in cellular allocation of phosphorus to polyphosphate (poly P) due to the growth cycle and variable copper availability in four diatom species grown in batch culture. I found substantial variability in the percentage of extractable P allocated to poly P (*e*-poly P) as a function of both the growth cycle and variable [Cu^{2+}], though the nature of this variability is not consistent between the 4 species tested. The range of poly P values I report is higher than any previous reports. This may be partly explained by the extraction procedure employed, which would include the poly P stored as PPB granules that some other analytical methods miss, and which may exclude some cellular constituents with P but little poly P. The presence of granular PPBs was visually confirmed in 3 of the 4 species investigated using DAPI fluorescence. I conclude that the variations observed here warrant further study on the cycling of poly P in the marine

environment, particularly its variability with the growth cycle.

3.2 Introduction

Interest in the molecule polyphosphate (poly P) in the marine environment has increased as a result of recent evidence (Diaz et al., 2008) indicating that phytoplankton-derived poly P is a precursor to authigenic apatite minerals in sediments. Though early studies indicated the majority of reactive P burial occurs in coastal upwelling regions during distinct time intervals, the discovery of dispersed, fine-grained authigenic apatite deposits in coastal, non-upwelling regions and deep-sea sediment cores (Ruttenberg and Berner, 1993; Filippelli and Delaney, 1994, 1996; Reimers and Ruttenberg, 1996; Slomp and Epping, 1996) amounts to a newly discovered sink that may account for as much as 80% of reactive P burial worldwide (Benitez-Nelson, 2000; Faul and Paytan, 2005; Paytan and McLaughlin, 2007). Moreover, Diaz et al. (2008) identified the flux of phytoplankton-derived poly P from surface water phytoplankton, including diatoms, as sufficiently large to be the sole source of poly P to underlying sediments.

Cells contain at least 3 chemically distinct pools of poly P: acid-soluble short-chain poly P, long-chain poly P soluble at neutral pH, and long-chain poly P in granular polyphosphate bodies (PPBs) (Clark et al., 1986). While the abundance of Ca^{2+} ions in seawater render any of these fractions likely apatite nucleation sites (the major components of apatite are Ca and PO_4), the co-location of PPBs with calcium in an organelle known as the acidocalcisome (Docampo et al., 2005; Seufferheld et al., 2008) suggests PPBs may be the pool of poly P most likely to nucleate apatite formation.

Poly P is ubiquitous in all cells, and has been shown to have diverse functionality. Such ubiquity and versatility has resulted in a diverse and poorly focused literature, often with more attention paid to determining the functionality of poly P than to constraining its variable concentration within the cell (see Seufferheld & Curzi (2010) for a review of functions of poly P). For example, few studies even mention that there are multiple types of poly P in the cell, and that these

different poly P stores may have different properties in the cell and in the environment. Furthermore, little of this literature has focused on marine phytoplankton. As a further illustration of challenges resulting from this lack of focus, Eixler et al. (2005) summarizes 3 general approaches that have been used to investigate PPBs: 1) preparation/staining of cells followed by light or electron microscopy, which is not quantitative, 2) extraction of granules followed by chemical analysis and comparison of orthophosphate equivalents, and 3) ^{31}P-NMR analysis *in vivo* or after extraction, which the authors state cannot detect PPBs. In the remainder of the paper, Eixler et al. (2005) test various extraction techniques (i.e. addressing the second general approach described above) in an effort to standardize methods for extraction and resolve uncertainties as to their comparative efficacy, especially with regards to PPBs. Eixler et al. (2005) settles on a procedure that yields consistent results in a practical, quick, and cost-effective method for the regular determination of cellular poly P that includes poly P stored as PPB granules. However, the authors' statement that ^{31}P-NMR can not detect PPB granules is not entirely accurate. Though it is true that the more common solution-based NMR cannot detect tightly bound species (such as PPBs), solid state ^{31}P-NMR techniques exist that can quantify poly P in PPBs (Cholli et al., 1985; Orchard et al., 2010; Faul and Paytan, 2005; Diaz et al., 2008). It thus appears that Eixler et al. (2005) may not have been aware of solid state ^{31}P-NMR. Nonetheless, while offering less resolution than solid-state ^{31}P-NMR on the types of polyphosphate species present, the error is comparable, and this method is lower-cost, quicker, simpler, and thus suitable for the rapid analysis of multiple samples as required in this study.

One identified function for poly P is the concentration and detoxification of toxic metals, including Zn, Cu, and Cd (Hashemi et al., 1994; Alvarez and Jerez, 2004; Jensen et al., 1982a), which were considered in the previous chapter. Of these metals, only Cu shows sufficiently high concentrations in natural marine environments to limit the growth of some phytoplankton species through its toxic effects (Mann et al. 2002). Furthermore, I could find no studies that report variability of poly P with the growth progression of cells in culture (hereafter referred to as

'growth cycle'). Thus, in this chapter, I seek to constrain the variability of poly P in the marine environment due to the growth cycle and potentially variable [Cu^{2+}], especially high [Cu^{2+}] observed in natural seawater and toxic to some phytoplankton. I focus on diatoms, for though all species produce poly P, as ballast species (Buesseler, 1998; Armstrong et al., 2001), diatoms are particularly important in delivering materials to the seafloor, and PPBs of comparable size to sedimentary apatite grains have been found in diatoms overlying those sediments (Diaz et al., 2008). Four diatom species are considered including 3 centric species from genus *Thalassiosira* (the coastal species *T. pseudonana* and *T. weissflogii*, as well as the oceanic *T. oceanica*)and 1 estuarine pennate species from genus *Surirella*. This diversity was selected to provide an initial perspective on how universal observed trends might be.

3.3 Methods

3.3.1 Culture growth and collection

Four species of diatom were investigated for this study: The coastal, centric diatoms *Thalassiosira pseudonana* (*Tp*) and *Thalassiosira weissflogii* (*Tw*), the oceanic centric diatom *Thalassiosira oceanica* (*To*), and the estuarine pennate *Surirella spp.* (*Sur*). Variable copper data from diatoms grown in two different conditions are reported. Eight cultures of both *Sur* and *Tp* were grown in the pH-controlled, high-volume (1 L), PO_4^{3-}-replete conditions described in chapter 2 of this thesis, and collected by filtration (growth data including absorbance, fluorescence, cell counts, and pH available in Appendix F). *Sur* in this high-volume experiment only were amended with $Si(OH)_4$ (400 µM final concentration), since it was found to limit growth. Since this method produces much more biomass than is needed for poly P analysis, small-volume cultures were also grown and analyzed. Eight cultures each of *Sur*, *Tp*, *To*, and *Tw* were grown on a 14:10 hour light:dark cycle in acid-cleaned 60 ml polycarbonate bottles with 100 µM EDTA Aquil media (Price et al., 1988), also PO_4^{3-}-replete, but without pH control. For both high-volume and low-volume cultures, Cu spikes were added in a

1:1 (mol:mol) solution with EDTA, and free copper concentrations were calculated using MINEQL at 20℃, all solids off, and with ionic strength calculated (Westall et al., 1976) (Table 3.1). Cultures grown using these small-volume procedures were collected by centrifugation. To distinguish between the *Sur* and *Tp* cultures grown under different culture conditions, I append 'f' to high-volume cultures collected by filtration, and 'c' to small-volume cultures collected by centrifugation. Growth data for all 4 species reported in Appendix F were used to determine the end of exponential growth for each of the species under consideration.

Samples were rinsed with Aquil salts (i.e. without added nutrients, vitamins, or trace-metals) to dilute residual PO_4^{3-} from the growth media below detection limits; i.e. 3 times for samples collected by centrifugation, and 10 times for samples collected by filtration. See methods in chapter 2 of this thesis for a more complete description of the rinsing procedure used for filtered cells. After collection, cells were stored in a -80℃ freezer until analysis. Cu-amended samples were collected after 8 days for all samples except *Sur*-f, which was collected after 14 days for the first 2 samples, and 17 for the remaining 6 (Appendix F).

To determine poly P variability with the growth cycle, four 500-ml PC bottle cultures, one for each species considered, were grown without Cu amendment and sampled at the same time of day (± 1 hour) between 0 and 21 days. These samples were collected via centrifugation and stored as described above.

3.3.2 Polyphosphate assay

Samples were analyzed in a colorimetric assay using a combination of methods adapted from Solorzano & Strickland (1968) and Eixler et al. (2005). Milli-Q (MQ) water was added to rinsed samples that were then autoclaved for 20 min at 110℃. After cooling, samples were filtered through a GF/F filter. The filtrate was separated into two equal portions: one to measure extractable soluble reactive phosphate (*e*-SRP), and the other for extractable total cellular phosphate (*e*-TCP). The difference between the two fractions was attributed to poly P, and this difference was divided by *e*-TCP to arrive at a final value for extractable %P allocated to poly P (*e*-poly P). That is:

Table 3.1: Total Copper [Cu_T] added to each sample in a 1:1 ratio with EDTA, and resulting free copper [Cu^{2+}] concentrations (M) as calculated by MINEQL (Westall et al., 1976). All samples were grown in Aquil media (Price et al., 1988) with 100 µM EDTA, and *Sur*-f were amended with silicic acid to a final concentration of 400 µM.

	Sur-f		*Tp*-f		*Sur*-c, *Tp*-c, *To* and *Tw*	
Sample	[Cu_T]	[Cu^{2+}]	[Cu_T]	[Cu^{2+}]	[Cu_T]	[Cu^{2+}]
1	3.0E-8	2.4E-14	1.0E-8	8.0E-15	2.3E-8	1.9E-14
2	1.0E-7	8.0E-14	7.0E-8	5.6E-14	6.9E-8	5.6E-14
3	3.0E-7	2.4E-13	1.0E-7	8.0E-14	2.1E-7	1.7E-13
4	7.0E-7	5.6E-13	7.0E-7	5.6E-13	6.2E-7	5.1E-13
5	1.0E-6	8.0E-13	1.0E-6	8.0E-13	1.9E-6	1.6E-12
6	3.0E-6	2.4E-12	3.0E-6	2.4E-12	5.6E-6	4.6E-12
7	1.0E-5	8.0E-12	7.0E-6	5.6E-12	1.7E-5	1.4E-11
8	5.0E-5	4.0E-11	1.0E-5	8.0E-12	5.0E-5	4.0E-11

(3.1) *e*-poly P = (*e*-TCP - *e*-SRP)/*e*-TCP

Eixler et al. (2005) report that 70% of total cellular phosphorus was extracted using this method (Eixler et al., 2005). In replicate measurements (n=14) of a single diatom culture, the standard deviation for analysis was 5%, indicating that this procedure extracts a fairly consistent ratio of poly P to phosphate from cells. Dilute HCl was added to the *e*-TCP samples to achieve a final concentration of 0.1 M. Vials were fitted with autoclave caps, weighed, then placed in a boiling water bath for 2 hours. After allowing to cool, vials were weighed again then brought to their pre-boil weight with MQ.

Just before adding the mixed reagent described in Solorzano & Strickland (1968) to all samples, dilute HCl was added to the standards, references, and *e*-SRP samples to equilibrate pH, volume, and ionic strength with *e*-TCP samples (Solorzano and Strickland, 1968). Samples were allowed to sit at least 30 minutes before analyzing at A_{882} on a Varian Cary 50 Bio UV-Visible Spectrophotometer in a 1 ml quartz cuvette.

All data points represent the average of 3 measurements of the same sample. A reference standard was generated for each assay, and run every 2 samples (i.e. 6 measurements, since each sample was measured in triplicate) to account for any drift during analysis and to determine the detection limits of the instrument, determined as 3 times the standard deviation of this reference standard. All data reported had measurements above the detection limits, and significant drift during measurement was not observed. The standard curve was prepared from reagent-grade KH_2PO_4 salt and dissolved into 1 L of MQ. Dilutions were prepared from this standard. R^2 values for the standard curve were consistently > 0.99.

The total time to complete all steps in this procedure for all data reported here was 2-3 days. Consistent timing for this procedure may be important, as it was found that 2 sets of 8 samples that were run twice, once immediately after the GF/F filtering step, and once 3-5 days after the initial analysis, had universally higher *e*-poly P values on the second analysis, apparently due to decreasing SRP readings, though TCP readings were relatively constant (*e*-poly P = 18% higher values, sd = 11% for the set allowed to sit 3 additional days, and 19% higher values, sd = 9% for the set allowed to sit an additional 5 days). Samples were sitting in acid-cleaned glass test-tubes and capped with autoclave caps during this time. In 2 GF/F-filtered samples allowed to sit longer (on the order of 10 days), white filaments began to appear in the filtrate. As it is unlikely that PO_4^{3-} was removed or poly P added during this waiting time, I infer that poly P was polymerizing in the test tube, either auto-catalyzed, or bacterially mediated. In either case, these observations emphasize the importance of prompt sample processing for this procedure. The second, elevated set of values were not used for analysis.

3.3.3 DAPI staining

To visually confirm the presence of PPBs, the cellular store of poly P that appears at present to be the best candidate for nucleating apatite formation in sediments, cells were stained with a solution of 2 mg/ml DAPI and allowed to sit for at least 5 min before rinsing and placing an aliquot on a slide. Cells were observed under UV-excitation using a long-pass filter and at 100x magnification

on an Olympus BX51 fluorescence microscope. An aliquot of GF/F filtrate from a sample of *Tw* was pelleted and stained with DAPI to confirm presence of PPBs in the filtrate that would then be analyzed.

3.3.4 N:P ratios

After rinsing with Aquil salts, cultures were subsampled for N:P analysis. To remove salts that can interfere with analysis, subsamples were shaken vigorously with a solution of 1 M ammonium formate to remove excess salts (Zhu and Lee, 1997). This rinse was repeated once more before filtering equivalent volumes of *Tp*, *To*, and *Tw* onto a combusted GF/F filter for CN analysis, and onto a 0.2 µm PC filter for total P analysis. Both filters were enclosed in separate combusted squares of aluminum foil. *Sur*-f samples were scraped off of the 1 µm PC filter using a pipette tip and dried in a 1.5 ml micro centrifuge tube. Samples were sent to the SOEST Laboratory for Analytical Biogeochemistry at the University of Hawaii and analyzed by Dr. Rebecca Briggs. There they were analyzed for N using a Exeter Analytical CE 440 Elemental Analyzer, and for P using a high-temperature ashing method of (Aspila et al., 1976).

3.4 Results

3.4.1 Microscopy

Small, sub-micron PPB granules were identified in all diatom species except *Sur* (Figure 3.1). *Sur* contained possible PPBs, but the yellow color was not sufficiently distinct from surrounding materials to allow much confidence in a positive identification. This may be due in part to the heavily silicified frustule of *Sur*. Granules of comparable size to those observed in cells were also recovered from the GF/F filtrate and fluoresced yellow under UV excitation consistent with DAPI-PPB complexes (Allan and Miller, 1980; Tijssen et al., 1982; Eixler et al., 2005) (Figure 3.2). The yellow color of granules in the cells appeared more muted than the filtrate, possibly due to intervening cellular constituents and the frustule. This

confirms that some of the P stored as poly P in the diatoms tested was present in the granular PPB fraction identified by Clark et al. (1986) and at present the best candidate as nucleation sites for apatite in sediments. Though PPB granules were not unambiguously identified in *Sur*, the same procedure was used to minimize differences in results. Though PPB granules were present, this does not eliminate the possibility that substantial poly P was also stored in the acid-soluble short-chain and neutral pH-soluble long chain poly P fractions. Though high-Cu and low-Cu cultures were examined, there was no discernible difference in the size or number of PPBs observed, though the small size of the bodies and apparent dimming through the cell wall made such comparisons impossible to quantify with the tools employed.

3.4.2 Individual culture sampled multiple days

Data indicate that a single batch culture allowed to grow over time first depletes its poly P stores, elevates to a peak concentration after 3-10 days depending on the species (approximately at the end of exponential growth, indicated by arrows), then gradually decreases its store of poly P to an apparently stable level (Figure 3.3). Results for *Sur* differ in that though there was an initial decline (captured by a single data point, which could be an outlier), there was no peak observed over the course of the growth cycle. This is one of the more prominent differences in the substantial variability observed in P allocated to poly P throughout the growth cycle. *To* shifts from allocating 4% of extractable P reserves to poly P on day 1 to a maximum of 73% by day 9. The comparable minimum-to-maximum variation is 8-33% for *Tp* between days 1 and 4, 14-33% for *Sur* between days 4 and 8, and 45-77% for *Tw* between days 3 and 6. *Tw* results may not capture the full variability as samples were not collected before day 3.

3.4.3 Multiple cultures grown at variable [Cu^{2+}]

In all diatom species investigated, variable [Cu^{2+}] appears to induce changes in *e*-poly P. For all species except *Tp*, *e*-poly P increases at higher [Cu^{2+}]. For *Tp*,

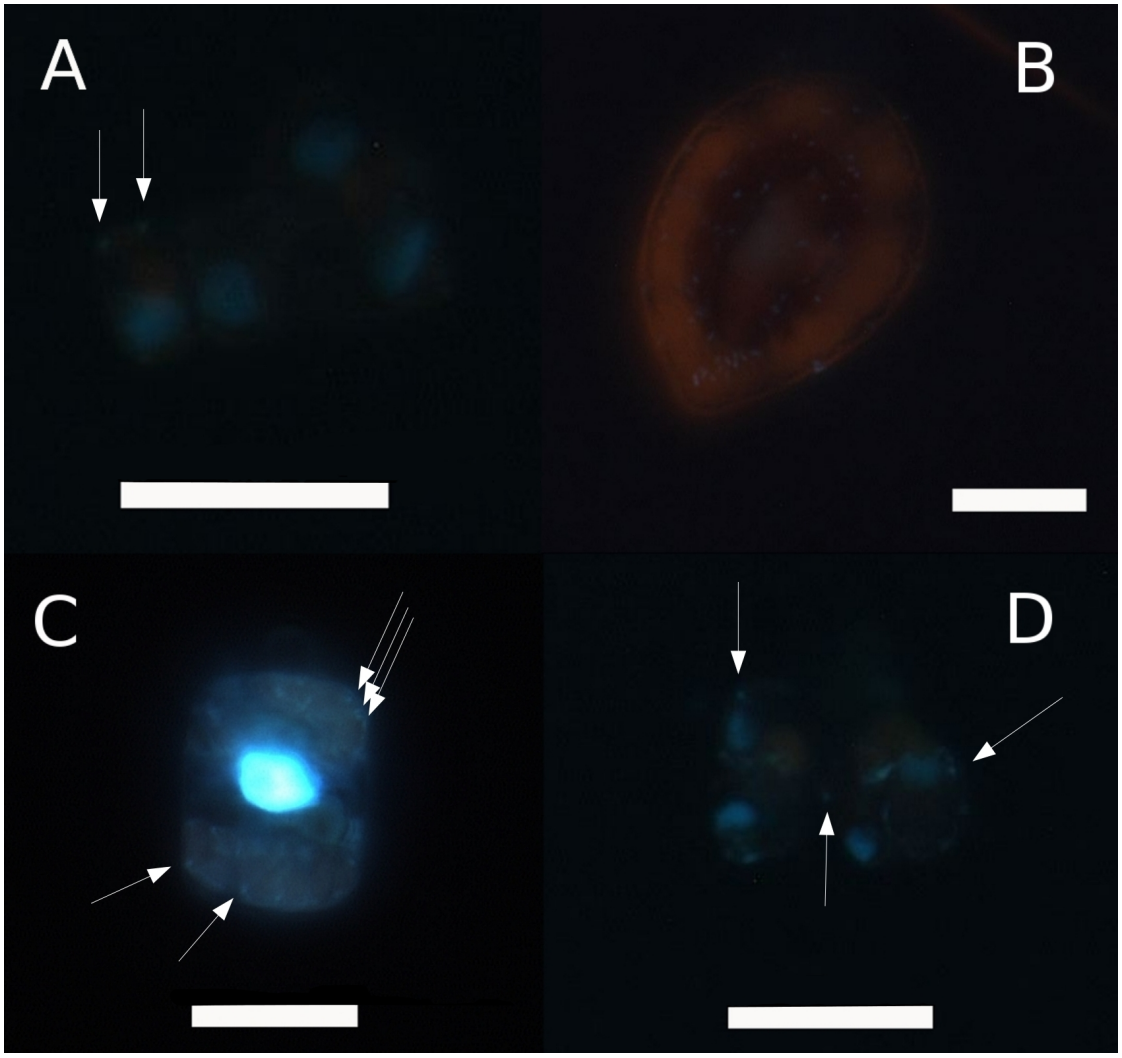

Figure 3.1: Fluorescent images of DAPI-stained cells and PPBs. All scale bars are 10 µm. Arrows point to yellow-green fluorescence of DAPI-PPB complexes in A) *To*, C) *Tw*, and D) *Tp*. While many PPB-sized objects are visible in B) *Sur*, they appear more blue than yellow-green, and may be bacteria.

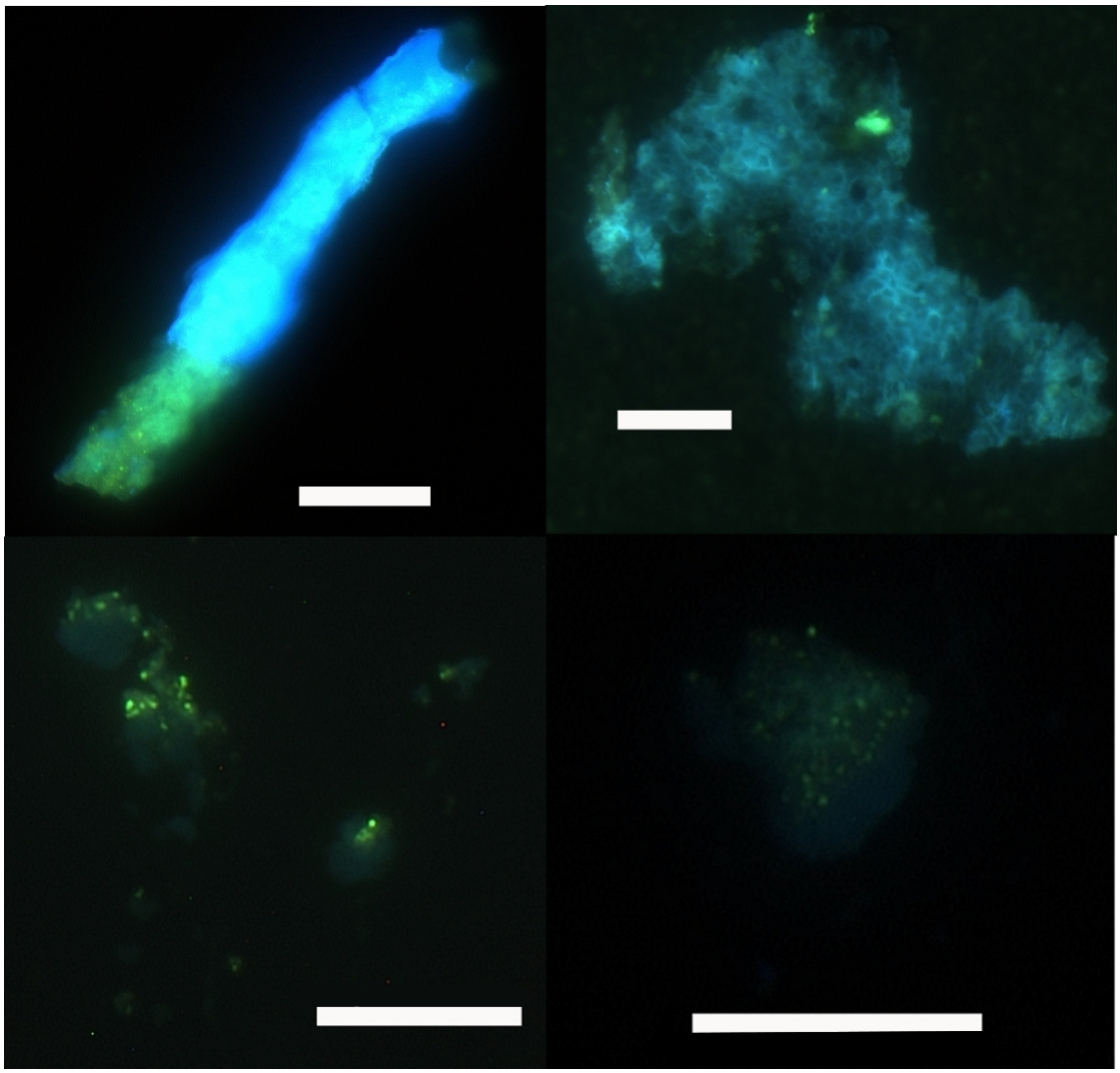

Figure 3.2: Four images of yellow-green fluorescence from DAPI-PPB complexes isolated from a *Tw* culture. Scale bars are all 10 µm, as in Figure 3.1. Yellow-green fluorescence is notably brighter in these images than in the diatoms, though the size of these PPB granules here an inside the diatoms is comparable.

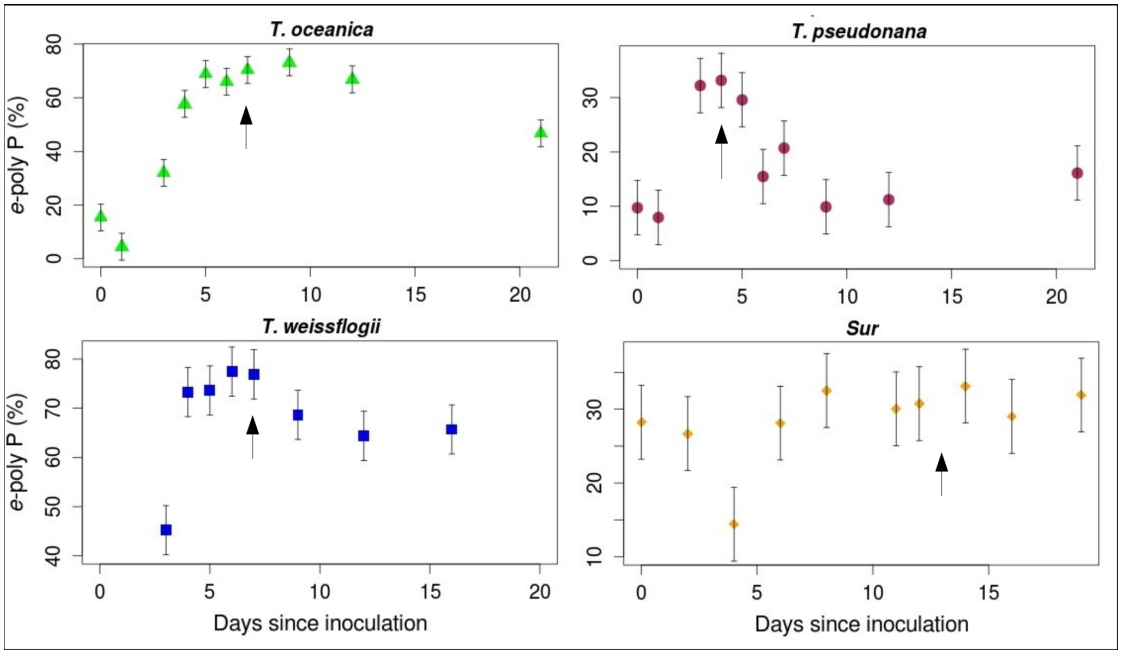

Figure 3.3: Clockwise from upper left, plots for *To*, *Tp*, *Sur*, and *Tw* comparing days since inoculation with measured *e*-poly P. Error bars are ± 5% as established by running separate aliquots of a single culture through the whole *e*-poly P procedure (n=14). All centric diatoms show a peak in *e*-poly P that roughly coincides with the end of exponential growth (end exponential growth indicated by arrows; see Figure 3.4 for data used to choose arrow location), and decline afterwards. *To*, *Tp*, and *Sur* show an initial decline from inoculation *e*-poly P, and as *Tw* is missing data points before day 3 but appears to stabilize *e*-poly P by day 12, it likely also experienced an initial decline in *e*-poly P from values at inoculation. Symbols and colors associated with each diatom will be consistent throughout this chapter.

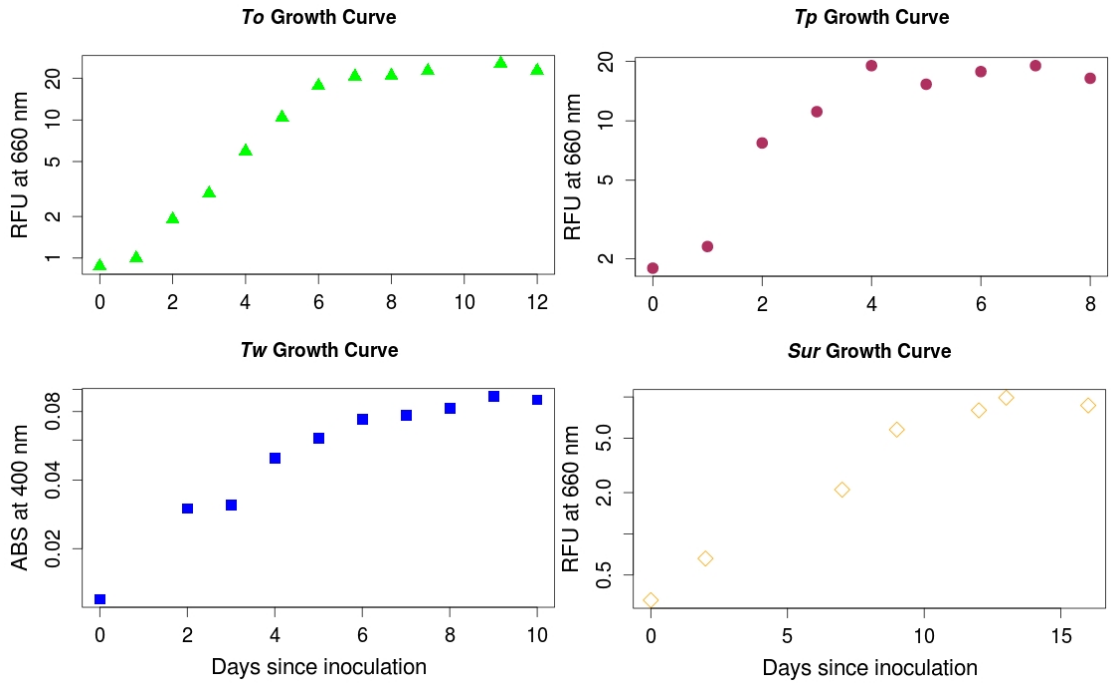

Figure 3.4: Clockwise from upper left, plots for *To*, *Tp*, *Sur*, and *Tw* comparing days since inoculation with measured fluorescence (RFU) at 660 nm for *To*, *Tp*, and *Sur*, or absorbance (ABS) at 400 nm for *Tw*. Note the log scale for the y axis. These plots were used to select placement of the arros indicating the end of exponential growth in Figure 3.3. Symbols and colors associated with each diatom will be consistent throughout this chapter.

both biological replicates have relatively high *e*-poly P at low [Cu^{2+}], decreasing as free copper concentrations increase. Above [Cu^{2+}] ~1E-12, *Tp* appears to substantially increase its *e*-poly P back to levels observed at the lowest [Cu^{2+}]. In the *Tp*-f replicate, this decreases again at the highest [Cu^{2+}], whereas it does not do so in the *Tp*-c replicate. Conditions in the large-volume, pH-controlled environment (*Tp*-f) apparently enabled *Tp* to allocate much more P to poly P. By contrast, pH control and differential collection dates appeared to make little difference to *Sur* with regard to how much poly P it accumulated. This is consistent with the low variation observed in the single culture sampled over multiple days.

Comparing the differences in maximum and minimum *e*-poly P due to the growth cycle and variable [Cu^{2+}], I consider a difference $\leq$ 10%, i.e. a 2 σ difference in *e*-poly P, as indicating comparable values. This defined, I find that the minimum-maximum difference due to variable [Cu^{2+}] is smaller than that due to the growth cycle for *To* (37-55% (Cu) vs. 4-73% (growth)), and *Tp*-c (19-33% vs. 8-33%), comparable for *Tw* (37-79% vs. 45-77%), *Sur*-c (25-39% vs. 14-33%), *Sur*-f (28-49% vs 14-33%), and larger for and *Tp*-f (20-68% vs. 8-33%).

All species show a $>$ 10% shift in P allocation to poly P, most of which occurs over a 10-fold difference in [Cu^{2+}] (Figure 3.5). While *Tw* and *Sur*-c show the highest poly P allocation at the highest [Cu^{2+}], for *Sur*-f and *To* this occurs at intermediate [Cu^{2+}], and for both *Tp* replicates this occurs at the lowest and at intermediate-high [Cu^{2+}]. The total %P as poly P and the capacity of cells to accumulate poly P appears to vary widely by species and, for *Tp* at least, with growth conditions.

3.4.4 Comparison of T-Tests

To establish whether the differences *e*-poly P due to variable [Cu^{2+}] were significant, I performed a Welch two-sample T-test comparing the 2, 3, and 4 cultures grown at the lowest and highest [Cu^{2+}]. This analysis was performed for all 6 Cu-challenged experiments individually, for all experiments combined, and for all experiments except *Tp* (Table 3.2). I report data comparing 2, 3, and 4 low/high cultures since a simple 'on/off' comparison of the highest and lowest

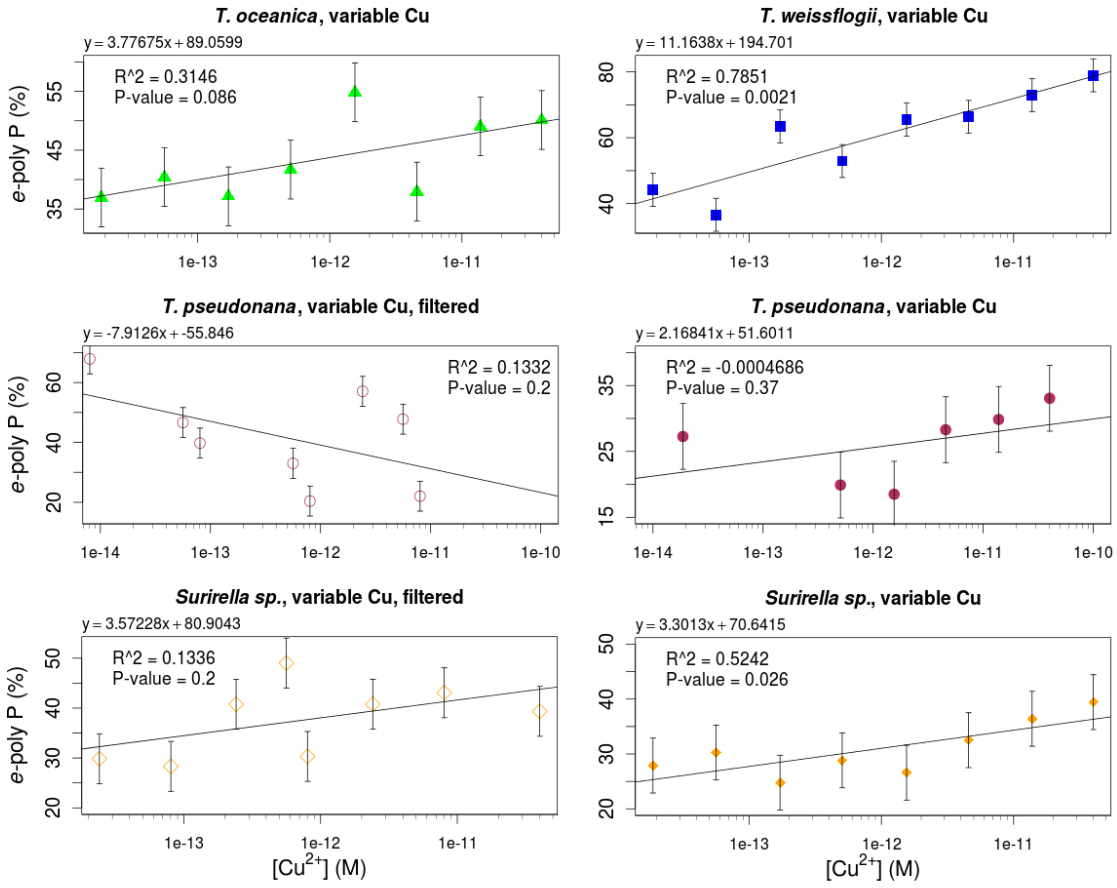

Figure 3.5: Plots showing the change in *e*-poly P at variable [Cu^{2+}]. Symbols and colors are the same as in Figure 3.3; open symbols indicate the culture was grown in large-volume and pH-controlled media and collected via filtration. R^2 and p-values are reported for a log-linearized fit to each data set, as well as the equation of fit.

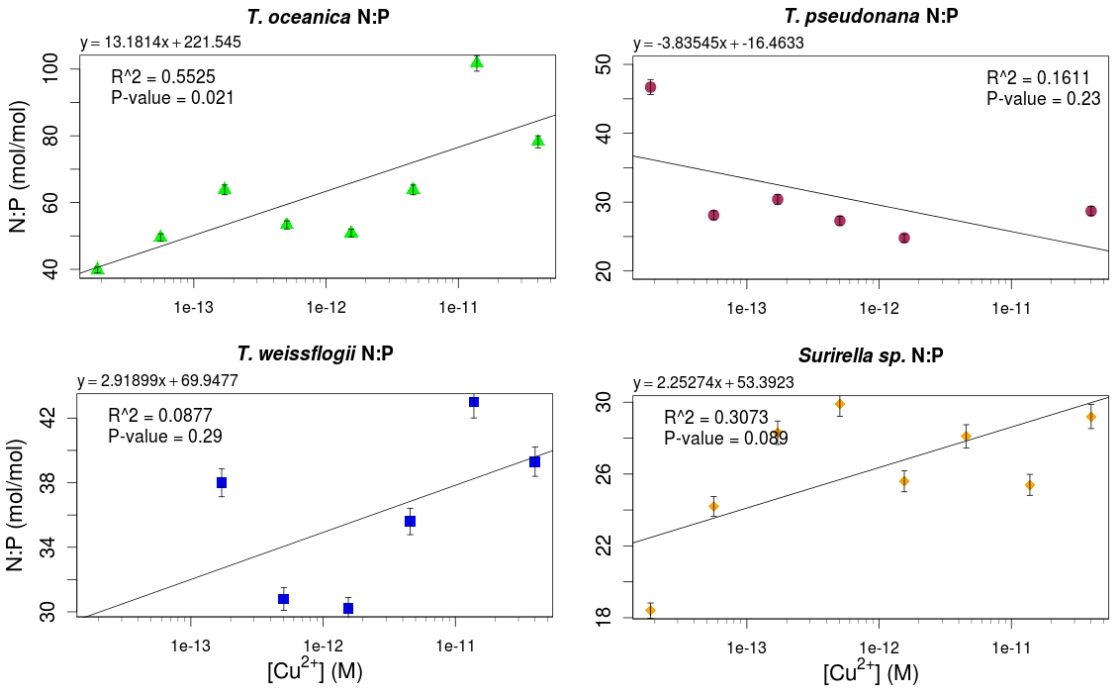

Figure 3.6: $[Cu^{2+}]$ vs N:P for all species. Only *To* shows a p-value < 0.05 or an $R^2 > 0.5$.

Table 3.2: p-values form a Welch's T-Test performed on *e*-poly P results of Cu-challenged cells. These results reflect a comparison between cultures grown at the 2, 3, and 4 lowest $[Cu^{2+}]$ with the cultures grown at the 2, 3, and 4 highest $[Cu^{2+}]$. E.g. 2 low/hi compares *Sur*-c grown at $[Cu^{2+}]$ of 1.87E-14 and 5.61E-14 against the two cultures grown at $[Cu^{2+}]$ of 1.38E-11 and 4.01E-11 (Table 3.1). *Tp*-c has no data in the 2 and 3 low/hi comparisons due to 2 data points that were lost during analysis, resulting in insufficient data for analysis.

P-values for a Welch's T-Test								
	Sur-c	*Sur*-f	*Tp*-c	*Tp*-f	*Tw*	*To*	All	No Tp
2 low/hi	**0.02452**	**0.03186**	NA	0.842	**0.01026**	**0.03916**	0.1183	**0.01089**
3 low/hi	**0.01595**	0.084	NA	0.7321	**0.03647**	0.09265	0.116	**0.0174**
4 low/hi	0.06266	0.4178	0.2474	0.7829	**0.01212**	**0.04133**	0.1753	**0.02836**

cultures might over-simplify the response, whereas comparing the top/bottom 4 could mask what is a real tendency for diatoms to accumulate poly P.

Sur, *Tw*, and *To* all show a statistically significant ($p < 0.05$) difference in the amount of P allocated to poly P between low and high $[Cu^{2+}]$. While only *Tw* shows a significant response for all comparisons, when combining results for these

three species, the difference between low-Cu and high-Cu cultures is significant at each window, and the p-values improve, approaching 0.01. Including *Tp* into this analysis whether considering the top/bottom 2, 3, or 4 points eliminates the statistical significance of the results.

3.4.5 N:P ratios for the data.

N:P ratios (Figure 3.6) generally increase with increasing [Cu^{2+}], though again *Tp* is an outlier. The trend is only significant for *To*. Similarly, comparing % poly P to N:P (Figure 3.7), all species show higher N:P ratios at higher poly P, though the trend is only significant for *Tp* and *Sur*. R^2 values are generally poor, with only %P as poly P vs N:P for *Tp* and [Cu^{2+}] vs N:P for *To* having values > 0.5. Such trends, if taken at face value, could be explained either by decreased total cellular P reserves as *e*-poly P increases, or increased cellular N reserves increase. If the latter, one would expect the C:N ratios to decrease, and C:P ratios to show no trend. However, these data (Appendix G) are mixed with even poorer R^2 and p-values.

3.5 Discussion

3.5.1 Comparison with previous results

The most appropriate comparisons with data presented here would be studies that report poly P in living marine phytoplankton grown in culture or collected *in situ*. Unfortunately, there are very few such studies (Table 3.3). Most research focuses on poly P's cellular function (Seufferheld and Curzi, 2010) or adjusting growth conditions to maximize P accumulation (Mino, 2000). Few studies focus on marine organisms, distinguish between different cellular poly P reserves, or focus on marine eukaryotes. In poly P studies, there is no standardization of methods for culture conditions, PPB visualization, or quantifying poly P abundance. Our data are roughly comparable at low Cu-abundances and at some points in the growth cycle with the limited data available, but are significantly higher than any previ-

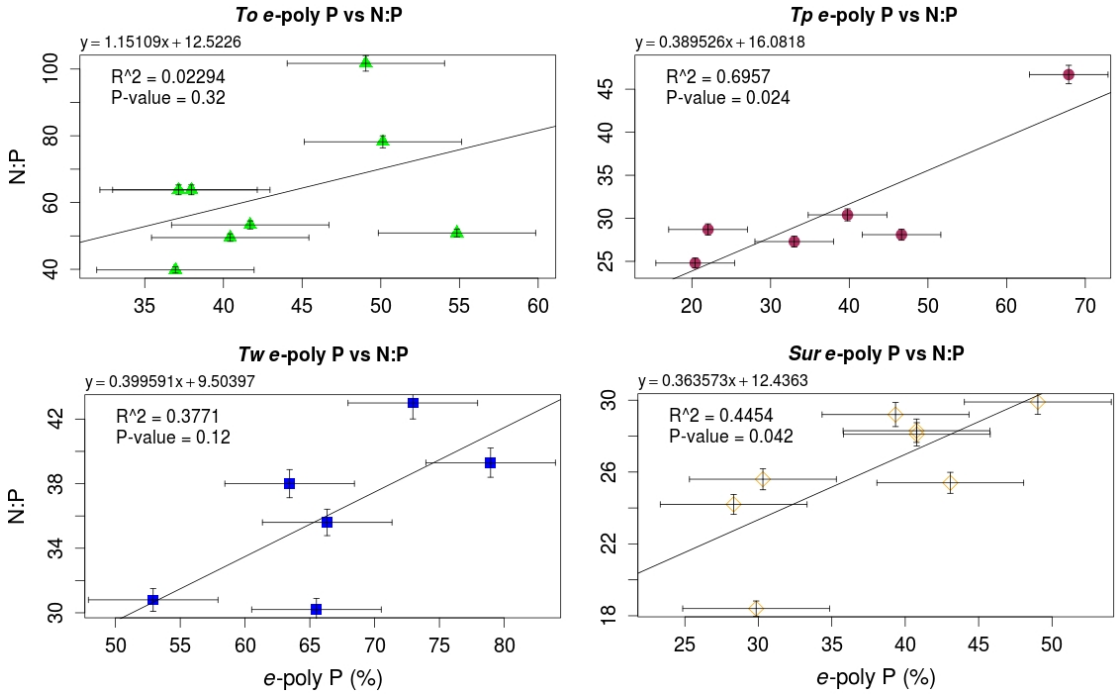

Figure 3.7: %P as poly P (i.e. *e*-poly P) vs N:P ratios for all species considered. Though all species show a positive trend towards higher N:P ratios with higher *e*-poly P, the statistics are again poor, as only *Sur* and *Tp* show a p-value < 0.05 and only *Tp* has an R^2 value > 0.5.

ous quantifications at some [Cu^{2+}], and high-growth rate time points in the growth cycle samples (Table 3.3). These higher values may be explained in part by the extraction technique. As mentioned previously, *e*-poly P would include granular poly P that would be missed using traditional (but not solid state) ^{31}P-NMR, and if there is little poly P in the fraction excluded by the GF/F step in this method (for instance, in the phospholipid membrane of cell walls), this would also result in higher *e*-poly P values. Assuming reported values reflect 70% of total cellular P (as found by Eixler et al., (2005)), and no poly P is included in the portion that is removed by GF/F filtration, *e*-poly P values may be elevated by as much as 30% with respect to a method that includes this P reservoir.

Only the Rhee (1973) paper listed in Table 3.3 sampled their culture through time. However, they report their data as growth rate, not as days since inoculation, their study organism was a freshwater phytoplankton, and no cells were collected after the onset of steady state. Thus, it offers an imperfect comparison. As I collected cells and measured *e*-poly P long after the onset of steady state, the relationship between growth rate and *e*-poly P observed in Rhee (1973) breaks down, as cultures with very low growth rates still have quite high *e*-poly P. Given the magnitude of variability with the growth cycle, other studies that do not subsample through time likely do not reflect the full variability of poly P allocation for their study organisms under the conditions tested. Likewise, studies that sample through time but cease sampling cells at the end of exponential growth will exaggerate the importance of growth rate in determining cellular *e*-poly P for *in situ* communities. Studies that seek to identify variability in the poly P contents of surface phytoplankton without observing changes through time are subject to large sampling biases. Likewise, *in vitro* studies that do not ensure that cells are at the same stage of growth at the time of sampling are prone to misattribution of the observed effects to the variable tested, when it may be accounted for by the cell cycle.

Table 3.3: A summary from papers reporting data for %P as poly P for various phytoplankton. While not exhaustive, this summary does include the most commonly cited papers in studies concerned with variability in the amount of P allocated to poly P by marine phytoplankton.

Study organism	Organism type	Freshwater/ Marine	*in vitro*/ *in situ*	Variable tested	%P as poly P	Reference	Multiple time points?	Method	Poly P conclusion summary
Amphidinium carteri	Diatom	Marine	*vitro*	n/a	30%	Solorzano and Strickland 1968	no	UV-oxidation, acid hydrolysis	Marine phytoplankton accumulate poly P when grown in excess phosphate.
Skeletonema costatum	Dinoflagellate	Marine			30%				
Scenedesmus spp.	Alga	Fresh	*vitro*	Growth rate	11-23%	Rhee, 1973	yes	Hot water extraction, fractionation	Poly P involved with growth rate.
Thalassiosira pseudonana	Diatom	Marine	*vitro*	N-limited	19-43%	Perry, 1976	no	UV-oxidation, acid hydrolysis	Poly P did not inhibit PO_4^{3-} uptake. P-limited cultures had no poly P.
				P-limited	0%				
Chlorella vulgaris	Alga	Fresh	*vitro*	Extraction method	45-80%	Eixler, 2005	no	Extraction; multiple agents	NaOH and hot water extract PPB granules with similar efficiencies, but hot water method is simpler.
Synechocystis spp. (PCC 6803)	Cyanobacteria	Fresh							
Natural assemblage	Diatom-dominated	Marine	*situ*	n/a	7%	Diaz, 2008	no	Solid-state ^{31}P-NMR	Phytoplanton-supplied poly P nucleates apatite formation in sediments.
Trichodesmium spp.	Cyanobacteria	Marine	*situ*	Nutrient availability	8-25%	Orchard, 2010	no	Solid-state ^{31}P-NMR	*Trichodesmium* accumulate more poly P in oligotrophic waters.
Thalassiosira pseudonana	Diatom	Marine	*vitro*	P replete	2%	Dyhrman 2012	no	Solid-state ^{31}P-NMR	P-stressed diatoms produce more poly P.
				P-limited	15%				
Surirella spp.	Diatom	Estuarine	*vitro*	Growth cycle	14-33%	This study	yes	Hot water extraction	
Thalassiosira pseudonana	”	Marine	”	”	8-33%	”	”	”	Diatoms greatly vary allocation of P to poly P during the growth cycle.
Thalassiosira weissflogii	”	”	”	”	45-77%	”	”	”	
Thalassiosira oceanica	”	”	”	”	4-73%	”	”	”	
Surirella spp.	”	Estuarine	”	$[Cu^{2+}]$	25-49%	”	no	”	Diatoms vary allocation of P to poly P in response to variable $[Cu^{2+}]$. Response inconsistent between the 4 species investigated.
Thalassiosira pseudonana	”	Marine	”	”	19-68%	”	”	”	
Thalassiosira weissflogii	”	”	”	”	37-79%	”	”	”	
Thalassiosira oceanica	”	”	”	”	37-55%	”	”	”	

3.5.2 Variability in poly P with the growth cycle

The finding that diatoms grown in nutrient-replete batch culture display such large shifts in *e*-poly P as a normal part of the growth cycle is useful for understanding poly P dynamics in the marine environment. Rhee (1973) finds that maximal growth rates coincide with maximal poly P accumulationRhee1973, but this study does not capture the slow draw-down of poly P reserves due to the timing of sampling. Thus, it would be an oversimplification to directly translate this conclusion to *in situ* communities. Assuming that batch experiments in which PO_4^{3-} is not limiting approximate diatom blooms, my results suggest diatoms may accumulate substantial quantities of poly P during a bloom, and that any poly P accumulation will slowly be drawn down as the bloom ages.

Thus, there may be elevated poly P within a bloom, as found by Solorzano & Strickland (1968) inside a dinoflagellate bloom, but this build-up will not necessarily translate to elevated poly P per cell delivered to sediments by sinking phytoplankton. However, blooms may elevate poly P in the water column via processes that interrupt cell growth at maximal growth rates, such as cell lysis or grazing. There is some evidence that any poly P released to the water column by such processes may be somewhat refractory. Poly P may account for 0-13% of total dissolved phosphorus in coastal ocean waters, with higher values near point sources for sewage and areas of high biological activity, such as bloom patches or kelp forests (Solorzano and Strickland, 1968; Paytan et al., 2003; Young and Ingall, 2010). The total soluble non-reactive phosphorus (SNP) pool, which would include polyphosphate, is estimated to have a lifetime between 2 and greater than 90 days in coastal waters and 50-300 days in the open ocean. Aqueous SNP abundance has been shown to vary widely with seasons, distance from shore, depth, biological activity, and plankton community composition (Benitez-Nelson (2000) and references therein).

However, such variability may simply be an artifact of analytical techniques that neither distinguish between poly P and other dissolved P constituents (Monaghan and Ruttenberg, 1999; Benitez-Nelson, 2000) nor adequately recover the dissolved low molecular weight (LMW; <1000 Da) fraction of SNP. A recent anal-

ysis with greater recovery of this fraction found a fairly consistent 8-13% of dissolved P as poly P between 4 diverse sampling locations (Young and Ingall, 2010), implying that poly P, especially in the LMW fraction, is refractory. Though any organism capable of producing alkaline phosphatase would be able to cleave the phosphate monoester bonds of poly P (Heppel et al., 1962; Suzumura et al., 1998), the consistent numbers over such a wide area indirectly argues that this pool of poly P is either unavailable or difficult to access. Possible explanations include the differential chemical solubility of short-chain, long-chain, and granular poly P; which may also mean differential bioavailability (Clark et al., 1986). Alternatively, limits to the size of particles that may be transported into the cell (e.g. 600 Da for gram-negative bacteria; Weiss et al., 1991) combined with protective structures dominated by phospholipid containing macromolecules as hypothesized in Suzumura et al. (1998) may protect phosphate mono-ester bonds from degradation.

An alternative fate for poly P released to the water column during blooms may be conversion to apatite while still in the water column, perhaps in microenvironments (Faul and Paytan, 2005). Poly P-to-apatite conversion has been noted to occur in as little as 48 hours in the presence of sulfur-reducing bacteria (Goldhammer et al., 2010). Such bacteria would not be expected in the water column, except perhaps the interior of fecal pellets. However, given our poor understanding of poly P dynamics, there may be other pathways for poly P conversion to apatite in the water column. Any such sink switching would decrease P remineralization, and thereby increase P retention efficiency in sediments.

3.5.3 Polyphosphate in variable Cu regimes

My results show that all species exhibit a response in their stores of poly P to the range of [Cu^{2+}] tested, though that response varies. Three of the four species considered, *Sur*, *To*, and *Tw*, increased their *e*-poly P as [Cu^{2+}] increased. By contrast, *Tp* did not appear to show any clear trend in either of the two replicates. However, both sets of cultures show initially high *e*-poly P decreasing until a [Cu^{2+}] of $\sim$ 1E-12 M, then increasing above this, perhaps decreasing again at the highest [Cu^{2+}]. This may be evidence for two modes of poly P management by *Tp* in

response to variable [Cu^{2+}], but more data are needed to clarify the response. As the diatoms studied were isolated from oceanic, coastal, and estuarine regimes, and include 3 centric species and 1 pennate species, a poly P response to Cu stress may be widespread in class Bacillariophyceae. Based on the variability found in this small sample set, the magnitude and nature of that response appears likely to vary widely throughout the class as a whole.

Though the responses observed here may be specific to Cu, PPBs have been implicated in detoxifying other metals such including Ti, Pb, Mg, Zn, Cd, Sr, Co, Hg, Ni, and Cu in organisms including cyanobacteria, green algae, and diatoms (Yu & Wang, (2004) and references therein). The responses observed may therefore reflect a general metal-stress response not specific to Cu. However, Dyhrman (2012) and Perry (1976) identify PPB accumulation as a stress response to N and P deficiency in *Tp*, respectively, and Brown & Kornberg (2004) identify several physical and chemical stressors that induce poly P accumulation as a general stress response. It is unclear whether the nature of poly P accumulation for metal toxicity stress is distinct from the general stress response.

3.5.4 N:P variability with increasing [Cu^{2+}]

Three of the 4 species (*Tp* being the outlier) show higher N:P ratios as [Cu^{2+}] increases, and all of the species show a positive trend towards higher N:P ratios at higher *e*-poly P. This is unexpected, since the traditional view of poly P accumulation is that it represents luxury phosphorus storage (Diaz et al., 2008). If this accumulated phosphate is indeed 'luxury', and in excess of the basic needs of the phytoplankter, one would expect N:P ratios to decrease as more P is stored in the form of poly P, yet this is not what is observed.

An alternative explanation for the observed trends is that diatoms accumulate more N in a high-poly P condition. This would lead to lower C:N ratios at high poly P, and there is some evidence for this in the data, but it is not as clear. Similarly, C:P ratios are inconsistent. Overall, weak correlations and inconsistent results in N:P, C:N, and C:P data warn against any strong conclusions on the effects of variable [Cu^{2+}] or elevated poly P on diatom N:P ratios. Yet the fact

that all species show positive trend towards higher N:P at higher %P as poly P is intriguing, and warrants further study.

3.5.5 Limitations of culture experiments

All diatoms tested showed the capacity for substantial allocation of P to poly P both during the growth cycle and with variable [Cu^{2+}]. Culture experiments are necessarily imperfect approximations of *in situ* community dynamics, and an obvious point of criticism in that regard is the high [PO_4^{3-}] in culture media. However, this factor alone cannot explain the observed high *e*-poly P. Though the [PO_4^{3-}] in cultures is well above the levels that would be found in coastal surface waters, N is generally considered the proximate limiting nutrient (Tyrrell, 1999), and Fe limits production in highly productive HNLC regions where diatoms dominate (Martin et al., 1990; Boyd et al., 2007), so diatoms would have luxury phosphate available to them in most marine environments (Moore et al., 2002).

Furthermore, though the paradigm has long been that poly P is a form of luxury P storage (Diaz et al., 2008), studies suggest that *Tp* and *Trichodesmium* may accumulate appreciable quantities of poly P because of P-limitation (Orchard et al., 2010; Dyhrman et al., 2012). Orchard (2012) attributes *Trichodesmium* accumulation of poly P up to 25% of total P to the 'overplus' P response (Voelz et al., 1966), whereas Dhyrman (2012) invoke a stress-response mechanism. The relationship between available [PO_4^{3-}] and poly P is therefore not straightforward. The surprising increase in N:P ratios with elevated poly P raises the possibility that the high [NO_3^-] in culture medium may also be a factor in poly P accumulation, though the nature of such a relationship, if any, is unclear.

3.6 Conclusions

In this study I sought to elucidate factors influencing the origins of poly P in the marine environment. My approach focused on how diatoms, a dominant class of marine phytoplankton important in delivering P to sediments, vary their allocation of P to poly P at different points in the growth cycle and in response to

variable [Cu^{2+}]. Cu is unique among potentially toxic metals in that its naturally occurring range in the ocean is sufficient to inhibit phytoplankton growth by its excess. In the 4 diatom species studied, including 2 coastal centric, one oceanic centric, and one estuarine pennate diatom, I find wide variability in the amount of P allocated to poly P both within a species under different conditions, and between species. The centric species all display a wide variation with the growth cycle, though a pattern of *e*-poly P accumulation during exponential growth followed by a slow draw-down during steady state emerges. *Sur* displays evidence of an initial draw-down for *e*-poly P, but does not display a peak.

In response to increasing [Cu^{2+}], *To*, *Tw*, and *Sur* allocate more P to poly P at higher concentrations ($p < .05$). *Tp* shows no trend. Due to poor statistical results, strong conclusions cannot be drawn from N:P. However, all species show a positive trend towards higher N:P at higher *e*-poly P, suggestive of either lower total cellular P at higher *e*-poly P or lower N. This warrants further study.

Chapter 4

An investigation into phytoplankton allocation of P to polyphosphate in the Humboldt and California Currents

4.1 Abstract

Few *in situ* data exist concerning phosphorus allocation to internal polyphosphate (poly P) stores in marine phytoplankton. Here I report findings from two cruises of opportunity in the relatively well-characterized California Current in summer and the comparatively understudied Humboldt Current in the late Austral summer off the coast of Chile. In addition to reporting community poly P data, I report microalgal community composition based on pigment to chlorophyll a ratios, I use Fe speciation and macronutrient data to assess the state of Fe-limitation with the proxies Si_{ex} and NO_3^-/dFe, and I report Cu-speciation data. I find phytoplankton communities store between 4-47% of their extractable P as poly P (*e*-poly P), with an average of 21% *e*-poly P at Humboldt Current sites, and 22% in the California Current. Despite previous work indicating that nutrient availability, general stress, phytoplankton speciation, and $[Cu^{2+}]$ may each influ-

ence poly P allocation in marine phytoplankton, I found no significant correlation between any oceanographic property measured and *e*-poly P. Breaking the data into various nutrient, Fe-limitation, and [Cu^{2+}] regimes, samples from low-nutrient regimes have higher average *e*-poly P values, but the difference is not statistically significant. I conclude that the wide variation in *e*-poly P allocation with the growth cycle observed in chapter 3 likely explains the lack of correlation, and may well be the dominant factor determining *in situ* poly P allocation.

4.2 Introduction

As highlighted in the previous chapter, polyphosphate (poly P) is an important yet understudied molecule in all cells, and in marine phytoplankton in particular. Its ubiquity and diverse functionality have led to a poorly focused literature, with many studies seeking to constrain its function within the cell, but few quantifying its variability with differing conditions; a more pertinent consideration for understanding the cycling of P in the marine environment.

Studies that have considered variability in P allocation in marine phytoplankton have found that it may vary as a function of nutrient availability (Solorzano and Strickland, 1968; Orchard et al., 2010; Perry, 1976), or as part of a general stress response (Dyhrman et al., 2012). Results presented in the previous chapter identify [Cu^{2+}] and the growth cycle as important considerations. In chapter 3, wide variation in the ability of even closely related diatoms to accumulate poly P in the same conditions were observed, and only certain species of bacteria appear to be able to accumulate poly P (Mino, 2000), both suggesting that community composition is an important factor determining poly P export from the photic zone. Thus, in the marine environment it appears that trace metal load, nutrients, physiological stress, phytoplankton community composition, and the progression of a bloom are all variables that may influence poly P production and export from the photic zone.

The only *in situ* data for poly P in marine phytoplankton communities come from Diaz et al. (2008), who report a single data point for poly P of a

spring bloom phytoplankton community in the Effingham Inlet; a pacific fjiord on Vancouver Island, British Columbia. Orchard et al., (2010) picked *in situ* colonies of *Trichodesmium* (7 data points), while Young and Ingall, (2010) and Solorzano and Strickland (1968) looked at the dissolved phase (6 and 24 data points, respectively). There is clearly a need for *in situ* poly P data from marine phytoplankton throughout the global ocean.

In the dissolved phase, initial indications are that poly P accounts for 8-13% of dissolved organic matter recovered by combined electrodialysis and reverse osmosis, most of which is in the low molecular weight fraction. The consistent values obtained at widespread sampling locations, and the absence of poly P measured by the more common ultrafiltration method suggest that poly P may be somewhat refractory once released into the water column, and that previous studies using ultrafiltration under-report poly P (Young and Ingall, 2010). Likewise, widely employed sampling techniques do not resolve poly P in the dissolved inorganic phosphorus fraction, and in fact include it in the dissolved organic fraction (Karl and Björkman, 2002), meaning that our understanding of P cycling in surface waters fails to properly account for poly P. Such an oversight amounts to a significant blind spot in our understanding of P cycling in the surface ocean, especially in light of recent evidence that poly P can act as a nucleation site for the mineral apatite, which effectively removes P from circulation (Diaz et al., 2008; Ingall, 2010; Goldhammer et al., 2010). Variability in the supply of poly P to sediments may therefore affect the residence time of P in the ocean, with significant long-term implications for the productivity of the global ocean (Tyrrell, 1999).

In this chapter I seek to determine whether nutrients, stress from Fe-limitation (as measured by the proxies NO_3^-/dFe and Si_{ex}), $[Cu^{2+}]$, or phytoplankton community composition (as determined by pigments) are correlated with *e*-poly P in the phytoplankton community sampled on two cruises of opportunity in the California and Humboldt Currents. These data were measured on subsamples taken from a single 30-50 L sample of seawater collected by Teflon pump, standard CTD, and a CTD specialized for trace metal sampling. I find that none of these factors are strongly associated with poly P allocation. Given the size of the

signal due to stage of growth observed in chapter 3 of this thesis, this may prove to be the salient variable for future studies considering *in situ* poly P allocation in phytoplankton communities to consider.

4.3 Methods

4.3.1 Oceanographic setting

There are 4 major eastern boundary currents (EBCs) around the globe whose upwelling driven by wind-stress curl (Bakun and Nelson, 1991) enables high productivity sustaining large fisheries important for human populations (Daneri et al., 2000; Alheit and Niquen, 2004). Samples for this chapter were collected on two cruises of opportunity in two of these EBCs off the coasts of Chile and California (see Table 4.1 for data on oceanographic context; Figures 4.2 and 4.1 for maps with sampling sites). Humboldt Current samples were collected as part of the INSPIRE student cruise between 16-104 kilometers off shore (http://oceanexplorer.noaa.gov/explorations/10chile/), while California Current samples were collected on the CCE-LTER Process cruise P1106MV at stations 80-133 kilometers offshore (http://cce.lternet.edu/). Both cruises were conducted aboard the R/V Melville, with sampling opportunities and locations dictated by goals of the larger research team. Target areas on the INSPIRE cruise included the Humboldt Current Triple Junction, the Concepción methane seep area, El Quisco methane seep area, and the Humboldt Current Trench. Water column depth varied from ∼500 m to 4008 m (Table 1). Humboldt Current sites 6-12 were sampled in close proximity to known methane seeps at water depths < 1000 m. Some of the Humboldt Current samples were also sampled in quite close proximity to each other. E.g. Samples 6 and 7 were sampled at the same location and only 17 hours apart from each other, while samples 9-12 were each sampled within 4 km of the previous sample, and all four were sampled within 48 hours (Table 4.1).

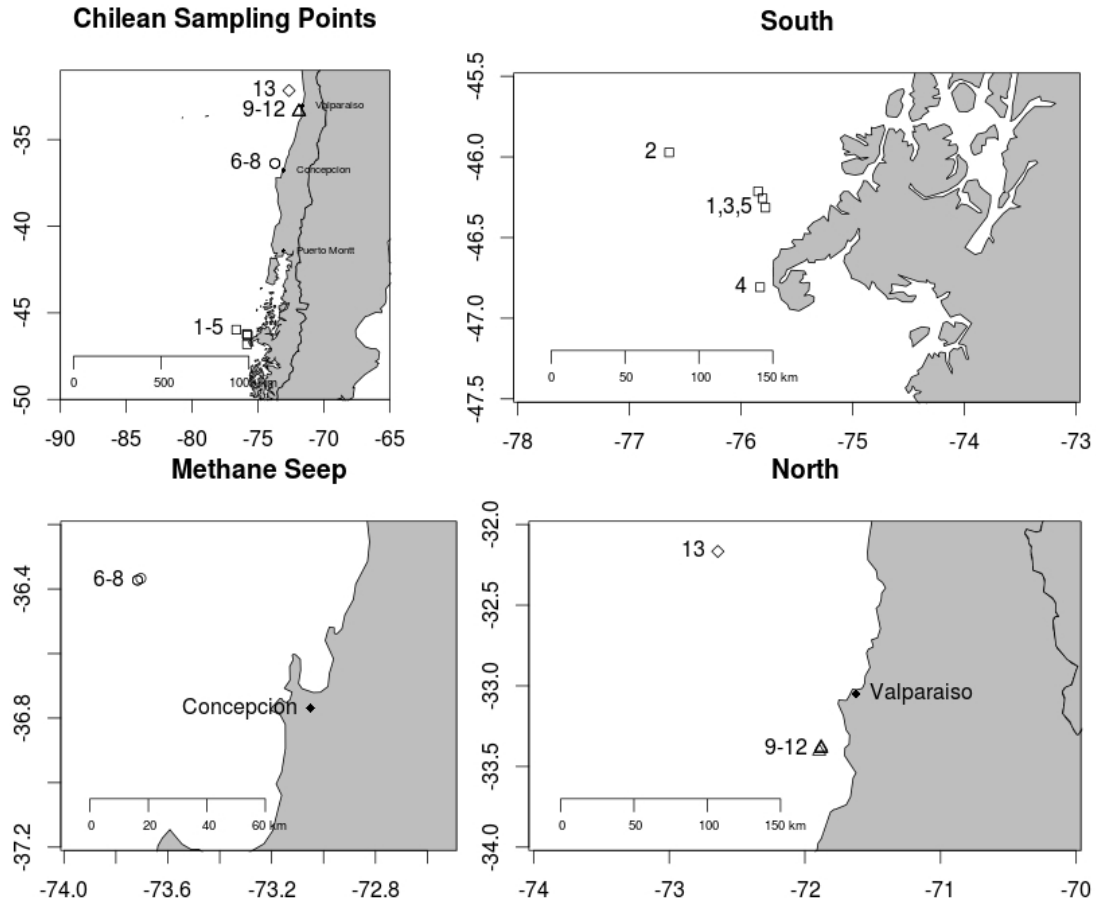

Figure 4.1: Maps of Chilean sampling sites. Clockwise from the upper left: *Chilean Sampling Points:* Overview of the entire area sampled. *South:* Southern sites sampled near the Chilean Triple Junction including samples 1-5 (squares). *North:* close up of the northern sites including samples 9-12 (triangles) taken near the El Quisco methane seep area, and sample 13 (diamond) taken over the Peru-Chile Trench. *Methane Seep:* close up of the area where samples 6-8 (circles) were taken in close proximity to the Concepción methane seep. The symbol assignments used for the different sites in this figure will be used for all relevant figures in this chapter.

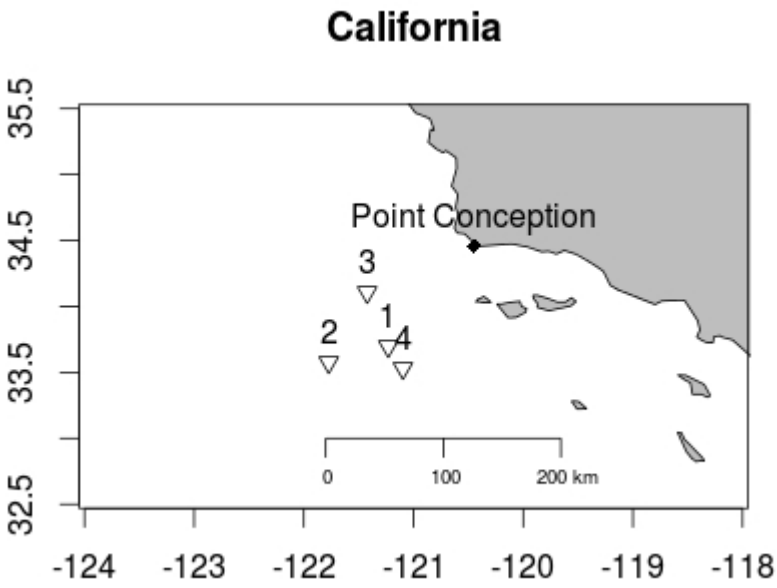

Figure 4.2: Map showing sampling sites on the CCE-LTER cruise included in this analysis. Upside-down triangles will be used to represent California Current samples in figures throughout this chapter.

Table 4.1: Oceanographic data for Humboldt and California Current Samples. 'd col' = depth of sample collection, 'd bot' = depth to bottom, 'day' = date sample collected, 'dist' = closest distance to shore, 'lat' = latitude, 'long' = longitude, 'O_2' = oxygen present in seawater, 'sal' = salinity, 'temp' = temperature, 'mld' = mixed layer depth, 'nd' = no data available.

Cruise	site	d col	d bot	day	dist	lat	long	O_2	sal	temp	mld
		m	*m*		*km*			*ml/L*	*PSU*	℃	*m*
Humboldt	1	5-10	2561	02/26/10	29	-46.312	-75.7815	nd	nd	nd	nd
Humboldt	2	5-10	3577	02/28/10	103	-45.9723	-76.6429	nd	nd	nd	nd
Humboldt	3	30-40	3005	03/03/10	40	-46.2135	-75.8466	5.8	32.4	13	∼10
Humboldt	4	10-20	3083	03/04/10	40	-46.8075	-75.8295	6	32.0	13.5	∼8
Humboldt	5	15	2968	03/05/10	35	-46.2566	-75.8069	5.6	32.3	13.5	∼15
Humboldt	6	25-30	811	03/09/10	60	-36.3725	-73.7166	4.8	34.0	13.6	∼45
Humboldt	7	35	811	03/09/10	60	-36.3725	-73.7166	4.7	34.1	13.0	∼42
Humboldt	8	14-20	747	03/10/10	59	-36.3667	-73.7037	4.5	34.1	13.5	∼35
Humboldt	9	20-25	∼500	03/12/10	16	-33.3884	-71.8803	5	34.4	17.0	∼25
Humboldt	10	30-35	∼500	02/13/10	17	-33.4054	-71.8947	5	34.4	17.0	∼25
Humboldt	11	20	∼500	03/14/10	16	-33.3797	-71.88	4.8	34.4	18.5	∼19
Humboldt	12	30	∼500	03/14/10	16	-33.3896	-71.8802	4.9	34.4	18.5	∼10
Humboldt	13	20-30	4008	03/15/10	104	-32.1667	-72.6417	4.7	34.4	18.5	∼35
California	1	25	∼3100	06/26/11	81	33.69713	-121.2299	5.6	33.2758	14.0815	39
California	2	60	∼3700	06/27/11	133	33.57598	-121.7727	5.5	32.9479	14.7288	61
California	3	30	∼3500	07/02/11	87.5	34.107	-121.4224	5.6	33.5385	13.5503	22
California	4	20	∼3400	07/07/11	80	33.53098	-121.0963	5.4	33.5624	14.939	62

4.3.2 Humboldt Current sample collection

Prior to the cruise, all equipment to come into contact with samples was extensively acid-cleaned according to the procedures described in chapter 2 of this thesis, and double-bagged for transport to and from the sampling locations. While the original procedure called for using Teflon tubing and a Teflon pump to sample seawater, the pump failed after only two sample sites. After this, a CTD was used for sample collection. Each of the 24-Niskin bottles in the rosette were inspected for breaks in the plastic covering of the spring inside the bottle. Eight were found to have no exposures of the metal spring, and water was sampled only from these Niskin bottles.

Sampling sites from the Humboldt Current are plotted in Figure 4.1. The sampling procedure was adapted from procedures designed for the collection of particulate and dissolved samples for trace metal analysis (Cullen et al., 1999; Cullen, 2001). 30-50 L of mixed layer seawater samples were collected using a Teflon Yamada diaphragm pump (model DP-10F; Humboldt Current sites 1 and 2) or the Niskin bottles of a CTD (Humboldt Current sites 3-13). Water was either pumped directly into a 50 L carboy (sites 1 and 2), or allowed to empty into it from a Niskin bottle via acid-cleaned Tygon tubing (sites 3-13). The carboy was rinsed with seawater from the sampling site 3x before collecting seawater for filtering. A clean area was established in the ship's lab, and all filter manipulations were carried out under a Class 100 Laminar flow hood. After initial collection of seawater into the carboy, all sample processing took place within this hood.

The following discussion of sampling methods is represented schematically in Figure 4.3. Two 2 L aliquots were sub-sampled directly from the 50 L carboy and filtered onto GF/F filters for subsequent pigment analysis. When filtration was complete, pigment samples were immediately placed in a -80°C freezer, and stored at that temperature until analysis. Two 100 ml aliquots were sub-sampled directly from the carboy into clear French square-bottom bottles and preserved in 4% formaldehyde for future visual characterization of the phytoplankton community. When these two steps were complete, sea water was allowed to flow through a stack of three in-line filters housed in clean, Savillex Teflon-filter holders holding 60 µm

Nitex, 5 µm polycarbonate (Whatman), and 0.4 µm polycarbonate (Whatman) filters. The first ∼200 mls was not collected, and served to condition the apparatus for each sampling site. The filtering process for Humboldt Current samples was alternatively aided by positive pressure and suction. Positive pressure was supplied from compressed air through two 0.1 µm in-line filters to a modified cap on the carboy. Suction was applied by a separate vacuum pump and collected in a 1 L Savillex Teflon filtration rig, which was secured in-line below the 0.4 µm filter. Approximately 2.2 L of water was filtered through the 0.4 µm filter. The first ∼500 mls were used to rinse the Savillex filtration rig, a 1 L fluorinated high-density polyethylene (FLPE) bottle, a 500 ml low-density polyethylene (LDPE) bottle, and a 250 ml LDPE bottle 3 times each. A further 1.7 L was filtered, with 1 L added to the FLPE bottle, and 500 ml and 200 ml to each of the LDPE bottles, respectively. The FLPE bottle was filled first, and once filled was re-bagged and placed in a -20℃ freezer. The 500 ml and 250 ml samples were similarly double-bagged, but not frozen. The 500 ml bottle was acidified before analysis on shore. Water in the 1L FLPE bottle was used to determine nutrients, Cu_T, as well as organic ligands for both Fe and Cu. The 500 ml LDPE bottle was used to determine Fe_T. The 250 ml bottle was collected for future ICP-MS analysis.

After 1.7 L had been sampled through the stack of 3 filters and preserved accordingly for analysis (Figure 4.3), the 0.4 µm filter was removed to promote more rapid filtration. Filtering time for the remaining sample in the carboy onto 5 µm filters varied between sites, ranging between 4.5 to 26 hours. When filtering became slow, a 2 L Erlenmeyer flask was fitted to the base of the 5 µm filter, and suction was applied (Humboldt Current samples only). This method enabled a further ∼2 L to be filtered before slow filtration rates prompted replacement of the 5 µm filter. The used filter was folded in half with clean Tefzel tweezers and placed in an acid-cleaned 15 ml polypropylene centrifuge tube, which was stored in a -80℃ freezer. At no site did the 60 µm filter obstruct flow. Between sample sites, the Savillex filter rig, Tefzel tweezers, and in-line filters were rinsed with MQ water immediately after filtration was completed.

4.3.3 California Current sample collection

Samples collected in the California Current were sampled using a CTD and rosette designed for trace-metal sampling lowered on a nonmetallic hydroline. Sampling sites are plotted in Figures 4.2. Cleaning of equipment was the same as for the Humboldt Current, but the sample collection process was generally simpler. Samples were filtered onto a single 5 µm PC filter in a Teflon filter holder directly from the trace metal clean Niskin bottles under positive pressure supplied by nitrogen gas until filter clogged. After clogging, the filter was replaced until 30-50 L had been filtered. 750 ml of filtrate was further filtered through a 0.2 µm PC filter; 250 mls for total Cu determination and acidified to pH 1.8, and 500 ml un-acidified for Cu speciation.

4.3.4 Polyphosphate analysis

Polyphosphate analysis proceeded as described in chapter 3 of this thesis. As reported there, the data here represents extractable polyphosphate (*e*-poly P; Chapter 3 equation 3.1). Both 0.4 µm and 5 µm filters were sampled by either a trace metal clean pipette to scrape off some of the cells, or by tearing off a portion of the filter using acid-cleaned Tefzel tweezers and placing either the ripped filter or the pipette tip into acid-cleaned borosilicate 30 ml culture tubes. As direct contact of filters with the final liquid used in the assay did not take place in chapter 3, controls of acid-cleaned filters were used to establish their contribution of phosphate or poly P to analysis.

4.3.5 Iron and copper analysis

Iron and copper totals, speciation, and ligand data were collected by Randelle Bundy in the Barbeau lab at the Scripps Institution of Oceanography at UC San Diego. Total iron was assessed using the FeLume flow injection analysis system (Waterville Analytical) with an Fe(II) sulfite reduction chemiluminescent flow injection analysis (FIA) method, described previously and in greater detail in King and Barbeau (2007), (2011); King et al., (2012). Briefly, in this method,

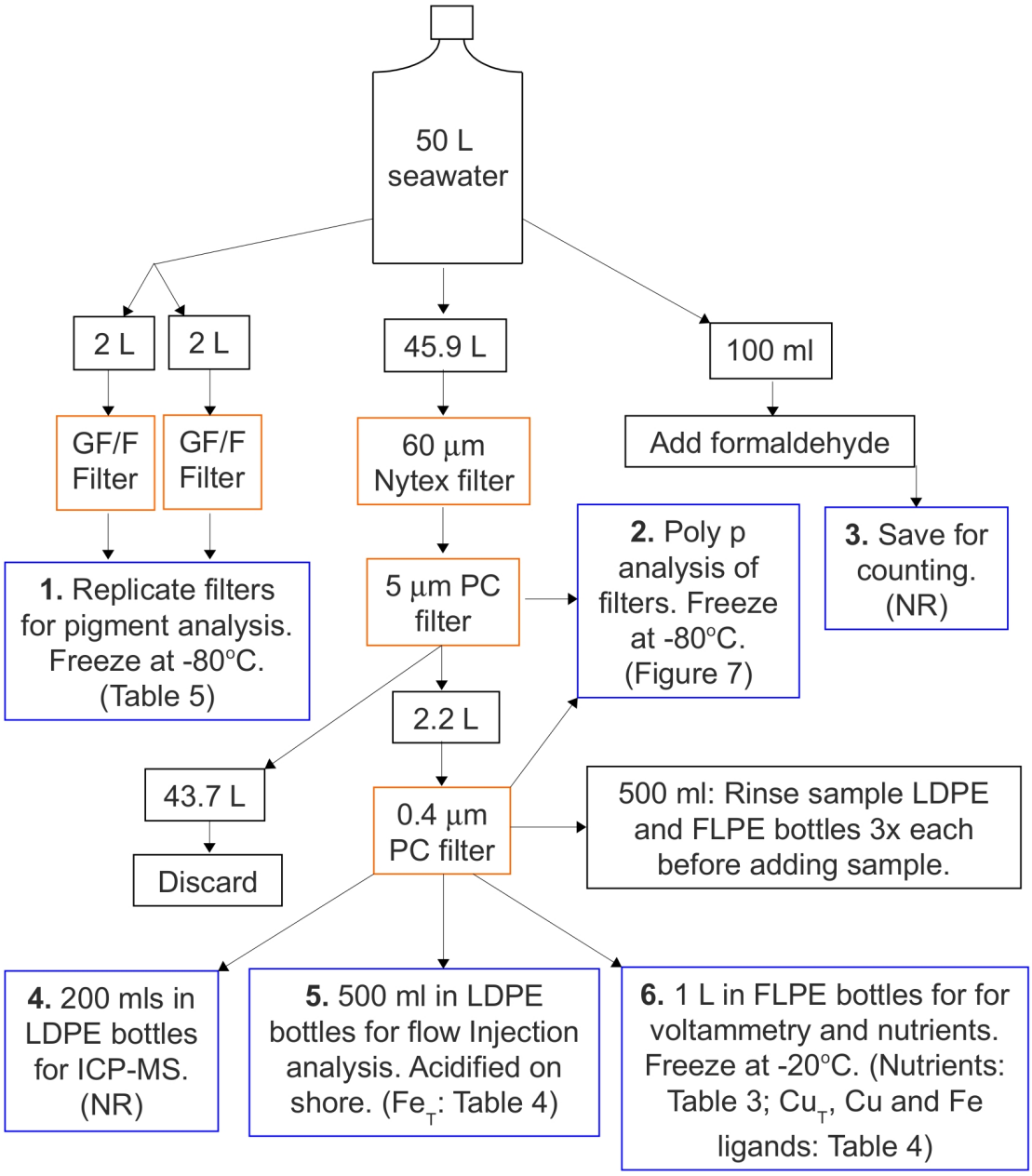

Figure 4.3: Schematic of sampling flow chart, and purpose (1-6) for each sample collected in the Humboldt Current. Fewer samples were collected from the simplified California Current sampling procedure. Orange boxes indicate a filtering step, whereas blue boxes represent a final sample. This chapter includes data from final samples in blue boxes 1, 2, 5, and 6. Samples for analyses 3 and 4 had not yet been processed as of this writing, as is indicated by 'NR' for 'not reported' in the appropriate boxes.

sodium sulfite is used to reduce iron in the sample, which after a concentration step onto nitriloacetic acid resin, is eluted in an HCl carrier solution then mixed with ammonia and luminol. Oxidiation of Fe(II) to Fe(III) catalyzes the oxidation of luminol, producing light at ∼426 nm that is then detected using a photomultiplier tube.

Total Cu was determined using adsorptive cathodic stripping voltammetry (ACSV; Buck Bruland, (2005)), and standard addition methods. With quartz lids, samples were UV-oxidized at ambient pH in a Jelight Model 342 UVO-Cleaner for 2 h at 10 mW/cm^2. 10 sub-samples were then pipetted into cleaned and conditioned Teflon voltammetric cups, buffered, and then appropriate copper standard additions were added to each cup. After moving the samples to a second set of voltammetric cups, the well-characterized competing ligand salicylaldoxime (SA) was added, samples were purged with oxygen-free argon gas, then analyzed on a BioAnalytical Systems (BASi) controlled growth mercury electrode (CGME).

An established competitive ligand exchange-adsorptive cathodic stripping-voltammetry (CLE-ACSV) method was used to measure the organic complexation of dFe (Rue and Bruland, 1995; Buck and Lohan, 2007) and Cu (Buck and Bruland, 2005; Bundy et al., 2012) with SA as the added ligand. A single sample for either Fe or Cu speciation determination was divided into 10 lidded Teflon Savillex vials (17 mL flat bottom), buffered, then known concentrations of dissolved inorganic Fe (ranging from 0 to 150 nM) or Cu (ranging from 0 to 20 nM) were added and allowed to equilibrate with the ambient ligands for at least 2 hours. 2.5 or 25 µM concentrations of SA were then added and equilibrated for at least 15 minutes at 25 µM, and 30 min at 2.5 µM (note, Fe was only characterized for Humboldt current samples). Each vial was run separately according to the same procedure as described above for ACSV. The linear current response was measured, and sensitivity determined from the linear portion of the titration curve where all the ligands are titrated with the added Fe or Cu. Results from the increasing Fe and Cu additions, after the titration of ambient ligands, were interpreted using linearization methods to calculate the concentrations of ambient Fe-binding ligands and their conditional stability constants (Scatchard, 1949; Ružić, 1982; van den

Berg, 1982; Mantoura and Riley, 1975).

4.3.6 Nutrient analysis

Nutrients (PO_4^{3-}, dissolved silica, NO_3^-, NO_2^-, and NH_4^+) were analyzed at the Oceanographic Data Facility (ODF) at the Scripps Institution of Oceanography at UC San Diego. Analyses are performed on a Seal Analytical continuous-flow AutoAnalyzer 3 (AA3). After each run, the charts were reviewed for any problems and final concentrations (in µmol/L) were calculated using SEAL Analytical AACE 6.07 software. Further information including references may be obtained at the ODF website: http://odf.ucsd.edu/index.php?id=473.

4.3.7 Pigment analysis

Pigments were analyzed on an Agilent 1100 series HPLC system using a method adapted from Zapata et al., (2000). The specifications for this method are: column: Waters Symmetry C8 column (3.5 4µm particle size, 4.6 x 150 mm, silica, reverse-phase); solvent A: methanol, acetonitrile and an aqueous pyridine solution (0.25M, pH=5) (50:25:25 v:v:v); solvent B: methanol, acetonitrile, and acetone (20:60:20 v:v:v); the gradient (time,%A, %B) 0, 100, 0; 12, 60, 40; 36, 0, 100; 38, 0, 100; 40, 100, 0.

Samples were extracted in 1.6 ml acetone doped with canthaxanthin as an internal standard and centrifuged for 5 minutes. 200 ml of the sample was placed in the auto sampler vial and kept at 1.2 ℃ prior to sampling. The auto sampler diluted the sample with MQ water to 70% acetone just prior to injecting 100 ml onto the column via the 500 ml sample loop. Data was processed using Agilents ChemStation for LC software (Rev.A.09.03).

Once processed, pigments were used to determine community composition as described in Goericke and Montoya (1998). Briefly, reasonable starting estimates for the ratio of various taxon-specific phytopigments to chlorophyll a based on published data were used to arrive at a minimum difference between measured and predicted total chlorophyll a using the Solver module in Microsoft Excel. These

estimates were then used to arrive at the percent contribution each taxon made to the entire phytoplankton community.

4.4 Results

4.4.1 Characterizing oceanographic context

Oceanographic data including depth of sample collection, water column depth, date collected, distance from shore, latitude, longitude, oxygen, salinity, temperature, and mixed layer depth are reported in Table 4.1. Nutrient data from samples are reported in Table 4.2. Nutrient levels are consistent with typical oceanographic values for these regions (Garcia et al., 2009), and N:P have a tight correlation. The N:P ratio is low relative to the Redfield ratio (10.4 instead of 16), but other studies have found similar N:P ratios in this region (Gruber and Sarmiento, 1997).

Table 4.2: Measured data for all sampling sites including nutrients, Fe-limitation proxies, Cu-speciation data, and *e*-poly P results. 'nd' indicates no data is available for that measurement at that site. Full Fe and Cu speciation data are included in Appendix I. As described in the methods, error for *e*-poly P results is ± 5%

Cruise	Site	Depth	NO_3	PO_4	Si	NO_2	NH_4	Si_{ex}	NO_3^-/dFe	log[Cu^{2+}]	*e*-poly P
		m	µM	µM	µM	µM	µM	µM	µM/nM	M	%
Humboldt	1	5-10	1.19	0.46	2.10	0.08	0.19	1.22	0.59	-15.96	16.88
Humboldt	2	5-10	4.82	0.46	1.05	0.04	0.24	-2.52	1.64	-16.52	44.90
Humboldt	3	30-40	7.23	0.85	0.80	0.16	0.74	-4.55	31.49	-15.98	3.73
Humboldt	4	10-20	0.20	0.37	0.40	0.01	0.00	0.26	0.49	-16.24	25.30
Humboldt	5	15	0.24	0.28	0.05	0.01	0.10	-0.13	0.51	-15.83	12.70
Humboldt	6	25-30	12.74	1.31	3.70	0.40	0.16	-5.73	11.68	-14.20	21.98
Humboldt	7	35	14.54	1.48	5.50	0.25	0.71	-5.26	12.75	-14.37	20.22
Humboldt	8	14-20	15.31	1.76	10.45	0.45	0.53	-0.88	6.12	-14.46	4.21
Humboldt	9	20-25	7.19	1.25	4.15	0.09	0.45	-1.17	7.90	-15.49	16.37
Humboldt	10	30-35	7.54	1.20	2.00	0.38	0.42	-3.58	13.47	-15.50	26.92
Humboldt	11	20	1.87	0.77	0.35	0.05	0.76	-1.03	2.19	-15.77	47.38
Humboldt	12	30	7.20	1.09	0.75	0.73	1.30	-4.57	nd	nd	12.07
Humboldt	13	20-30	2.10	0.82	0.50	0.05	0.37	-1.05	nd	nd	21.17
California	1	25	3.79	0.56	2.4	0.2	0.18	-1.39	nd	-16.19	23.33
California	2	60	0.01	0.25	1.3	0.04	0.21	1.29	nd	-16.59	26.30
California	3	30	8.46	0.97	1.6	0.29	0.08	-6.86	nd	nd	21.40
California	4	20	2.47	0.37	2	0.12	0.49	-0.47	nd	nd	17.20

Table 4.3: Percent contributions of different groups of microalgae to total chlorophyll a in Humboldt samples. TChl a = total chlorophyll a (µg/L), Dino = dinoflagellates, Diat = diatoms, Prym = prymnesiophytes, Pelag = pelagophytes, Synec = synechococcus, Chloro = chlorophytes, Crypto = cryptophytes, and Pro = prochlorococcus. All values are in %. Negative values are an artefact the minimization between predicted and measured Chl a.

Humboldt site	TChl a	Dino	Diat	Prym	Pelag	Synec	Chloro	Crypto	Pro
1	7.14	6	68	11	1	1	9	4	0
2	2.16	23	2	63	-1	3	7	3	0
3	0.57	18	35	22	1	3	17	5	0
4	3.51	13	58	13	0	2	10	3	0
5	1.96	8	71	13	0	2	0	5	0
6	1.12	4	17	12	0	20	25	22	0
7	1.10	1	8	10	0	28	27	27	0
8	1.72	2	8	10	0	33	43	4	0
9	0.98	2	4	15	2	52	12	5	7
10	0.85	3	6	25	5	18	23	6	12
11	0.15	10	-4	35	9	20	14	0	16
12	0.56	4	6	34	11	-5	32	7	12
13	0.16	13	-4	62	6	4	10	0	10

4.4.2 Speciation data

Speciation data for both Fe and Cu is reported in Appendix I. No speciation data is available for Humboldt Current sites 12 or 13, as sampling opportunities exceeded expectations and supplies of trace-metal clean bottles for trace metal analysis samples were exhausted. Speciation results for California Current samples were returned only for Cu for the first two samples, but at two analytical windows.

While Humboldt Current samples 6-8 were initially analyzed at a lower analytical window, it was found that the ligands were exceptionally strong, with a conditional stability constant $\log K_{CuL,Cu2+}{}^{cond} > 13.5$; which I take as the cutoff between 'strong' and 'weak' copper ligands (Bundy et al., 2012). Cu L_s

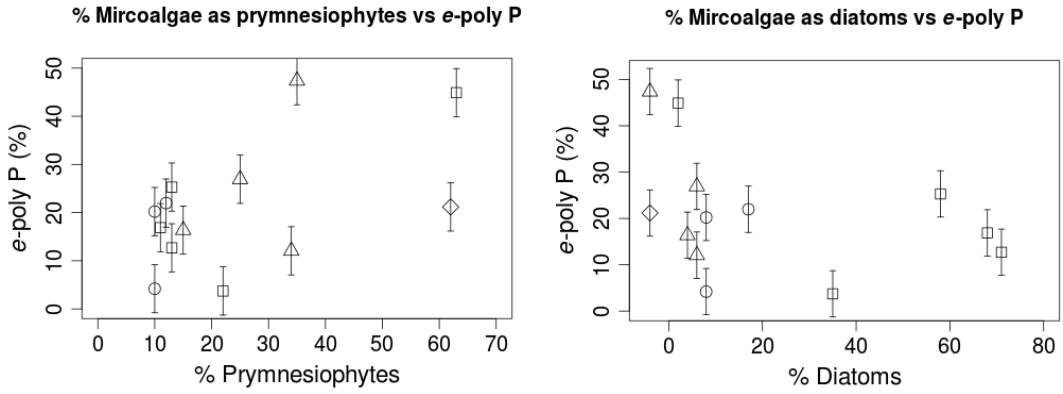

Figure 4.4: Percent microalgal community composed by prymnesiophytes (left) and diatoms (right) vs *e*-poly P. Though the trend with increasing poly P is positive for prymnesiophytes and negative for diatoms, neither trend is statistically significant.

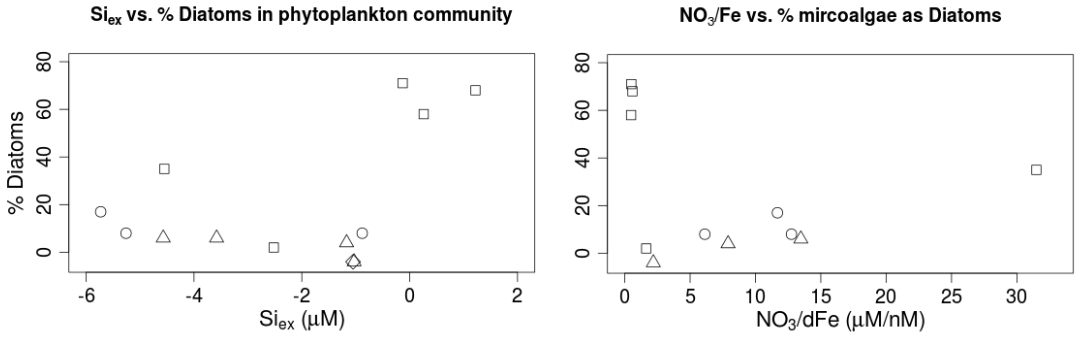

Figure 4.5: Si_{ex} (left) and NO_3^- /dFe (right) vs. % microalgal community composed of diatoms. When Si_{ex} is $\sim$ 0 or positive, diatoms make up $>$ 50% of the microalgal community. Diatom composition decreases sharply at Si_{ex} $\sim$ -1, then increases as Si_{ex} becomes more negative. This trend is mirrored when comparing % diatoms to NO_3^- /dFe, as might be expected since both are proxies for iron limitation.

strength averaged 15.39 for Humboldt Current samples, and varied between 14.83 and 16.03 (n=8). Cu L_w strength averaged 13.94 for Humboldt Current samples, and varied between 13.9 and 13.95 (n=3). In the California Current samples, $\log K_{CuLs,Cu2+}{}^{cond}$, had values of 16.03 and 16.45 at the higher analytical window, and $\log K_{CuLw}$, Cu^{2+}cond had values of 14.3 and 14.8. $\text{Log}K_{CuLw,Cu2+}{}^{cond}$ were 13.48 and 13.67. At no station were copper ligands saturated, resulting in relatively low $[Cu^{2+}]$ at all stations, with $\log[Cu^{2+}]$ ranging from -16.24 to -14.45 in Humboldt Current samples, and values of -16.18 and -16.59 in the California Current. Ligand concentrations averaged 7.48 nM in the Humboldt Current, and ranged between 4.75 and 13.79 nM. The excess in Cu ligands (i.e. $[L_s]$-$[Cu_T]$) appeared to be low close to shore (< 20 miles), to increase substantially between 20-30 km offshore, and then decrease to much lower levels further from shore.

Similarly, Fe ligands were in excess at all Humboldt Current stations (no Fe data are available for California Current samples), with concentrations ranging between 2.72 and 6.01 nM with an average concentration of 4.07 ± 1.16 nM. Total Fe concentrations ranged from 0.23-2.93 nM, which is in line with other measurements of Fe made in a coastal upwelling regime off the coast of Peru (Bruland et al., 2005). Excess ligands (i.e. $[L_s]$ -[dFe]) ranged from 1.86-3.76 nM; a much smaller range than eL_{Cu} and with no discernible trend. Iron concentrations are highest in the first two, pump-collected Humboldt Current samples, and at sites 6-8, where stormy conditions prevailed and a deep mixed layer was observed. Iron ligand strength averaged $\log K_{FeLs,Fe'}{}^{cond} = 11.65 \pm 0.32$, and varied between 11.16 and 12.3. There is a strong correlation between the concentration of Fe ligands and the total Fe concentration, with a similar slope as noted in previous studies (King et al., 2012).

4.4.3 Proxies for iron limitation

Proxies for iron limitation have been used in the California Current to determine the *in situ* state of iron deficiency in phytoplankton communities. Though most effectively deployed in tandem with batch experiments and Fe-addition, I use them nonetheless to establish a baseline of data for this region. I report results in

my samples using two of these proxies, NO_3^-/dFe and Si_{ex}, and data are reported in Figure 4.6.

NO_3^-/dFe is calculated simply by dividing the total nitrate by the total dissolved Fe (dFe) measured. Si_{ex} is calculated as:

$$Si_{ex} = [Si(OH)_4] - [NO_3^-] * R_{Si:NO3}^-$$

where $R_{Si:NO3}^-$ is the ratio of Si:NO_3^- in upwelled source waters (King and Barbeau, 2011). When R is 1, its approximate value in the California Current, this term may be ignored. The area of the Humboldt Current sampled is largely fed by Subantarctic Water, with an influence from Antarctic Intermediate Water (Carr and Kearns, 2003). These source waters are some of the most depleted with respect to Si in the world (Sarmiento 2004), so it is unreasonable to expect an $R_{Si:NO3}^-$ of 1 for upwelled waters. To apply a more appropriate correction, I use the average of the Si:NO_3^- ratio at 200 m depth between 47-32^{o}S latitude and 71-77^{o}W longitude from the JFM World Ocean Atlas, 2009 (Garcia et al., 2009). These data (n=47) have a mean of 0.74, with a standard deviation of 0.2. I have used this value for $R_{Si:NO3}^-$ in the Humboldt Current Si_{ex} data reported in Table 4.2.

Si_{ex} values for the Humboldt Current range from -5.7 to 1.2, and NO_3^-/dFe values range from 1 to 31.5. King et al. (2012) found that a NO_3^-/dFe > 8 indicated iron limitation, though King and Barbeau, (2007) find evidence for Fe-limitation in bottle experiments when the NO_3^-/dFe was low as $\sim$5. By this measure, approximately half of my samples display evidence of iron limitation. Si_{ex} values are quite low relative to previous studies. For example, King and Barbeau (2011) find only 120 instances of mixed layer Si_{ex} values < 1 out of 8415 stations sampled (i.e. 1.4% of all observations) in a 24 year period from 1985-2009 in the California Current, whereas 9 of 13 Humboldt Current samples have values $<$ -1.

4.4.4 Pigment data

Phytoplankton community composition data were collected for the Humboldt Current samples by analyzing phytopigments and minimizing the difference

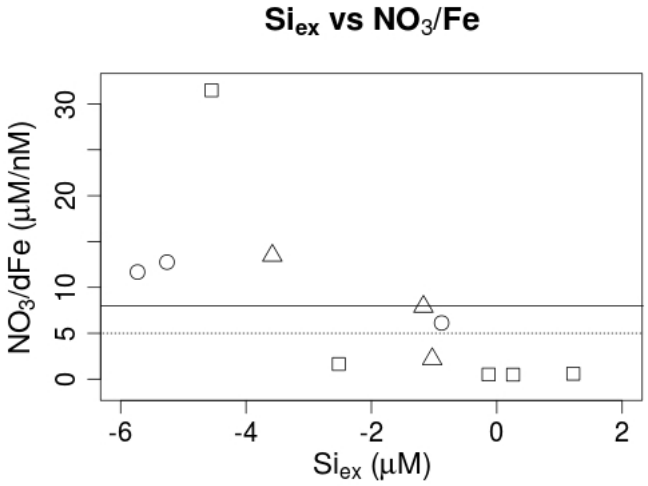

Figure 4.6: Si_{ex} vs NO_3^-/dFe; proxies for iron limitation. Negative Si_{ex} values suggest preferential draw-down of Si relative to NO_3^- by Fe-limited diatoms, while a ratio of NO_3^-/dFe > 8 (solid line) has been found to indicate iron limitation, though bottle experiments have shown phytoplankton may be Fe-limited when NO_3^-/dFe is as low as 5 (dotted line).

between predicted and measured chlorophyll a. The difference minimization was fairly good, with a maximum deviation of 29%, though most sites achieved 0% difference (Table 4.3). A stable solution could not be found when peridinin was included in the minimization, so it was excluded and a reasonable estimate was used instead. Poly P was not found to correlate significantly with any phytoplankton group, though prymnesiophytes are the most abundant taxon at the highest 2 poly P measurements (Figure 4.4).

Diatoms are most abundant ($> 50\%$ of the population) at the most positive Si_{ex} values, and least abundant when Si_{ex} is -1. Similarly, diatoms are most abundant at the lowest three NO_3^-/dFe values, are nearly absent at low NO_3^-/dFe, and increase as NO_3^-/dFe values increase (Figure 4.5). No other group of phytoplankton shows such coherent trends in both these markers for Fe-limitation.

4.4.5 Polyphosphate procedure

The addition/subtraction of phosphate or poly P by filters during analysis was assessed, as introduction of the polycarbonate filter added an additional source of error to measurements not present in chapter 3. Multiple controls with and without a P std added were established to determine whether the filter added to the blank, removed phosphate, or added polyphosphate to the analyses. Results indicate that sampling procedures do not add significant P to the analysis (n=12). The absorbance reading at A_{882} was observed to increase in the TCP fraction relative to the SRP fraction by an average of 0.0008. This was indistinguishable from the detection limits of the instrument, determined as 3x the standard deviation of a reference standard run after every 6 measurements. I therefore conclude that the 5 µm PC filters added no poly P to the measurements.

0.4 µm filter blanks were also investigated (n = 7), though these filters appeared to contribute to detection of poly P. A_{882} readings differed between the SRP and TCP samples by an average of 0.0032, with a standard deviation of 0.0028. This was roughly equivalent to a 0.005-0.01 mg PO_4^{3-}/L increased reading due to poly P. The high variability precluded simply subtracting out a standard amount, the data were thus deemed unreliable, and are not reported.

Extractable poly P data for Humboldt and California Current samples are in Table 4.2. In all but one case, later replicate measurements of Humboldt Current samples were found to drift towards higher *e*-poly P values. Though both California and Humboldt Current samples were kept on ice during sampling to prevent cell rupture, it was observed that thawing did occur in Humboldt Current samples. While this upward drift could be casued by removal of orthophosphate or addition/polymerization of polyphosphate, I consider removal of orthophosphate onto the filter or centrifuge tube walls after cell rupture more likely. Such drift was not observed with California Current samples, presumably since they were sampled without allowing complete thawing before returning to the freezer. I therefore report only the first measurement of the Humboldt Current samples (which was measured in triplicate), and the average of three replicates (each measured in triplicate) for California Current samples. California Current sample 4 was measured

n=8 with a sd of ∼5%. This is taken as the error of analysis for all samples.

4.4.6 Polyphosphate data and analysis

Values ranged from 4 to 47% of extractable cellular phosphorus as poly P in Humboldt Current samples (mean = 21%, sd = 13%), and 17-26% in California Current samples (mean = 22%, sd = 4%). No significant linear correlation was found between *e*-poly P and any nutrient, trace metal, phytoplankton taxon, or physical property measured. The data were subdivided into regimes based on the distribution of NO_3^-, [Cu^{2+}], and Fe-limitation proxies. The definitions for each regime are listed in Table 4.4. Plotting NO_3^- against temperature and salinity suggested 4 nutrient regimes (Figure 4.7), so samples were divided into an oligotrophic regime, one low- and one high-nutrient transition regime, and one nutrient-replete regime (see Table 4.4 for regime definitions). The correlation between nitrate and phosphate was strong for this sample set ($R^2 = 0.824$, p-val = 1.1E-5), and diatoms and small phytoplankton are expected to most commonly encounter nitrogen limitation in this region (Moore et al., 2002), so nitrate instead of phosphate was used to establish nutrient regimes. Only 13 samples had associated Cu-speciation data (Humboldt Current sites 1-11, California Current sites 1 and 2), with values ranging over 3 orders of magnitude. As all values were quite low, and lacking any published expectation of how these levels might affect poly P, these data were arbitrarily divided into 'high', 'medium', and 'low' [Cu^{2+}] regimes.

Fe-limitation regimes were determined using both Si_{ex} and NO_3^-/dFe. Si/NO_3^- was also considered, but its correlation with NO_3^-/dFe was much worse than the correlation between Si_{ex} and NO_3^-/dFe (p-val = 0.013, $R^2 = 0.461$ for Si_{ex} vs. p-val = 0.099, $R^2 = 0.193$ for Si/NO_3), so was not considered further as a useful Fe proxy in this data set. While King and Barbeau (2011) provide a numerical basis for dividing samples into Fe-replete, conditionally Fe-limited, and Fe-limited regimes based on NO_3^-/dFe data and on-ship Fe-addition bottle experiments, the same numerical basis is not available for Si_{ex}. As Fe data were only available for some of the samples though Si_{ex} was available for all samples, it was desirable to link Si_{ex} and Fe/NO_3^- so all samples could be incorporated into

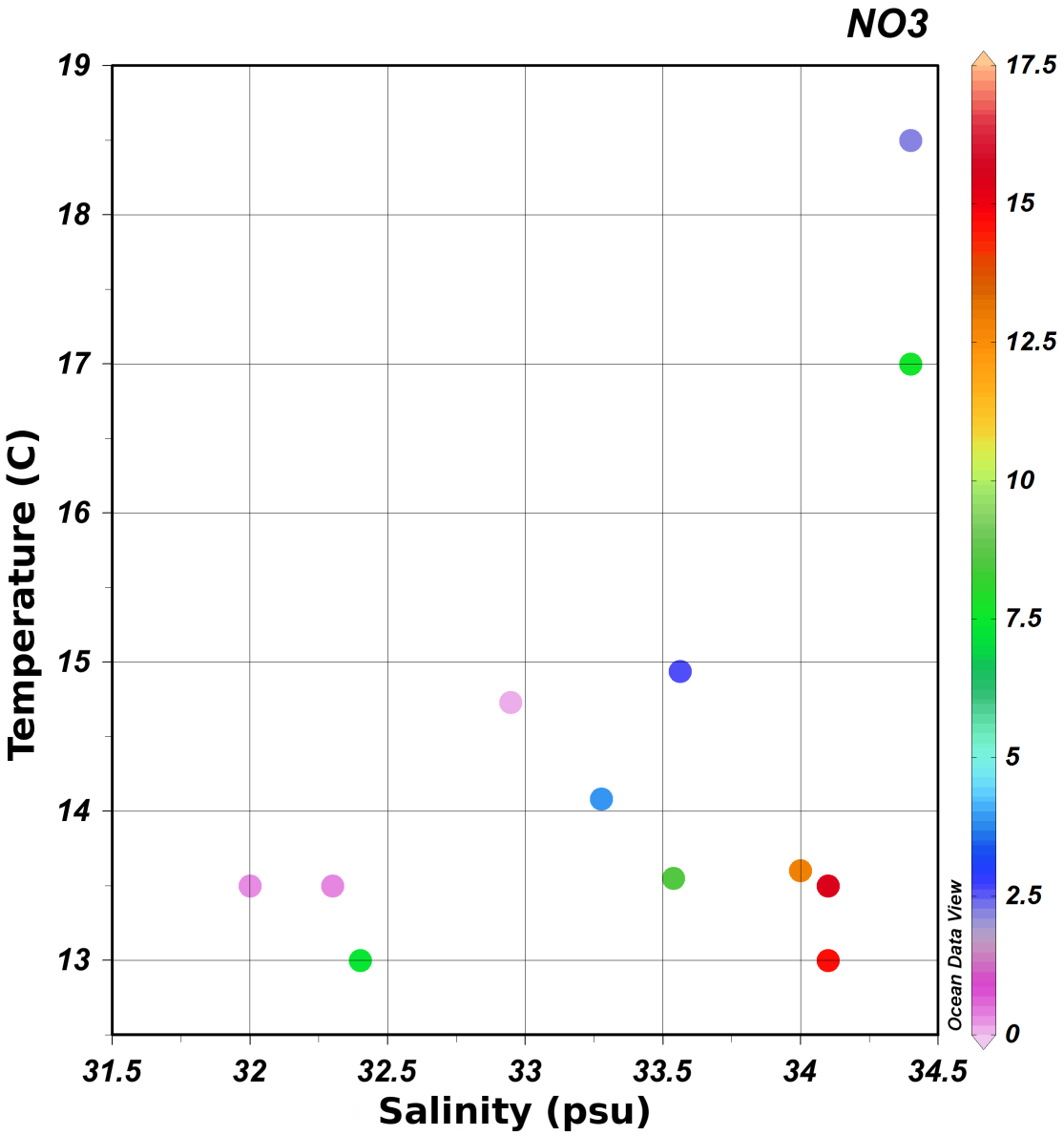

Figure 4.7: Salinity (psu) vs temperature (℃) vs. measured nitrate (µM/L) for Humboldt and California Current samples.

the analysis. These two properties were thus plotted against each other, and the linear regression comparing Si_{ex} and NO_3^-/dFe ($R^2 = 0.461$, p-val = 0.013) was used to arrive at numerical thresholds for the Fe-replete, conditionally Fe-limited, and Fe-limited regimes using Si_{ex} values.

With the regimes thus established and defined, average *e*-poly P data from the community were compared in each regime using a Welch two-sample T-test. The high and low regimes were compared with each other (Table 4.4), though no comparison displayed a statistically significant difference. Nutrient regimes showed the strongest difference in average *e*-poly P when all data were included (Table 4.4), but this result should be treated with caution, due to the small sample size, high variability within those regimes, and considering the error of the measurements.

4.4.7 Cu^{2+} and Nutrients

Nutrients were found to have a statistically significant ($p < .01$) correlation to log[Cu^{2+}] (Appendix I). The correlation was strongest with nitrate, decreasing for phosphate, nitrite, and dSi, respectively. Ammonia displayed no correlation with Cu^{2+}, nor did Cu_T or Fe_T .

4.5 Discussion

4.5.1 Reflection on methods

This study roughly doubles the existing published data for poly P measurements of marine phytoplankton collected *in situ*. Average values are in line with previously published results, though included here are 2 sites with poly P values substantially higher than any previously published results (Humboldt Current sites 2 and 11). Co-determining poly P along with nutrients, metal speciation, and phytoplankton community composition is unprecedented, and provides an excellent means for evaluating any influence these variables may have on *e*-poly P in a single packet of water.

Using the extraction method for poly P enabled the rapid and relatively

Table 4.4: A summary of parameters used to establish regimes for comparing poly P. Results from a Welch two-sample t-test are reported below the defined parameters for nutrient regimes (top section), Fe-limitation parameters (middle section), and $[Cu^{2+}]$ (bottom section). No parameter considered showed a significant (p-val < 0.05) difference in community poly P allocation between the regimes considered.

Nutrient Regimes

	NO_3^-		
Regime	Definition	PPB avg	n
Low	$[NO_3^-] < 1$	21.43±7.57	3
Med-low	$1 \leq [NO_3^-] < 5$	28.48±13.91	6
Med-high	$5 \leq [NO_3^-] < 10$	16.1±8.87	5
High	$10 \leq [NO_3^-]$	15.47±9.79	3

p-value = 0.4538 (High vs Low); 0.061 (Low+Med-low vs Med-high+High)

Fe-Limitation Regimes

	NO_3^-/Fe			Si_{ex}		
Regime	Definition	PPB avg	n	Definition	PPB avg	n
Fe-limited	NFe > 8	18.21±15.93	5	$Si_{ex} < -2$	21.6±8.22	6
Conditional	8 ≥ NFe > 5	10.29±8.60	2	$-2 \leq Si_{ex} < -1$	27.06±13.85	4
Fe-replete	5 ≥ NFe	29.43±10.06	4	$-1 \leq Si_{ex}$	17.09±12.80	7

NO_3^-/dFe p-value = 0.2408 (Fe-limited vs Fe-replete)

Si_{ex} p-value = 0.4614 (Fe-limited vs Fe-replete)

Cu Speciation Regimes

Regime	Definition	PPB avg	n
Low	$\log[Cu^{2+}] < -16$	15.8±10.04	4
Med	$-16 \leq \log[Cu^{2+}] < -15$	21.85±15.07	6
High	$-15 \leq \log[Cu^{2+}]$	29.03±9.79	3

p-value = 0.1195

low-cost evaluation of poly P in natural phytoplankton assemblages. While this approach excludes a portion of the cell in the analysis, it nonetheless yields consistent results (Eixler et al., 2005, chapter 3). The low cost and high speed with readily available materials and instrumentation enables multiple determinations of *e*-poly P in virtually any lab with a UV-visible spectrophotometer. Subsequent determinations highlight the importance of proper sampling methods for examining poly P. While thawing of the samples would not be a problem for trace-metal characterization of the phytoplankton community using this method (for which it was originally designed; Cullen et al., 1999; Cullen, 2001), it is problematic for P. Care should be taken to ensure that samples are not allowed to thaw during sampling either by keeping samples on dry ice when sampling, or quickly processing small batches of samples at a time. Consideration might also be given to using different materials for filtration and storage, but this could limit the ability to do poly P and trace-metal work on the same sample.

4.5.2 Nutrients and poly P

The literature is contradictory as to whether high or low [PO_4^{3-}] results in poly P accumulation. There are reports indicating that poly P increases with elevated PO_4^{3-} (Perry, 1976; Solorzano and Strickland, 1968), and that it increases under low-PO_4^{3-} stress as part of a P 'overplus' response (Voelz et al., 1966; Orchard et al., 2010), or as part of a generalized stress response (Dyhrman et al., 2012). The data I report here does not offer support to these hypotheses. While I do find slightly higher average poly P at lower [PO_4^{3-}], which would support the 'overplus' and/or general stress hypotheses, the difference is not statistically significant, especially after considering measurement error (Table 4.4).

4.5.3 Fe-limitation and poly P

While no study has directly linked Fe-limitation specifically to enhanced poly P accumulation, studies have hypothesized that poly P accumulation may occur as part of a generalized stress response in diatoms (Dyhrman et al., 2012)

and other organisms (Seufferheld et al., 2008). It is on this basis that I evaluate the Fe-limitation state of phytoplankton communities for comparison with poly P measurements. While many sites exhibited evidence of Fe-limitation, no correlation between this and *e*-poly P is observed. This may indicate that any generalized stress response involving poly P does not include the response to Fe-limitation, or that any such signal in this limited sample set is too small to resolve.

4.5.4 Copper and poly P

All [Cu^{2+}] measurements in this study were quite low, so it is not surprising that no significant correlation between [Cu^{2+}] and *e*-poly P was observed. Quantitative evidence for copper affecting phytoplankton allocation of P to poly P is limited to the previous chapter of this thesis, and in that study most diatoms did not show a response below ∼1E-12 [Cu^{2+}], a concentration far above any concentration measured in this study.

4.5.5 Community composition and poly P

Though poly P was not found to correlate significantly with any phytoplankton group (Figure 4.4, Appendix H), prymnesiophytes are the dominant taxa at the highest 2 poly P measurements. While this may indicate prymnesiophytes have an unusual ability to accumulate poly P, more data would be needed to verify this claim, especially since a high % of prymnesiophytes (62%) co-occurs with a poly P concentration of 21%, the average over all Humboldt Current sites, at site 13. Analyses of variable poly P allocation with the growth cycle of phytoplankton taxa other than diatoms in both laboratory and field settings will likely be useful in enhancing our understanding of spatial and temporal variability of poly P in the marine environment.

Diatoms are most abundant (> 50% of the population) at the most positive Si_{ex} values (Humboldt Current sites 1, 4 and 5), and least abundant when Si_{ex} is ∼ -1 (Figure 4.5). The three most positive Si_{ex} values also coincide with the lowest nutrient concentrations of the Humboldt Current sites sampled. High diatom con-

centrations ($> 17\%$) and positive Si_{ex} values were only observed at southern, colder sampling sites (Tables 4.1 and 4.3). It appears then that at the time of sampling, southern sites were Fe-replete, allowing drawdown of both NO_3^- and dissolved silica in roughly a 1:1 ratio. Either as the Humboldt Current flows north or due to upwelling of different source waters, substantial Fe-limitation and drawdown of Si relative to NO_3^- by diatoms is a characteristic of more northerly waters, as are higher overall nutrient concentrations.

4.5.6 Importance of the growth cycle for poly P

The general lack of statistically significant correlation between any of these variables and poly P may be related to the magnitude of variability observed in *e*-poly P with the growth cycle (Chapter 3). If *e*-poly P variability with the growth cycle is the dominant driver of short-term poly P allocation in phytoplankton communities in the surface ocean, then the wide variability in *e*-poly P observed in this study is exactly what would be expected in a study that randomly samples different phytoplankton communities in various stages of growth. Thus, future studies wishing to assess the effects of nutrients, metals, Fe-limitation, or phytoplankton assemblage on *in situ* poly P will likely have to control for variability due to the growth cycle of the community being sampled.

4.5.7 Data in EBCs

These data show that phytoplankton communities allocate a wide range of P to *e*-poly P in EBCs that is not strongly correlated with nutrients, Fe-limitation, $[Cu^{2+}]$, or phytoplankton community composition. The average allocation is substantial, indicating that poly P released to the water column from cell lysis due to cell death or grazing is considerable. There is evidence that at least some of this poly P is refractory, and current standard methods of analysis do not adequately resolve this fraction of dissolved phosphorus. The role of poly P in P cycling in the surface ocean is thus poorly constrained, but possibly important. While P is not likely to be the limiting nutrient in the California or Humboldt Currents sampled

here (Moore et al., 2002), in regions where PO_4^{3-} is the limiting nutrient, a better understanding of poly P cycling could be important.

Considering the ability of poly P to nucleate apatite formation, EBCs are a good starting place to begin investigating poly P allocation in phytoplankton communities due to the large export from the photic zone in EBCs. However, the wide distribution of fine-grained apatite deposits throughout marine sediments (Ruttenberg and Berner, 1993; Benitez-Nelson, 2000) indicates that highly productive EBCs are not the only important locations for understanding the poly P apatite removal and sequestration mechanism identified in Diaz et al. (2008). Initial studies have shown comparable accumulation of poly P to the values found here in *Trichodesmium spp* in an oligotrophic gyre (Orchard et al., 2010). These regions deserve further study as well.

4.5.8 Conclusions

Here I evaluate nutrient, $[Cu^{2+}]$, Fe-limitation, and phytoplankton community composition data with respect to community *e*-poly P using data collected on 2 cruises of opportunity in the California and Humboldt Currents. I find a relatively high amount of P allocated to *e*-poly P in general (average = 21% in Humboldt Current sites, and 22% in the California Current), but with variability from 4-47%. However, I find no significant correlation between *e*-poly P and any other variable tested. This may be explained by the random nature of the sampling, and the wide variability in *e*-poly P that occurs with the growth cycle.

Appendix A

Growth Data for Chapter 2

A.1 Tables A.1-5 pertain to Cu-treated cells, A.6-11 to Zn-treated cells, and A.12-17 to Cd-treated cells

Table A.1: Absorbance at 400 nm. Blanked instrument with DI water before and after measuring all 8 samples. "nd" means no data, and "collected" indicates a samplewas filtered the day before. Filtering and rinsing 2 samples took 3-6 hours.

Absorbance at 400 nm										
Sample#	Blank	1	2	3	4	5	6	7	8	Blank
Cu_T added (M)	before	1.0E-8	3.0E-8	1.0E-7	3.0E-7	1.0E-6	3.0E-6	1.0E-5	5.0E-5	after
08/27/09	0.045	0.054	0.052	0.052	0.051	0.052	0.05	0.051	0.051	0.043
08/28/09	0.043	0.053	0.052	0.053	0.052	0.053	0.053	0.056	0.055	0.046
08/29/09	0.045	0.061	0.062	0.068	0.065	0.074	0.071	0.074	0.076	0.046
08/30/09	0.045	0.095	0.095	0.124	0.115	0.144	0.137	0.145	0.142	0.048
08/31/09	0.047	0.164	0.162	0.184	0.179	0.198	0.197	0.193	0.2	0.046
09/01/09	0.046	0.204	0.201	0.217	0.219	0.243	0.237	0.226	0.236	0.044
09/02/09	0.043	0.251	0.24	0.251	0.271	0.29	0.281	0.268	0.286	0.044
09/03/09	0.046	0.298	0.286	0.306	nd	0.348	0.334	0.312	0.333	nd
09/04/09	0.045	collected	collected	collected	collected	0.396	0.375	0.362	0.377	0.045

Table A.2: Fluorescence at 660 nm. Blanked instrument with DI water before and after measuring all 8 samples. "nd" means no data, and "collected" indicates a samplewas filtered the day before. Filtering and rinsing 2 samples took 3-6 hours.

Fluorescence at 660 nm										
Sample#	Blank	1	2	3	4	5	6	7	8	Blank
Cu_T added (M)	before	1.0E-8	3.0E-8	1.0E-7	3.0E-7	1.0E-6	3.0E-6	1.0E-5	5.0E-5	after
08/27/09	0.08	0.84	0.72	0.870	0.75	0.68	0.89	0.78	0.76	0.23
08/28/09	0	0.89	0.93	0.900	1	1.06	0.9	1.11	0.91	0.07
08/29/09	0.06	1.55	1.52	2.140	2.03	3	2.65	2.98	2.81	0.06
08/30/09	0.045	4.46	4.42	8.110	7.13	9.53	8.92	9.58	9.77	0.048
08/31/09	0.047	11.92	11.06	13.050	13.1	12.91	12.58	12.47	13.61	0.046
09/01/09	0.046	15.08	14.15	14.330	15.69	15.22	14.35	14.5	16.34	0.044
09/02/09	-0.02	17.15	15.08	14.830	17.28	16.97	14.48	15.69	17.17	0.02
09/03/09	0.09	18.24	16.27	17.280	18.49	18.67	17.34	16.43	19.07	nd
09/04/09	-0.02	sampled	sampled	sampled	sampled	25.12	22.65	32.38	36.74	0.16

Table A.3: pH meter was calibrated daily with a slope > 0.95.

	pH							
Sample#	1	2	3	4	5	6	7	8
Cu_T added (M)	1.0E-8	3.0E-8	1.0E-7	3.0E-7	1.0E-6	3.0E-6	1.0E-5	5.0E-5
08/27/09	8.16	8.16	8.090	8.1	8.13	8.12	8.08	7.93
08/28/09	8.12	8.11	8.090	8.1	8.1	8.06	8.09	8.06
08/29/09	8.14	8.14	8.150	8.14	8.14	8.12	8.13	8.1
08/30/09	8.2	8.2	8.300	8.23	8.31	8.28	8.32	8.26
08/31/09	8.37	8.36	8.370	8.33	8.37	8.36	8.37	8.33
09/01/09	8.31	8.32	8.350	8.35	8.34	8.33	8.34	8.33
09/02/09	8.3	8.32	8.450	8.3	8.28	8.27	8.29	8.27
09/03/09	8.33	8.31	8.320	8.3	8.29	8.27	8.27	8.25

Table A.4: Cell counts by hemocytometer. Counts include the cultures with the highest and lowest ABS. 2 counts were made for each sample, and are vertically stacked. Counts are not included for innoculation day, since all cultures wereinoculated to have the same starting concentration of 1E5 cells/ml.

	Cell Counts by hemocytometer							
Sample#	1	2	3	4	5	6	7	8
Cu_T added (M)	1.0E-8	3.0E-8	1.0E-7	3.0E-7	1.0E-6	3.0E-6	1.0E-5	5.0E-5
08/28/09	4						19	
	4						17	
08/29/09	24				56			
	15				38			
08/30/09		70						240
		110						153
08/31/09		141						214
		154						226
09/01/09		138						288
		207						207
09/02/09		232			325			
		286			337			
09/03/09		248						340
		295						350

Table A.5: The difference in the time frame used to calculate the growth rate for cultures 1 and 2 vs. 3-8 may be explained by the fact that the cultures were inoculated from different growth stocks. Though all cultures were inoculated to the same initial density of cells, they were inoculated from 3 different bottles. 1-2 were inoculated from the same bottle, which may have been at a different stage in growth as compared to the other two bottles used to inoculate the remaining cultures.

Maximal Growth Rate, Days 1-4				
Sample #	Cu_T added (M)	Growth Rate	Average	stdev
1	1.0E-8	0.68	0.72	0.05
2	3.0E-8	0.66		
3	1.0E-7	0.73		
4	3.0E-7	0.65		
5	1.0E-6	0.73		
6	3.0E-6	0.76		
7	1.0E-5	0.72		
8	5.0E-5	0.79		

Table A.6: Absorbance at 400 nm. Blanked instrument with DI water before and after measuring all 8 samples. "nd" means no data, and "collected" indicates a samplewas filtered the day before. Filtering and rinsing 2 samples took 3-6 hours.

Absorbance at 400 nm										
Sample#	Blank	1	2	3	4	5	6	7	8	Blank
Zn_T added (M)	before	8.5E-10	7.6E-9	6.9E-8	6.2E-7	1.9E-6	5.6E-6	1.7E-5	5.0E-5	after
05/22/11	0.056	0.085	0.065	0.067	0.062	0.064	0.062	0.063	0.063	0.056
05/23/11	0.055	0.067	0.068	0.069	0.069	0.069	0.068	0.07	0.068	0.056
05/24/11	0.054	0.078	0.081	0.091	0.095	0.092	0.091	0.093	0.092	0.056
05/25/11	0.055	0.105	0.118	0.145	0.144	0.149	0.146	0.146	0.144	0.056
05/26/11	0.056	0.156	0.172	0.178	0.175	0.183	0.174	0.176	0.155	0.058
05/27/11	0.058	0.174	0.19	0.219	0.185	0.21	0.19	0.197	0.172	0.057
05/28/11	0.076	0.215	0.236	0.25	0.23	0.261	0.239	0.241	0.207	0.062
05/29/11	0.062	0.203	0.23	0.247	0.237	0.263	0.241	0.233	0.208	0.061

Table A.7: Fluorescence at 660 nm. Blanked instrument with DI water before and after measuring all 8 samples. "nd" means no data, and "collected" indicates a samplewas filtered the day before. Filtering and rinsing 2 samples took 3-6 hours.

Fluorescence at 660 nm										
Sample#	Blank	1	2	3	4	5	6	7	8	Blank
Zn_T added (M)	before	8.5E-10	7.6E-9	6.9E-8	6.2E-7	1.9E-6	5.6E-6	1.7E-5	5.0E-5	after
05/22/11	0.15	0.61	0.54	0.54	0.71	0.49	0.4	0.76	0.69	-0.07
05/23/11	0.08	0.84	1.28	1.39	1.6	1.47	1.66	1.53	1.44	0.03
05/24/11	-0.04	2.15	3.21	4.67	4.77	4.62	5.01	5.21	4.66	0.15
05/25/11	0.01	4.48	7.9	9.42	9.55	9.49	9.75	9.45	8.35	0.19
05/26/11	0.37	7.18	10.23	11.84	12.48	14.85	11.55	11.44	9.75	-0.12
05/27/11	0.26	7.97	12.06	13.66	12.65	14.37	13.2	13.16	11.02	-0.2
05/28/11	0.17	9.89	18.83	21.14	13	15.01	12.96	12.01	13.39	0.07
05/29/11	0.14	8.73	13.14	15.61	15.1	18.03	13.09	12.39	8.72	0.1

Table A.8: pH meter was calibrated daily with a slope > 0.95.

pH								
Sample#	1	2	3	4	5	6	7	8
Zn_T added (M)	8.5E-10	7.6E-9	6.9E-8	6.2E-7	1.9E-6	5.6E-6	1.7E-5	5.0E-5
05/22/11	8.3	8.31	8.3	8.23	8.32	8.27	8.24	8.04
05/23/11	8.22	8.22	8.22	8.14	8.22	8.22	8.22	8.09
05/24/11	8.26	8.24	8.26	8.2	8.26	8.28	8.25	8.21
05/25/11	8.24	8.3	8.39	8.3	8.38	8.39	8.39	8.26
05/26/11	8.29	8.24	8.34	8.28	8.34	8.32	8.31	8.17
05/27/11	8.28	8.33	8.34	8.29	8.34	8.33	8.3	8.13
05/28/11	8.28	8.35	8.36	8.31	8.4	8.37	8.34	8.14
05/29/11	8.29	8.32	8.32	8.29	8.31	8.32	8.27	8.11

Table A.9: Cell counts by hemocytometer. Counts include the cultures with the highest and lowest ABS. 2 counts were made for each sample, and are vertically stacked. Counts are not included for innoculation day, since all cultures wereinoculated to have the same starting concentration of 1E5 cells/ml.

Cell Counts by hemocytometer								
Sample#	1	2	3	4	5	6	7	8
Zn_T added (M)	8.5E-10	7.6E-9	6.9E-8	6.2E-7	1.9E-6	5.6E-6	1.7E-5	5.0E-5
05/23/11	9	15		9		14		
	11	18		14		10		
05/24/11	34	37		59			59	
	21	29		63			50	
05/25/11	76	120		115		156		
	96	92		137		114		
05/26/11	108	157			158			47
	112	120			144			74
05/27/11	153	173			172			101
	141	153			183			106
05/28/11	138	253	200			183		
	200	215	175			149		
05/29/11	232	229			188		128	
	167	176			187		114	

Table A.10: MQ added to each culture using a clean pipette from a cleaned bottle.

	MQ added							
Sample#	1	2	3	4	5	6	7	8
	8.5E-10	7.6E-9	6.9E-8	6.2E-7	1.9E-6	5.6E-6	1.7E-5	5.0E-5
05/22/11								
05/23/11								
05/24/11	35	50	50	50	25	60	50	35
05/25/11								
05/26/11	75	100	85	100	75	75	75	75
05/27/11								
05/28/11	100	100	100	75	100	100	100	100
05/29/11								

Table A.11: Growth rates. Avg and stdev 1-8 indicate the average and standard deviation of samples 1-8, while Avg and stdev 2-8 indicate the average and standard deviation of samples 2-8. The growth rate for culture 1 falls outside both standard deviations.

Sample#	Zn_T added (M)	Growth Rate	Avg, 1-8	stdev, 1-8	Avg, 2-8	stdev, 2-8
1	1.0E-8	0.50	0.67	0.09	0.69	0.06
2	3.0E-8	0.67				
3	1.0E-7	0.71				
4	3.0E-7	0.65				
5	1.0E-6	0.74				
6	3.0E-6	0.80				
7	1.0E-5	0.63				
8	5.0E-5	0.62				

Table A.12: Absorbance at 400 nm. Blanked instrument with DI water before and after measuring all 8 samples. 'nd' means no data, and 'collected' indicates a sample was filtered the day before. Filtering and rinsing 2 samples took 3-6 hours. A 9th culture of diatoms was grown later, since the bubbling aparatus could only accommodate 8 cultures at a time

					Absorbance at 400 nm									
Sample#	Blank	1	2	3	4	5	6	7	8	Blank		Blank	9	Blank
Cd_T added (M)	before	9.40E-11	8.50E-10	7.60E-9	6.90E-8	2.10E-7	6.20E-7	1.90E-6	5.60E-6	after		before	5.00E-5	after
03/25/11	0.055	0.063	0.062	0.063	0.065	0.067	0.064	0.064	0.061	0.053	04/13/11	0.054	0.065	0.055
03/26/11	0.056	0.084	0.084	0.081	0.089	0.084	0.082	0.084	0.08	0.055	04/14/11	0.054	0.082	0.055
03/27/11	0.054	0.151	0.141	0.146	0.15	0.146	0.146	0.145	0.145	0.054	04/15/11	0.055	0.129	0.056
03/28/11	0.055	0.181	0.182	0.186	0.196	0.18	0.18	0.186	0.183	0.056	04/16/11	0.055	0.172	0.075
03/29/11	0.054	0.224	0.217	0.221	0.253	0.215	0.218	0.231	0.214	0.054	04/17/11	0.075	0.22	0.077
03/30/11	0.056	0.253	0.243	0.255	0.297	0.243	0.251	0.269	0.252	0.054	04/18/11	0.058	0.225	0.055
03/31/11	0.054	0.276	0.278	0.274	0.312	0.268	0.279	0.296	0.275	0.054	04/19/11	0.055	0.248	0.054
04/01/11	0.059	collected	collected	0.297	0.301	0.294	0.315	0.319	0.303	0.054	04/20/11	0.056	0.281	0.058

Table A.13: Fluorescence at 400 nm. Blanked instrument with DI water before and after measuring all 8 samples. 'nd' means no data, and 'collected' indicates a sample was filtered the day before. Filtering and rinsing 2 samples took 3-6 hours. A 9th culture of diatoms was grown later, since the bubbling aparatus could only accommodate 8 cultures at a time

	Fluorescence at 660 nm													
Sample#	Blank	1	2	3	4	5	6	7	8	Blank		Blank	9	Blank
Cd_T added (M)	before	9.40E-11	8.50E-10	7.60E-9	6.90E-8	2.10E-7	6.20E-7	1.90E-6	5.60E-6	after		before	5.00E-5	after
03/25/11	0.11	2.05	1.84	1.12	1.32	1.24	1.2	1.35	1.19	0.12	04/13/11	0.19	1.36	0.19
03/26/11	0.17	3.1	3.09	3.14	3.5	3.15	3.16	3.19	3.13	0.12	04/14/11	0.01	2.53	0.06
03/27/11	0.09	11.4	11.54	11.68	11.07	11.77	11.04	11.57	11.91	0.08	04/15/11	0.05	8.91	0.04
03/28/11	0.12	13.52	13.69	15.29	17.19	14.29	14.28	15.58	14.86	0.21	04/16/11	0	11.34	0.11
03/29/11	0.14	13.59	15.45	14.74	18.81	13.81	15.59	16.01	14.46	0.15	04/17/11	0.72	13.47	1.13
03/30/11	0.1	14.63	14.93	14.59	19.51	13.51	16.21	17.12	16.7	0.11	04/18/11	0.13	14.01	0.16
03/31/11	0.13	15.51	16.79	16.17	22.66	15.8	17.84	18.65	17.58	0.09	04/19/11	0.12	13.9	0.02
04/01/11	0.05	collected	collected	15.95	20.88	15.52	19.09	20.56	18.47	0.17	04/20/11	nd	16.36	0.07

Table A.14: pH meter was calibrated daily with a slope >0.95.

					pH					
Sample#	1	2	3	4	5	6	7	8		9
Cd_T added (M)	9.40E-11	8.50E-10	7.60E-9	6.90E-8	2.10E-7	6.20E-7	1.90E-6	5.60E-6		5.00E-5
03/25/11	8.27	8.27	8.28	8.28	8.27	8.27	8.28	8.32	04/13/11	8.48
03/26/11	8.22	8.2	8.16	8.22	8.23	8.22	8.21	8.24	04/14/11	8.3
03/27/11	8.31	8.31	8.3	8.61	8.32	8.3	8.29	8.32	04/15/11	8.41
03/28/11	8.17	8.18	8.18	8.18	8.18	8.17	8.16	8.18	04/16/11	8.38
03/29/11	8.31	8.3	8.3	8.35	8.32	8.31	8.31	8.32	04/17/11	8.92
03/30/11	8.21	8.21	8.21	8.2	8.2	8.22	8.22	8.23	04/18/11	8.36
03/31/11	8.19	8.2	8.19	8.17	8.23	8.22	8.19	8.21	04/19/11	8.41
04/01/11	collected	collected	8.14	8.15	8.16	8.15	8.14	8.18	04/20/11	8.35

Table A.15: Counts include the cultures with the highest and lowest ABS. 2 counts were made for each sample, and are vertically stacked. Counts are not included for innoculation day, since all cultures were innoculated to have the same starting concentration of 1E5 cells/ml.

Cell Counts by hemocytometer										
Sample#	1	2	3	4	5	6	7	8		9
CdT added (M)	9.40E-11	8.50E-10	7.60E-9	6.90E-8	2.10E-7	6.20E-7	1.90E-6	5.60E-6		5.00E-5
03/26/11		45	61	32					04/13/11	nd
		44	45	50					04/14/11	56
03/27/11	153	97		115				141		36
	116	128		76				128	04/15/11	103
03/28/11	127			155		130				93
	151			167		140			04/16/11	93
03/29/11	180			230	186					142
	152			198	160				04/17/11	nd
03/30/11		218		252	182				04/18/11	nd
		168		227	201				04/19/11	nd
03/31/11	191			224	204		188		04/20/11	237
	203			313	146		246			213
04/01/11	184	205			214					
	223	190			231					

Table A.16: MQ added to each culture using a clean pipette from a cleaned bottle.

MQ added										
	1	2	3	4	5	6	7	8	9	
	9.40E-11	8.50E-10	7.60E-9	6.90E-8	2.10E-7	6.20E-7	1.90E-6	5.60E-6	5.00E-5	
03/25/11									04/13/11	
03/26/11									04/14/11	
03/27/11	70	70	75	25	92	75	75	70	04/15/11	75
03/28/11	25	50	50	60	65	50	25	50	04/16/11	50
03/29/11	50	25	25	25	25	25	40	25	04/17/11	
03/30/11									04/18/11	75
03/31/11	85	75	90	90	100	75	75	75	04/19/11	
04/01/11									04/20/11	

Table A.17: Growth rate data for all Cd-treated samples.

Growth Rate, Days 2-3				
Sample#	Cd_T added (M)	Growth Rate	Average	stdev
1	9.4E-11	0.65	0.64	0.03
2	8.5E-10	0.66		
3	7.6E-9	0.66		
4	6.9E-8	0.58		
5	2.1E-7	0.66		
6	6.2E-7	0.63		
7	1.9E-6	0.64		
8	5.6E-6	0.67		
9	5.0E-5	0.63		

Appendix B

ICP results and errors used for Chapter 1

B.1 Metal to Si, P, and Zn 66 ratios for combined standard additions and external curve calculations

Table B.1: Me/Si, Me/P an Me/Zn66 ratios calculated by combined standard additions and external standard curve as described in the methods. "OP" designates the organic (intracellular) fraction, whereas "SP" designates the silica (frustule) fraction. 'Me_T' refers to the total metal concentration in M added to the experimental culture in a 1:1 ratio with EDTA, '$[Me^{2+}]$' refers to the calculated free metal concentration, and columns 'Cd111', 'Cu63', 'Cu65', 'Zn64', and 'Zn66' report the ratio of that specific isotope to either Si, P, or Zn66. All measurements are reported as mol/mol.

Sample	Me_T	$[Me^{2+}]$	Cd111	Cu63	Cu65	Zn64	Zn66
				Me/Si			

Continued on next page

Continued from previous page

Sample	Me_T	$[Me^{2+}]$	Cd111	Cu63	Cu65	Zn64	Zn66
standard additions + external curve							
OPCu1-8	1.00E-8	8.02E-15		6.04E-4	7.66E-4	3.23E-3	2.53E-3
OPCu1-7	1.00E-7	8.03E-14		1.74E-3	1.85E-3	1.26E-3	1.55E-3
OPCu1-6	1.00E-6	8.02E-13		3.63E-3	3.93E-3	5.21E-3	4.49E-3
OPCu1-5	1.00E-5	8.02E-12		9.79E-3	1.06E-2	2.45E-3	2.51E-3
OPCu3-8	3.00E-8	2.41E-14					
OPCu3-7	3.00E-7	2.41E-13					
OPCu3-6	3.00E-6	2.41E-12					
OPCu5-5	5.00E-5	4.01E-11					
SPCu1-8	1.00E-8	8.02E-15		2.13E-7	2.79E-7	2.89E-6	2.71E-6
SPCu1-7	1.00E-7	8.03E-14		4.68E-7	7.30E-7	4.68E-6	3.47E-6
SPCu1-6	1.00E-6	8.02E-13		2.75E-7	4.76E-7	3.84E-6	4.62E-6
SPCu1-5	1.00E-5	8.02E-12		6.09E-7	9.66E-7	7.22E-6	7.56E-6
SPCu3-8	3.00E-8	2.41E-14		3.45E-7	5.45E-7	8.62E-6	8.53E-6
SPCu3-7	3.00E-7	2.41E-13					
SPCu3-6	3.00E-6	2.41E-12		3.02E-7	4.98E-7	8.51E-6	7.80E-6
SPCu5-5	5.00E-5	4.01E-11		3.14E-6	3.21E-6	3.12E-5	2.98E-5
OPZn8-10	8.47E-10	2.38E-13		5.86E-3	5.32E-3	1.59E-3	1.43E-3
OPZn7-9	7.62E-9	2.13E-12		9.05E-3	7.97E-3	9.86E-3	1.15E-2
OPZn6-8	6.86E-8	1.93E-11		9.23E-3	8.84E-3	1.73E-2	1.62E-2
OPZn6-7	6.17E-7	1.74E-10		1.27E-2	1.30E-2	4.05E-2	4.16E-2
OPZn1-6	1.85E-6	5.32E-10		6.28E-3	5.90E-3	2.05E-2	1.89E-2
OPZn5-6	5.56E-6	1.57E-9		7.12E-3	7.61E-3	2.54E-2	2.16E-2
OPZn1-5	1.67E-5	4.76E-9		4.40E-3	4.65E-3	2.74E-2	2.29E-2
OPZn5-5	5.00E-5	1.40E-8		5.87E-3	5.69E-3	7.59E-2	6.75E-2
SPZn8-10	8.47E-10	2.38E-13		9.64E-8	2.04E-7	1.53E-6	1.69E-6
SPZn7-9	7.62E-9	2.13E-12		6.34E-8	8.60E-8	9.21E-7	8.71E-7
SPZn6-8	6.86E-8	1.93E-11		1.29E-9	7.46E-8	5.91E-7	5.31E-7
SPZn6-7	6.17E-7	1.74E-10		3.17E-7	3.65E-7	3.59E-6	3.88E-6
SPZn1-6	1.85E-6	5.32E-10		9.20E-8	1.19E-7	1.62E-6	2.05E-6

Continued on next page

Continued from previous page

Sample	Me_T	$[Me^{2+}]$	Cd111	Cu63	Cu65	Zn64	Zn66
SPZn5-6	5.56E-6	1.57E-9				2.57E-6	2.02E-6
SPZn1-5	1.67E-5	4.76E-9		1.30E-8	9.18E-8	4.85E-6	5.78E-6
SPZn5-5	5.00E-5	1.40E-8		1.95E-7	1.45E-7	1.11E-5	9.42E-6
OPCd9-11	9.41E-11	1.49E-14	2.02E-5	6.15E-3	7.14E-3	1.63E-2	1.49E-2
OPCd8-10	8.47E-10	1.35E-13	3.34E-5	6.09E-3	7.38E-3	1.06E-2	9.08E-3
OPCd7-9	7.62E-9	1.21E-12	1.10E-4	5.42E-3	4.82E-3	1.06E-2	9.51E-3
OPCd6-8	6.86E-8	1.10E-11	2.99E-4	2.06E-3	2.12E-3	5.96E-3	6.11E-3
OPCd2-7	2.06E-7	3.34E-11	3.76E-3	8.52E-3	9.58E-3	2.72E-2	2.35E-2
OPCd6-7	6.17E-7	9.84E-11	1.31E-3	2.62E-3	2.74E-3	8.94E-3	1.81E-2
OPCd1-6	1.85E-6	3.01E-10	1.96E-3	2.35E-3	2.12E-3	8.33E-3	7.47E-3
OPCd5-6	5.56E-6	8.88E-10	2.45E-3	3.40E-3	3.47E-3	8.56E-3	6.84E-3
OPCd5-5	5.00E-5	7.91E-9	4.57E-3	5.83E-3	5.75E-3	1.06E-2	1.18E-2
SPCd9-11	9.41E-11	1.49E-14	1.04E-8	2.58E-7	2.06E-7	1.45E-6	1.61E-6
SPCd8-10	8.47E-10	1.35E-13	1.04E-8	1.58E-7	1.39E-7	8.57E-7	9.84E-7
SPCd7-9	7.62E-9	1.21E-12	8.29E-9	1.30E-7	1.30E-7	7.97E-7	6.09E-7
SPCd6-8	6.86E-8	1.10E-11	5.34E-8	1.25E-6	1.21E-6	1.79E-5	2.50E-5
SPCd2-7	2.06E-7	3.34E-11	1.45E-8	1.91E-7	1.65E-7	1.60E-6	1.33E-6
SPCd6-7	6.17E-7	9.84E-11	5.37E-8	4.65E-7	2.31E-7	4.14E-6	3.68E-6
SPCd1-6b	1.85E-6						
SPCd5-6	5.56E-6	8.88E-10	4.30E-8	1.29E-7	7.46E-8	8.70E-7	7.46E-7
SPCd5-5	5.00E-5	7.91E-9	1.11E-7	2.51E-7	2.95E-7	1.32E-6	1.23E-6
			Me/P				
			standard additions + external curve				
OPCu1-8	1.00E-8	8.02E-15		7.16E-4	9.09E-4	3.84E-3	3.00E-3
OPCu1-7	1.00E-7	8.03E-14		3.47E-3	3.69E-3	2.52E-3	3.09E-3
OPCu1-6	1.00E-6	8.02E-13		5.35E-3	5.79E-3	5.35E-3	4.60E-3
OPCu1-5	1.00E-5	8.02E-12		1.14E-2	1.24E-2	2.86E-3	2.93E-3
OPCu3-8	3.00E-8	2.41E-14		2.26E-3	2.38E-3	4.20E-3	4.10E-3

Continued on next page

Continued from previous page

Sample	Me_T	$[Me^{2+}]$	Cd111	Cu63	Cu65	Zn64	Zn66
OPCu3-7	3.00E-7	2.41E-13		3.20E-3	3.25E-3	3.64E-3	3.33E-3
OPCu3-6	3.00E-6	2.41E-12		6.20E-3	5.57E-3	4.40E-3	3.88E-3
OPCu5-5	5.00E-5	4.01E-11		1.50E-2	1.40E-2	5.88E-3	5.62E-3
SPCu1-8	1.00E-8	8.02E-15		8.26E-3	1.08E-2	1.12E-1	1.05E-1
SPCu1-7	1.00E-7	8.03E-14		1.66E-2	2.60E-2	1.67E-1	1.23E-1
SPCu1-6	1.00E-6	8.02E-13		2.86E-2	4.95E-2	3.98E-1	4.79E-1
SPCu1-5	1.00E-5	8.02E-12		3.12E-2	4.95E-2	3.70E-1	3.87E-1
SPCu3-8	3.00E-8	2.41E-14		7.08E-3	1.12E-2	1.77E-1	1.75E-1
SPCu3-7	3.00E-7	2.41E-13					
SPCu3-6	3.00E-6	2.41E-12					
SPCu5-5	5.00E-5	4.01E-11		4.92E-1	5.02E-1	3.25E+0	3.11E+0
OPZn8-10	8.47E-10	2.38E-13		1.54E-3	1.40E-3	2.02E-4	1.81E-4
OPZn7-9	7.62E-9	2.13E-12		1.81E-3	1.59E-3	1.97E-3	2.31E-3
OPZn6-8	6.86E-8	1.93E-11		6.83E-4	5.87E-4	2.41E-3	1.54E-3
OPZn6-7	6.17E-7	1.74E-10		1.38E-3	1.41E-3	4.39E-3	4.50E-3
OPZn1-6	1.85E-6	5.32E-10		1.14E-3	1.07E-3	3.71E-3	3.42E-3
OPZn5-6	5.56E-6	1.57E-9		1.53E-3	1.64E-3	5.47E-3	4.65E-3
OPZn1-5	1.67E-5	4.76E-9		1.31E-3	1.38E-3	8.13E-3	6.81E-3
OPZn5-5	5.00E-5	1.40E-8		2.99E-4	2.52E-4	9.74E-3	6.19E-3
SPZn8-10	8.47E-10	2.38E-13		5.78E-3	1.22E-2	9.15E-2	1.01E-1
SPZn7-9	7.62E-9	2.13E-12		4.97E-3	6.73E-3	7.22E-2	6.82E-2
SPZn6-8	6.86E-8	1.93E-11		9.86E-5	5.71E-3	4.52E-2	4.07E-2
SPZn6-7	6.17E-7	1.74E-10		4.79E-3	5.53E-3	5.42E-2	5.86E-2
SPZn1-6	1.85E-6	5.32E-10		3.85E-3	5.00E-3	6.79E-2	8.58E-2
SPZn5-6	5.56E-6	1.57E-9				2.10E-1	1.65E-1
SPZn1-5	1.67E-5	4.76E-9		6.20E-4	4.37E-3	2.31E-1	2.75E-1
SPZn5-5	5.00E-5	1.40E-8		1.33E-2	9.91E-3	7.55E-1	6.41E-1
OPCd9-11	9.41E-11	1.49E-14	3.65E-6	7.40E-4	1.29E-3	1.57E-3	1.76E-3
OPCd8-10	8.47E-10	1.35E-13	1.21E-5	2.20E-3	2.67E-3	3.82E-3	3.28E-3
OPCd7-9	7.62E-9	1.21E-12	5.55E-5	2.74E-3	2.43E-3	5.36E-3	4.80E-3

Continued on next page

Continued from previous page

Sample	Me_T	$[Me^{2+}]$	Cd111	Cu63	Cu65	Zn64	Zn66
OPCd6-8	6.86E-8	1.10E-11	2.99E-4	2.06E-3	2.11E-3	5.96E-3	6.11E-3
OPCd2-7	2.06E-7	3.34E-11	3.82E-4	7.58E-4	1.19E-3	1.79E-3	2.12E-3
OPCd6-7	6.17E-7	9.84E-11	9.96E-4	1.99E-3	2.08E-3	3.25E-3	1.37E-2
OPCd1-6	1.85E-6	3.01E-10	1.88E-3	2.26E-3	2.04E-3	8.00E-3	7.17E-3
OPCd5-6	5.56E-6	8.88E-10	4.74E-3	8.83E-4	1.44E-3	1.95E-3	2.13E-3
OPCd5-5	5.00E-5	7.91E-9	1.17E-2	7.58E-4	1.22E-3	1.67E-3	1.86E-3
SPCd9-11	3.14E-11	1.49E-14	3.29E-4	8.19E-3	6.53E-3	4.19E-2	4.65E-2
SPCd8-10	2.82E-10	1.35E-13	4.79E-4	7.27E-3	6.42E-3	3.95E-2	4.53E-2
SPCd7-9	2.54E-9	1.21E-12	3.43E-4	5.37E-3	5.40E-3	3.30E-2	2.52E-2
SPCd6-8	2.29E-8	1.10E-11	1.53E-3	3.59E-2	3.48E-2	5.14E-1	7.16E-1
SPCd2-7	6.86E-8	3.34E-11	4.80E-4	6.32E-3	5.47E-3	5.30E-2	4.40E-2
SPCd6-7	2.06E-7	9.84E-11	2.64E-3	2.29E-2	1.13E-2	2.03E-1	1.81E-1
SPCd1-6b	6.17E-7						
SPCd5-6	5.56E-6	8.88E-10	3.13E-3	9.40E-3	5.44E-3	6.34E-2	5.44E-2
SPCd5-5	5.00E-5	7.91E-9	4.11E-3	9.26E-3	1.09E-2	4.85E-2	4.52E-2
				Me/Zn66			
				standard additions + external curve			
OPCu1-8	1.00E-8	8.02E-15		2.39E-1	3.03E-1	1.28E+0	1.00E+0
OPCu1-7	1.00E-7	8.03E-14		1.12E+0	1.19E+0	8.16E-1	1.00E+0
OPCu1-6	1.00E-6	8.02E-13		9.20E-1	9.43E-1	1.16E+0	1.00E+0
OPCu1-5	1.00E-5	8.02E-12		3.90E+0	4.23E+0	9.77E-1	1.00E+0
OPCu3-8	3.00E-8	2.41E-14		5.51E-1	5.80E-1	1.03E+0	1.00E+0
OPCu3-7	3.00E-7	2.41E-13		9.61E-1	9.75E-1	1.09E+0	1.00E+0
OPCu3-6	3.00E-6	2.41E-12		1.60E+0	1.44E+0	1.13E+0	1.00E+0
OPCu5-5	5.00E-5	4.01E-11		2.66E+0	2.49E+0	1.05E+0	1.00E+0
SPCu1-8	1.00E-8	8.02E-15		7.83E-2	1.03E-1	1.07E+0	1.00E+0
SPCu1-7	1.00E-7	8.03E-14		1.35E-1	2.10E-1	1.35E+0	1.00E+0
SPCu1-6	1.00E-6	8.02E-13		5.96E-2	1.03E-1	8.31E-1	1.00E+0

Continued on next page

Continued from previous page

Sample	Me_T	$[Me^{2+}]$	Cd111	Cu63	Cu65	Zn64	Zn66
SPCu1-5	1.00E-5	8.02E-12		8.06E-2	1.28E-1	9.55E-1	1.00E+0
SPCu3-8	3.00E-8	2.41E-14		4.05E-2	6.39E-2	1.01E+0	1.00E+0
SPCu3-7	3.00E-7	2.41E-13					
SPCu3-6	3.00E-6	2.41E-12		4.93E-3	2.09E-2	1.09E+0	1.00E+0
SPCu5-5	5.00E-5	4.01E-11		6.44E-2	8.33E-2	1.05E+0	1.00E+0
OPZn8-10	8.47E-10	2.38E-13		4.78E+0	4.00E+0	1.11E+0	1.00E+0
OPZn7-9	7.62E-9	2.13E-12		7.85E-1	6.91E-1	8.55E-1	1.00E+0
OPZn6-8	6.86E-8	1.93E-11		5.69E-1	5.46E-1	1.07E+0	1.00E+0
OPZn6-7	6.17E-7	1.74E-10		3.06E-1	3.13E-1	9.74E-1	1.00E+0
OPZn1-6	1.85E-6	5.32E-10		3.33E-1	3.13E-1	1.09E+0	1.00E+0
OPZn5-6	5.56E-6	1.57E-9		3.29E-1	3.52E-1	1.18E+0	1.00E+0
OPZn1-5	1.67E-5	4.76E-9		1.92E-1	2.03E-1	1.19E+0	1.00E+0
OPZn5-5	5.00E-5	1.40E-8		8.69E-2	8.43E-2	1.12E+0	1.00E+0
SPZn8-10	8.47E-10	2.38E-13		5.70E-2	1.21E-1	9.03E-1	1.00E+0
SPZn7-9	7.62E-9	2.13E-12		7.28E-2	9.88E-2	1.06E+0	1.00E+0
SPZn6-8	6.86E-8	1.93E-11		2.43E-3	1.40E-1	1.11E+0	1.00E+0
SPZn6-7	6.17E-7	1.74E-10		8.16E-2	9.42E-2	9.25E-1	1.00E+0
SPZn1-6	1.85E-6	5.32E-10		4.49E-2	5.83E-2	7.92E-1	1.00E+0
SPZn5-6	5.56E-6	1.57E-9				1.27E+0	1.00E+0
SPZn1-5	1.67E-5	4.76E-9		2.25E-3	1.59E-2	8.39E-1	1.00E+0
SPZn5-5	5.00E-5	1.40E-8		2.07E-2	1.54E-2	1.18E+0	1.00E+0
OPCd9-11	9.41E-11	1.49E-14	1.36E-3	4.12E-1	4.79E-1	1.09E+0	1.00E+0
OPCd8-10	8.47E-10	1.35E-13	3.68E-3	6.71E-1	8.13E-1	1.17E+0	1.00E+0
OPCd7-9	7.62E-9	1.21E-12	1.16E-2	5.70E-1	5.06E-1	1.12E+0	1.00E+0
OPCd6-8	6.86E-8	1.10E-11	4.90E-2	3.37E-1	3.46E-1	9.75E-1	1.00E+0
OPCd2-7	2.06E-7	3.34E-11	1.60E-1	3.62E-1	4.07E-1	1.16E+0	1.00E+0
OPCd6-7	6.17E-7	9.84E-11	7.26E-2	1.45E-1	1.52E-1	4.08E-1	1.00E+0
OPCd1-6	1.85E-6	3.01E-10	2.63E-1	3.15E-1	2.84E-1	1.11E+0	1.00E+0
OPCd5-6	5.56E-6	8.88E-10	3.58E-1	4.98E-1	5.08E-1	1.25E+0	1.00E+0
OPCd5-5	5.00E-5	7.91E-9	6.30E+0	4.08E-1	6.57E-1	8.98E-1	1.00E+0

Continued on next page

Continued from previous page

Sample	Me_T	$[Me^{2+}]$	Cd111	Cu63	Cu65	Zn64	Zn66
SPCd9-11	3.14E-11	1.49E-14	5.65E-3	1.90E-1	2.18E-1	9.01E-1	1.00E+0
SPCd8-10	2.82E-10	1.35E-13	1.06E-2	1.60E-1	1.42E-1	8.71E-1	1.00E+0
SPCd7-9	2.54E-9	1.21E-12	1.36E-2	2.13E-1	2.14E-1	1.31E+0	1.00E+0
SPCd6-8	2.29E-8	1.10E-11	2.13E-3	5.01E-2	4.86E-2	7.18E-1	1.00E+0
SPCd2-7	6.86E-8	3.34E-11	1.09E-2	1.44E-1	1.24E-1	1.20E+0	1.00E+0
SPCd6-7	2.06E-7	9.84E-11	1.46E-2	1.26E-1	6.27E-2	1.13E+0	1.00E+0
SPCd1-6b	6.17E-7						
SPCd5-6	5.56E-6	8.88E-10	5.76E-2	1.73E-1	1.00E-1	1.17E+0	1.00E+0
SPCd5-5	5.00E-5	7.91E-9	9.08E-2	2.05E-1	2.41E-1	1.07E+0	1.00E+0

B.2 Metal to Si, P, and Zn 66 errors for combined standard additions and external curve calculations

Table B.2: Me/Si, Me/P an Me/Zn66 ERROR for combined std adds and extl curve. error calculated by adding instrument error from Si and element of interest, then multiplying by Me/Si value. Original error is the mean root sq of the instrumental error.

Sample	Me_T	$[Me^{2+}]$	Cd111	Cu63	Cu65	Zn64	Zn66
OPCu1-8	1.00E-8	8.02E-15		9.71E-5	8.80E-5	4.92E-4	3.37E-4
OPCu1-7	1.00E-7	8.03E-14		3.22E-4	3.12E-4	2.55E-4	3.80E-4
OPCu1-6	1.00E-6	8.02E-13		4.80E-4	5.45E-4	1.72E-3	1.39E-3
OPCu1-5	1.00E-5	8.02E-12		1.41E-3	1.48E-3	4.27E-4	5.09E-4
OPCu3-8	3.00E-8	2.41E-14					
OPCu3-7	3.00E-7	2.41E-13					
OPCu3-6	3.00E-6	2.41E-12					
OPCu5-5	5.00E-5	4.01E-11					

Continued on next page

Continued from previous page

Sample	Me_T	$[Me^{2+}]$	Cd111	Cu63	Cu65	Zn64	Zn66
SPCu1-8	1.00E-8	8.02E-15		4.60E-8	5.48E-8	2.53E-7	4.23E-7
SPCu1-7	1.00E-7	8.03E-14		7.48E-8	1.38E-7	5.67E-7	5.36E-7
SPCu1-6	1.00E-6	8.02E-13		4.79E-8	1.05E-7	4.39E-7	6.45E-7
SPCu1-5	1.00E-5	8.02E-12		1.31E-7	2.12E-7	8.50E-7	1.06E-6
SPCu3-8	3.00E-8	2.41E-14		3.73E-8	5.87E-8	4.92E-7	8.08E-7
SPCu3-7	3.00E-7	2.41E-13					
SPCu3-6	3.00E-6	2.41E-12		4.92E-8	5.09E-8	7.19E-7	7.19E-7
SPCu5-5	5.00E-5	4.01E-11		7.34E-7	4.48E-7	4.17E-6	5.60E-6
OPZn8-10	8.47E-10	2.38E-13		5.25E-4	5.24E-4	1.75E-4	2.83E-4
OPZn7-9	7.62E-9	2.13E-12		1.65E-3	1.47E-3	2.09E-3	2.90E-3
OPZn6-8	6.86E-8	1.93E-11		1.88E-3	1.73E-3	2.82E-3	2.90E-3
OPZn6-7	6.17E-7	1.74E-10		2.68E-3	3.07E-3	8.27E-3	9.95E-3
OPZn1-6	1.85E-6	5.32E-10		8.31E-4	1.01E-3	2.70E-3	2.46E-3
OPZn5-6	5.56E-6	1.57E-9		1.11E-3	1.20E-3	2.95E-3	2.89E-3
OPZn1-5	1.67E-5	4.76E-9		7.40E-4	7.36E-4	3.51E-3	2.76E-3
OPZn5-5	5.00E-5	1.40E-8		8.31E-4	1.07E-3	7.94E-3	7.10E-3
SPZn8-10	8.47E-10	2.38E-13		2.74E-8	6.96E-8	3.67E-7	4.99E-7
SPZn7-9	7.62E-9	2.13E-12		1.47E-8	2.17E-8	1.12E-7	2.03E-7
SPZn6-8	6.86E-8	1.93E-11		2.95E-10	2.56E-8	6.04E-8	1.18E-7
SPZn6-7	6.17E-7	1.74E-10		5.67E-8	6.51E-8	4.48E-7	5.87E-7
SPZn1-6	1.85E-6	5.32E-10		2.27E-8	2.87E-8	2.10E-7	3.91E-7
SPZn5-6	5.56E-6	1.57E-9				3.01E-7	2.83E-7
SPZn1-5	1.67E-5	4.76E-9		2.84E-9	2.28E-8	4.73E-7	6.37E-7
SPZn5-5	5.00E-5	1.40E-8		4.06E-8	3.68E-8	9.94E-7	8.64E-7
OPCd9-11	9.41E-11	1.49E-14	4.43E-6	1.36E-3	1.81E-3	3.75E-3	3.46E-3
OPCd8-10	8.47E-10	1.35E-13	3.27E-6	7.58E-4	9.11E-4	1.19E-3	1.05E-3
OPCd7-9	7.62E-9	1.21E-12	1.60E-5	8.32E-4	9.18E-4	1.84E-3	1.54E-3
OPCd6-8	6.86E-8	1.10E-11	2.74E-5	3.15E-4	3.18E-4	6.04E-4	8.41E-4
OPCd2-7	2.06E-7	3.34E-11	5.30E-4	1.48E-3	1.69E-3	4.34E-3	4.25E-3
OPCd6-7	6.17E-7	9.84E-11	8.90E-5	3.26E-4	3.38E-4	7.67E-4	1.93E-3

Continued on next page

Continued from previous page

Sample	Me_T	$[Me^{2+}]$	Cd111	Cu63	Cu65	Zn64	Zn66
OPCd1-6	1.85E-6	3.01E-10	3.59E-4	5.48E-4	4.81E-4	1.63E-3	1.78E-3
OPCd5-6	5.56E-6	8.88E-10	1.86E-4	3.24E-4	3.74E-4	6.60E-4	6.63E-4
OPCd5-5	5.00E-5	7.91E-9	2.85E-4	6.89E-4	6.64E-4	1.17E-3	9.69E-4
SPCd9-11	9.41E-11	1.49E-14	6.47E-10	3.35E-8	2.78E-8	2.29E-7	1.41E-7
SPCd8-10	8.47E-10	1.35E-13	8.12E-10	2.69E-8	1.96E-8	1.02E-7	1.45E-7
SPCd7-9	7.62E-9	1.21E-12	6.29E-10	1.92E-8	2.34E-8	8.16E-8	7.64E-8
SPCd6-8	6.86E-8	1.10E-11	4.45E-9	1.39E-7	1.20E-7	1.59E-6	3.21E-6
SPCd2-7	2.06E-7	3.34E-11	8.73E-10	3.32E-8	2.28E-8	1.79E-7	1.51E-7
SPCd6-7	6.17E-7	9.84E-11	6.07E-9	1.01E-7	5.11E-8	6.39E-7	7.90E-7
SPCd1-6	1.85E-6						
SPCd5-6	5.56E-6	8.88E-10	2.82E-9	3.33E-8	1.62E-8	1.15E-7	1.37E-7
SPCd5-5	5.00E-5	7.91E-9	5.27E-9	4.03E-8	4.26E-8	1.63E-7	1.59E-7

Me/P ERROR

std adds and extl curve combined

OPCu1-8	1.00E-8	8.02E-15		1.38E-4	1.33E-4	7.06E-4	4.95E-4
OPCu1-7	1.00E-7	8.03E-14		5.71E-4	5.47E-4	4.56E-4	6.93E-4
OPCu1-6	1.00E-6	8.02E-13		6.84E-4	7.77E-4	1.65E-3	1.33E-3
OPCu1-5	1.00E-5	8.02E-12		1.32E-3	1.37E-3	4.16E-4	5.10E-4
OPCu3-8	3.00E-8	2.41E-14		2.26E-4	3.31E-4	4.53E-4	4.49E-4
OPCu3-7	3.00E-7	2.41E-13		2.55E-4	3.86E-4	3.03E-4	2.89E-4
OPCu3-6	3.00E-6	2.41E-12		4.62E-4	4.38E-4	4.11E-4	3.30E-4
OPCu5-5	5.00E-5	4.01E-11		1.28E-3	1.03E-3	6.00E-4	6.87E-4
SPCu1-8	1.00E-8	8.02E-15		2.51E-3	3.08E-3	1.97E-2	2.57E-2
SPCu1-7	1.00E-7	8.03E-14		4.38E-3	7.57E-3	3.73E-2	3.18E-2
SPCu1-6	1.00E-6	8.02E-13		8.48E-3	1.69E-2	9.44E-2	1.26E-1
SPCu1-5	1.00E-5	8.02E-12		9.23E-3	1.48E-2	7.34E-2	8.57E-2
SPCu3-8	3.00E-8	2.41E-14		1.37E-3	2.17E-3	2.53E-2	3.17E-2
SPCu3-7	3.00E-7	2.41E-13					

Continued on next page

Continued from previous page

Sample	Me_T	$[Me^{2+}]$	Cd111	Cu63	Cu65	Zn64	Zn66
SPCu3-6	3.00E-6	2.41E-12					
SPCu5-5	5.00E-5	4.01E-11		1.41E-1	9.66E-2	7.41E-1	8.76E-1
OPZn8-10	8.47E-10	2.38E-13		1.93E-4	1.87E-4	2.93E-5	4.23E-5
OPZn7-9	7.62E-9	2.13E-12		2.45E-4	2.20E-4	3.26E-4	4.73E-4
OPZn6-8	6.86E-8	1.93E-11		2.60E-4	8.66E-5	2.68E-4	1.09E-4
OPZn6-7	6.17E-7	1.74E-10		1.38E-4	1.77E-4	4.11E-4	5.80E-4
OPZn1-6	1.85E-6	5.32E-10		1.14E-4	1.49E-4	3.70E-4	3.36E-4
OPZn5-6	5.56E-6	1.57E-9		2.04E-4	2.20E-4	5.11E-4	5.17E-4
OPZn1-5	1.67E-5	4.76E-9		2.00E-4	1.98E-4	9.19E-4	7.16E-4
OPZn5-5	5.00E-5	1.40E-8		2.20E-4	3.55E-5	1.82E-3	6.31E-4
SPZn8-10	8.47E-10	2.38E-13		1.71E-3	4.33E-3	2.32E-2	3.12E-2
SPZn7-9	7.62E-9	2.13E-12		1.63E-3	2.35E-3	1.57E-2	2.24E-2
SPZn6-8	6.86E-8	1.93E-11		3.37E-5	2.60E-3	9.73E-3	1.36E-2
SPZn6-7	6.17E-7	1.74E-10		1.27E-3	1.46E-3	1.14E-2	1.39E-2
SPZn1-6	1.85E-6	5.32E-10		1.34E-3	1.70E-3	1.56E-2	2.50E-2
SPZn5-6	5.56E-6	1.57E-9				4.76E-2	4.13E-2
SPZn1-5	1.67E-5	4.76E-9		1.92E-4	1.49E-3	4.37E-2	5.55E-2
SPZn5-5	5.00E-5	1.40E-8		3.85E-3	3.31E-3	1.29E-1	1.11E-1
OPCd9-11	9.41E-11	1.49E-14	3.49E-7	2.37E-4	1.20E-4	1.75E-4	1.60E-4
OPCd8-10	8.47E-10	1.35E-13	1.02E-6	2.44E-4	2.93E-4	3.77E-4	3.36E-4
OPCd7-9	7.62E-9	1.21E-12	4.38E-6	2.37E-4	3.01E-4	5.73E-4	4.57E-4
OPCd6-8	6.86E-8	1.10E-11	2.32E-5	2.86E-4	2.88E-4	5.20E-4	7.55E-4
OPCd2-7	2.06E-7	3.34E-11	2.51E-5	2.07E-4	1.39E-4	1.92E-4	1.46E-4
OPCd6-7	6.17E-7	9.84E-11	6.63E-5	2.45E-4	2.54E-4	2.50E-4	1.44E-3
OPCd1-6	1.85E-6	3.01E-10	1.55E-4	2.98E-4	2.57E-4	7.57E-4	9.89E-4
OPCd5-6	5.56E-6	8.88E-10	3.32E-4	3.77E-4	1.80E-4	2.44E-4	1.98E-4
OPCd5-5	5.00E-5	7.91E-9	4.10E-4	1.60E-4	1.47E-4	1.52E-4	1.18E-4
SPCd9-11	3.14E-11	1.49E-14	4.17E-5	1.59E-3	1.30E-3	9.00E-3	6.71E-3
SPCd8-10	2.82E-10	1.35E-13	7.08E-5	1.75E-3	1.35E-3	7.43E-3	9.82E-3
SPCd7-9	2.54E-9	1.21E-12	5.01E-5	1.17E-3	1.35E-3	5.69E-3	4.93E-3

Continued on next page

Continued from previous page

Sample	Me_T	$[Me^{2+}]$	Cd111	Cu63	Cu65	Zn64	Zn66
SPCd6-8	2.29E-8	1.10E-11	2.74E-4	7.43E-3	6.77E-3	9.47E-2	1.60E-1
SPCd2-7	6.86E-8	3.34E-11	6.68E-5	1.60E-3	1.19E-3	1.01E-2	8.48E-3
SPCd6-7	2.06E-7	9.84E-11	5.85E-4	7.43E-3	3.74E-3	5.35E-2	5.85E-2
SPCd1-6	6.17E-7						
SPCd5-6	5.56E-6	8.88E-10	6.83E-4	3.86E-3	2.01E-3	1.81E-2	1.82E-2
SPCd5-5	5.00E-5	7.91E-9	6.59E-4	2.53E-3	2.80E-3	1.15E-2	1.10E-2
			Me/Zn66 ERROR				
			std adds and extl curve combined				
OPCu1-8	1.00E-8	8.02E-15		6.45E-2	6.80E-2	3.35E-1	2.43E-1
OPCu1-7	1.00E-7	8.03E-14		2.79E-1	2.77E-1	2.16E-1	3.08E-1
OPCu1-6	1.00E-6	8.02E-13		2.88E-1	3.16E-1	5.97E-1	4.94E-1
OPCu1-5	1.00E-5	8.02E-12		7.28E-1	7.70E-1	2.12E-1	2.45E-1
OPCu3-8	3.00E-8	2.41E-14		7.30E-2	9.97E-2	1.44E-1	1.42E-1
OPCu3-7	3.00E-7	2.41E-13		8.96E-2	1.29E-1	1.06E-1	1.01E-1
OPCu3-6	3.00E-6	2.41E-12		1.40E-1	1.32E-1	1.21E-1	9.83E-2
OPCu5-5	5.00E-5	4.01E-11		3.47E-1	2.95E-1	1.53E-1	1.67E-1
SPCu1-8	1.00E-8	8.02E-15		2.86E-2	3.54E-2	2.51E-1	3.04E-1
SPCu1-7	1.00E-7	8.03E-14		3.95E-2	6.76E-2	3.43E-1	2.87E-1
SPCu1-6	1.00E-6	8.02E-13		1.77E-2	3.54E-2	1.97E-1	2.63E-1
SPCu1-5	1.00E-5	8.02E-12		2.26E-2	3.63E-2	1.75E-1	2.06E-1
SPCu3-8	3.00E-8	2.41E-14		6.62E-3	1.04E-2	1.14E-1	1.50E-1
SPCu3-7	3.00E-7	2.41E-13					
SPCu3-6	3.00E-6	2.41E-12		1.30E-3	3.36E-3	1.47E-1	1.43E-1
SPCu5-5	5.00E-5	4.01E-11		1.83E-2	1.05E-2	1.47E-1	1.94E-1
OPZn8-10	8.47E-10	2.38E-13		2.40E+0	9.91E-1	3.07E-1	3.64E-1
OPZn7-9	7.62E-9	2.13E-12		2.02E-1	1.80E-1	2.46E-1	3.27E-1
OPZn6-8	6.86E-8	1.93E-11		9.88E-2	9.05E-2	1.42E-1	1.49E-1
OPZn6-7	6.17E-7	1.74E-10		5.08E-2	5.99E-2	1.55E-1	1.95E-1

Continued on next page

Continued from previous page

Sample	Me_T	$[Me^{2+}]$	Cd111	Cu63	Cu65	Zn64	Zn66
OPZn1-6	1.85E-6	5.32E-10		4.62E-2	5.57E-2	1.50E-1	1.37E-1
OPZn5-6	5.56E-6	1.57E-9		4.89E-2	5.28E-2	1.28E-1	1.26E-1
OPZn1-5	1.67E-5	4.76E-9		2.97E-2	2.94E-2	1.37E-1	1.07E-1
OPZn5-5	5.00E-5	1.40E-8		1.07E-2	1.42E-2	9.67E-2	8.65E-2
SPZn8-10	8.47E-10	2.38E-13		2.17E-2	5.28E-2	3.04E-1	3.91E-1
SPZn7-9	7.62E-9	2.13E-12		3.18E-2	4.52E-2	3.46E-1	4.38E-1
SPZn6-8	6.86E-8	1.93E-11		1.06E-3	7.73E-2	3.45E-1	4.29E-1
SPZn6-7	6.17E-7	1.74E-10		2.38E-2	2.74E-2	2.19E-1	2.64E-1
SPZn1-6	1.85E-6	5.32E-10		1.67E-2	2.12E-2	2.00E-1	3.14E-1
SPZn5-6	5.56E-6	1.57E-9				3.04E-1	2.62E-1
SPZn1-5	1.67E-5	4.76E-9		6.53E-4	5.08E-3	1.42E-1	1.82E-1
SPZn5-5	5.00E-5	1.40E-8		5.20E-3	4.57E-3	1.56E-1	1.34E-1
OPCd9-11	9.41E-11	1.49E-14	1.92E-4	5.95E-2	8.46E-2	1.68E-1	1.55E-1
OPCd8-10	8.47E-10	1.35E-13	4.83E-4	1.06E-1	1.27E-1	1.70E-1	1.49E-1
OPCd7-9	7.62E-9	1.21E-12	1.48E-3	7.73E-2	8.75E-2	1.74E-1	1.44E-1
OPCd6-8	6.86E-8	1.10E-11	6.66E-3	6.66E-2	6.75E-2	1.42E-1	1.82E-1
OPCd2-7	2.06E-7	3.34E-11	1.88E-2	5.46E-2	6.23E-2	1.58E-1	1.57E-1
OPCd6-7	6.17E-7	9.84E-11	8.74E-3	2.56E-2	2.67E-2	7.48E-2	1.59E-1
OPCd1-6	1.85E-6	3.01E-10	4.22E-2	6.63E-2	5.81E-2	1.93E-1	2.16E-1
OPCd5-6	5.56E-6	8.88E-10	5.57E-2	8.70E-2	9.52E-2	1.96E-1	1.77E-1
OPCd5-5	5.00E-5	7.91E-9	4.44E-1	1.01E-1	1.03E-1	1.14E-1	9.88E-2
SPCd9-11	3.14E-11	1.49E-14	7.52E-4	4.68E-2	4.85E-2	2.08E-1	1.60E-1
SPCd8-10	2.82E-10	1.35E-13	2.12E-3	4.69E-2	3.72E-2	2.10E-1	2.69E-1
SPCd7-9	2.54E-9	1.21E-12	2.59E-3	5.58E-2	6.29E-2	2.84E-1	2.40E-1
SPCd6-8	2.29E-8	1.10E-11	3.93E-4	1.06E-2	9.69E-3	1.36E-1	2.29E-1
SPCd2-7	6.86E-8	3.34E-11	1.76E-3	3.96E-2	2.98E-2	2.57E-1	2.15E-1
SPCd6-7	2.06E-7	9.84E-11	4.11E-3	4.86E-2	2.45E-2	3.63E-1	3.83E-1
SPCd1-6	6.17E-7						
SPCd5-6	5.56E-6	8.88E-10	1.27E-2	7.15E-2	3.72E-2	3.36E-1	3.38E-1
SPCd5-5	5.00E-5	7.91E-9	1.39E-2	5.45E-2	6.02E-2	2.47E-1	2.35E-1

B.3 R^2 values for standard additions

Table B.3: R^2 values for std adds

Sample	[Me^{2+}]	Cd111	Cu63	Cu65	Zn64	Zn66
OPCu1-8		0.9954	0.9991	0.9970	1.0000	0.9984
OPCu1-7		0.9965	0.9994	0.9987	0.9829	0.9904
OPCu1-6		0.9966	1.0000	0.9962	0.8608	0.9180
OPCu1-5		0.9998	0.9976	0.9919	0.9999	0.9989
OPCu3-8		1.0000	0.9996	0.9990	0.9997	0.9992
OPCu3-7		0.9998	1.0000	0.9999	0.9997	0.9996
OPCu3-6		0.9999	0.9998	0.9992	0.9999	0.9993
OPCu5-5		0.9789	0.9800	0.9900	0.9975	0.9998
SPCu1-8		0.9990	1.0000	0.9984	0.9933	0.9995
SPCu1-7		1.0000	0.9996	0.9969	0.9998	0.9901
SPCu1-6		0.9998	1.0000	0.9990	0.9862	0.9921
SPCu1-5		0.9975	0.9993	0.9996	0.9759	0.9980
SPCu3-8		0.9997	0.9997	0.9989	0.9872	0.9876
SPCu3-7		0.9984	0.9809	0.9979	1.0000	0.9997
SPCu3-6		0.9949	1.0000	0.9973	0.9377	0.9431
SPCu5-5		0.9995	0.9995	0.9998	0.8953	0.8783
OPZn8-10		0.9997	1.0000	0.9975	0.8808	0.8849
OPZn7-9		0.9816	0.9985	0.9992	0.9993	0.9942
OPZn6-8		0.7197	0.9988	0.9999	0.9941	0.9990
OPZn6-7		1.0000	0.9998	0.9995	0.9997	0.9892
OPZn1-6		0.9724	0.9999	0.9995	0.9753	0.9815
OPZn5-6		0.9999	0.9997	1.0000	0.9982	0.9940
OPZn1-5		0.9809	0.9972	0.9956	0.9985	1.0000
OPZn5-5		0.0292	0.9999	1.0000	0.9979	0.9776
SPZn8-10		0.9999	0.9997	1.0000	0.9983	0.9938
SPZn7-9		1.0000	1.0000	0.9998	0.9990	0.9998
SPZn6-8		1.0000	0.9999	0.9997	0.9990	1.0000
SPZn6-7		0.9999	0.9993	0.9973	0.9894	0.9901

Continued on next page

Continued from previous page

Sample	[Me^{2+}]	Cd111	Cu63	Cu65	Zn64	Zn66
SPZn1-6		0.9999	0.9986	0.9999	0.9945	0.9972
SPZn5-6		0.9999	0.8184	0.8292	0.9894	0.9594
SPZn1-5		0.9997	0.9999	0.9999	0.9988	1.0000
SPZn5-5		0.9997	0.9874	0.9971	0.9695	0.9880
OPCd9-11	0.9964	0.9476	0.9902	0.9991	0.9874	0.9889
OPCd8-10	0.9984	0.9539	0.9988	0.9972	0.9999	0.9988
OPCd7-9	0.9976	0.9998	0.9993	0.9953	0.9932	0.9966
OPCd6-8	0.9994	0.9985	0.9975	0.9985	0.9989	0.9981
OPCd2-7	0.9998	0.8591	0.9509	0.9871	0.9951	0.9819
OPCd6-7	0.9991	0.9892	0.9944	0.9897	0.9024	0.9912
OPCd1-6	0.9995	0.9971	0.9988	0.9953	0.9969	0.9892
OPCd5-6	0.9709	0.9398	0.9997	0.9980	0.9964	0.9968
OPCd5-5	0.9962	0.9361	0.9941	0.9812	0.8670	0.8591
SPCd9-11	0.9996	0.9991	0.9995	0.9948	0.9296	0.9178
SPCd8-10	0.9996	0.9948	0.9994	0.9990	0.9957	0.9990
SPCd7-9	0.9995	0.9997	1.0000	0.9998	1.0000	0.9988
SPCd6-8	0.9999	0.9989	0.9992	0.9999	0.9785	1.0000
SPCd2-7	1.0000	0.9998	1.0000	0.9999	0.9999	0.9991
SPCd6-7	1.0000	0.9989	1.0000	0.9968	0.9991	0.9979
SPCd1-6b	1.0000	1.0000	1.0000	1.0000	1.0000	1.0000
SPCd5-6	0.9998	0.9900	0.9979	0.9999	0.9997	0.9990
SPCd5-5	0.9994	1.0000	0.9996	0.9979	0.9957	0.9940

Appendix C

Single Element Plots, Me:Si

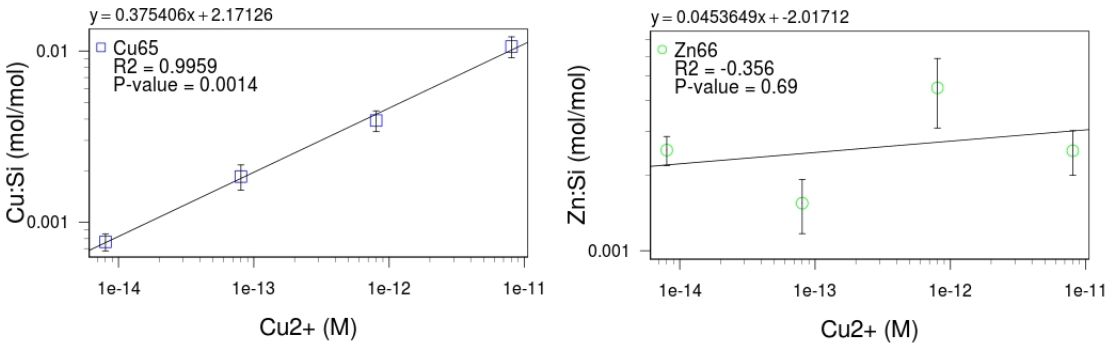

Figure C.1: Intracellular fraction, variable Cu. Expanded view of plots in figure 2.3, top left corner with linear fit, equation, R^2, and p-value.

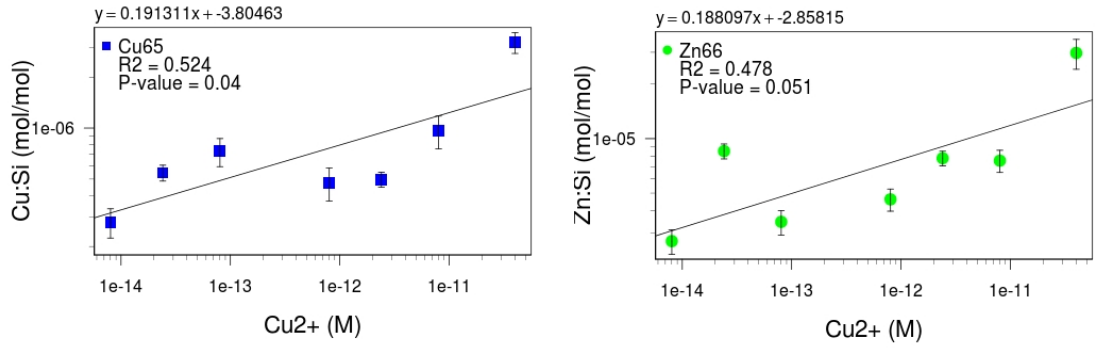

Figure C.2: Frustule fraction, variable Cu. Expanded view of plots in figure 2.3, top right corner with linear fit, equation, R^2, and p-value.

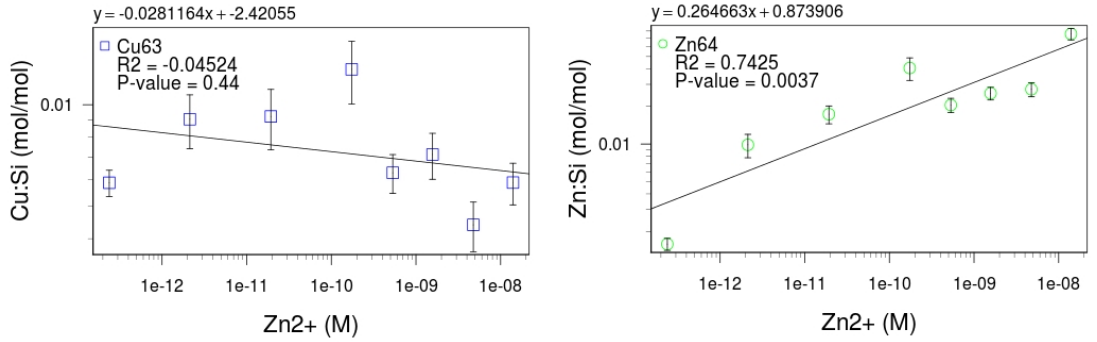

Figure C.3: Intracellular fraction, variable Zn. Expanded view of plots in figure 2.3, middle left with linear fit, equation, R^2, and p-value.

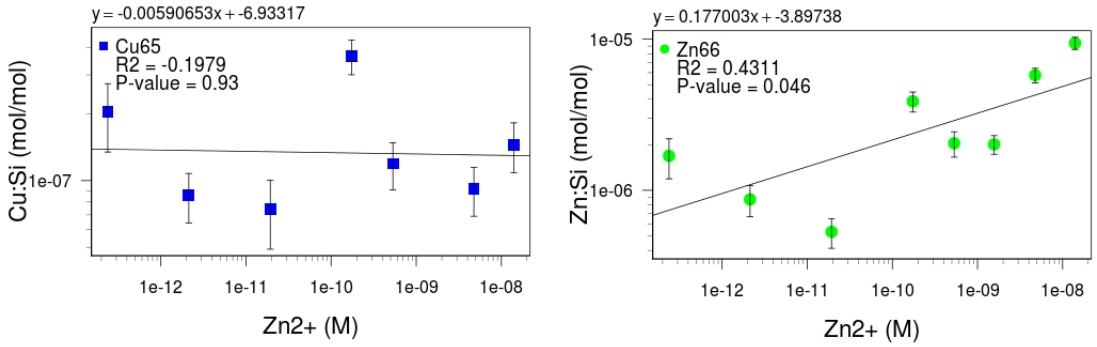

Figure C.4: Frustule fraction, variable Zn. Expanded view of plots in figure 2.3, middle right with linear fit, equation, R^2, and p-value.

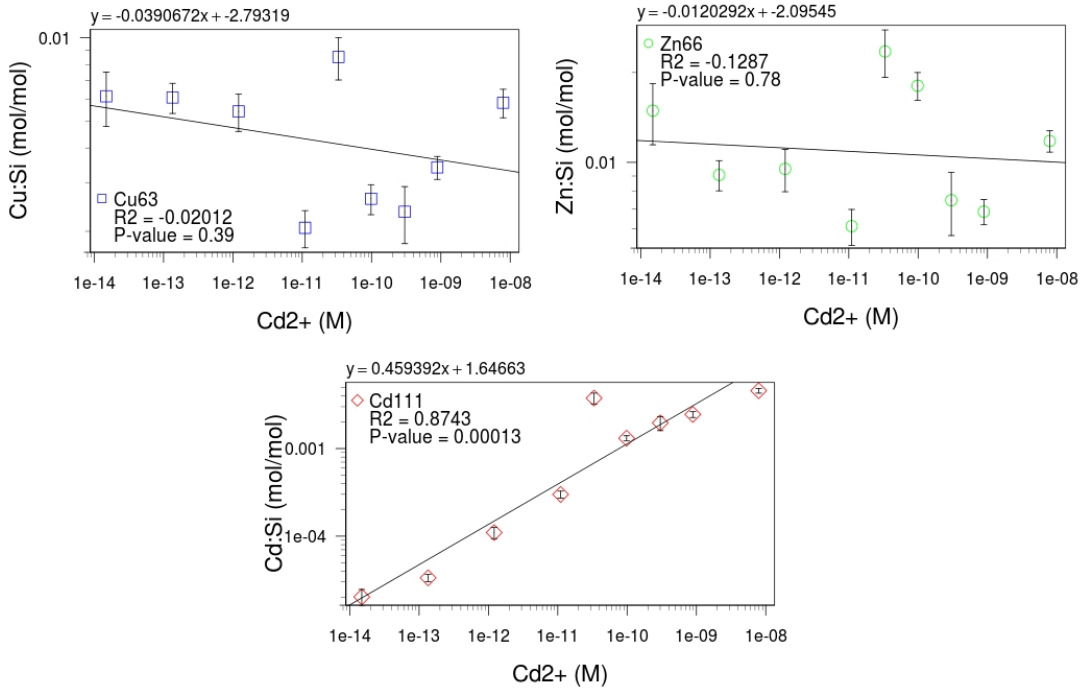

Figure C.5: Intracellular fraction, variable Cd. Expanded view of plots in figure 2.3, bottom left corner with linear fit, equation, R^2, and p-value.

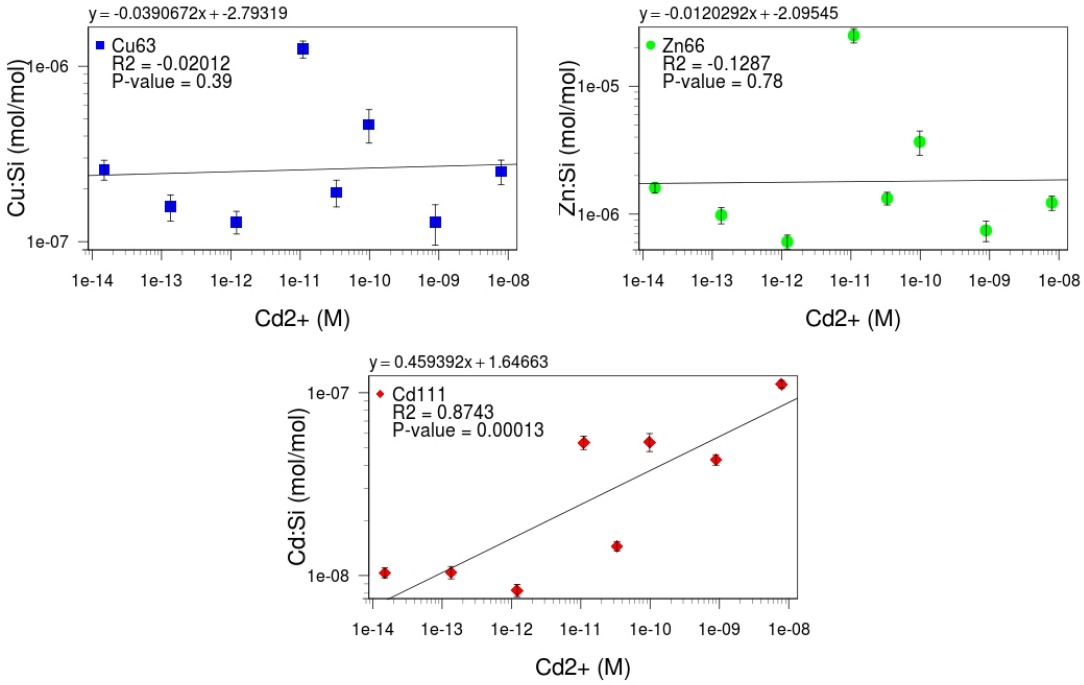

Figure C.6: Frustule fraction, variable Cd. Expanded view of plots in figure 2.3, bottom right corner with linear fit, equation, R^2, and p-value.

Appendix D

Single Element Plots, Me:P

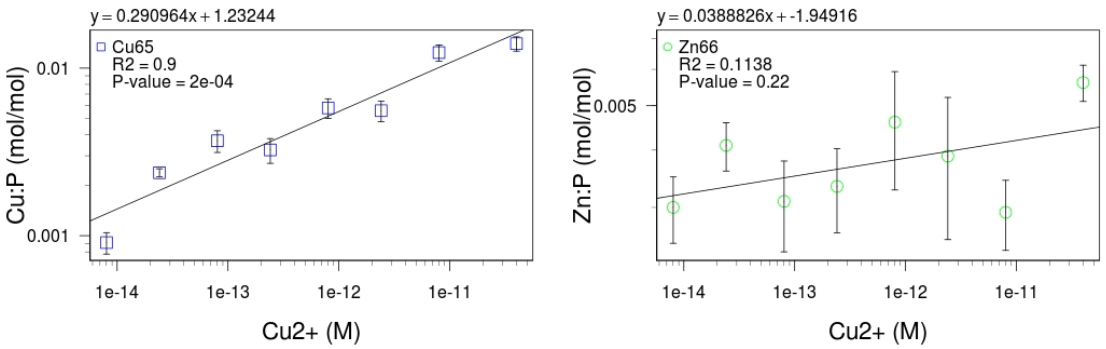

Figure D.1: Intracellular fraction, variable Cu. Expanded view of plots in figure 2.4, top left corner with linear fit, equation, R^2, and p-value.

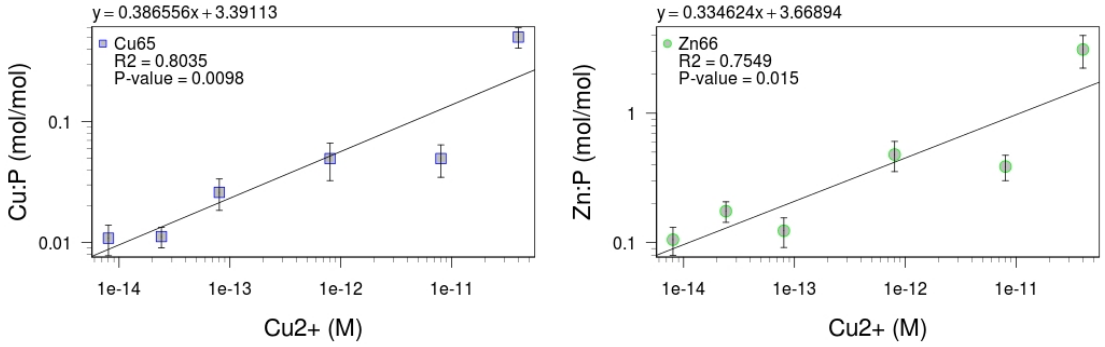

Figure D.2: Frustule fraction, variable Cu. Expanded view of plots in figure 2.4, top right corner with linear fit, equation, R^2, and p-value.

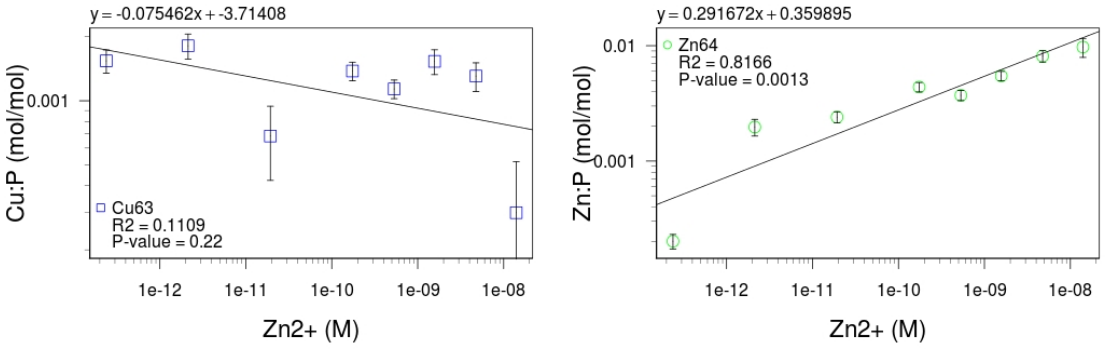

Figure D.3: Intracellular fraction, variable Zn. Expanded view of plots in figure 2.4, middle left with linear fit, equation, R^2, and p-value.

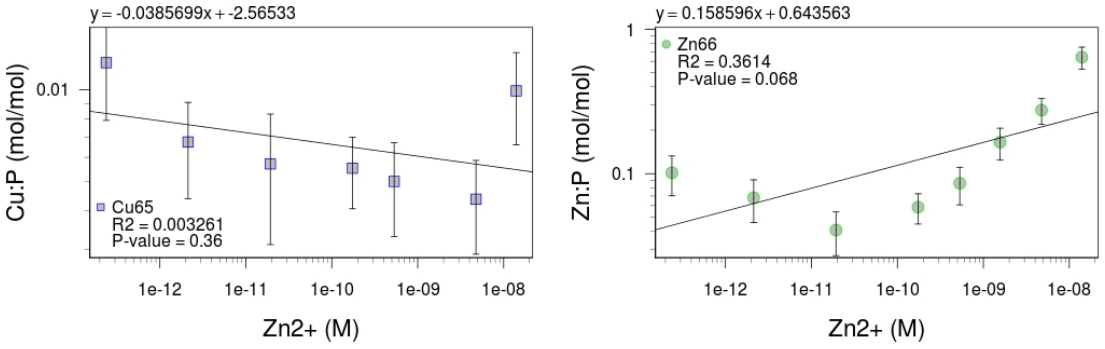

Figure D.4: Frustule fraction, variable Zn. Expanded view of plots in figure 2.4, middle right with linear fit, equation, R^2, and p-value.

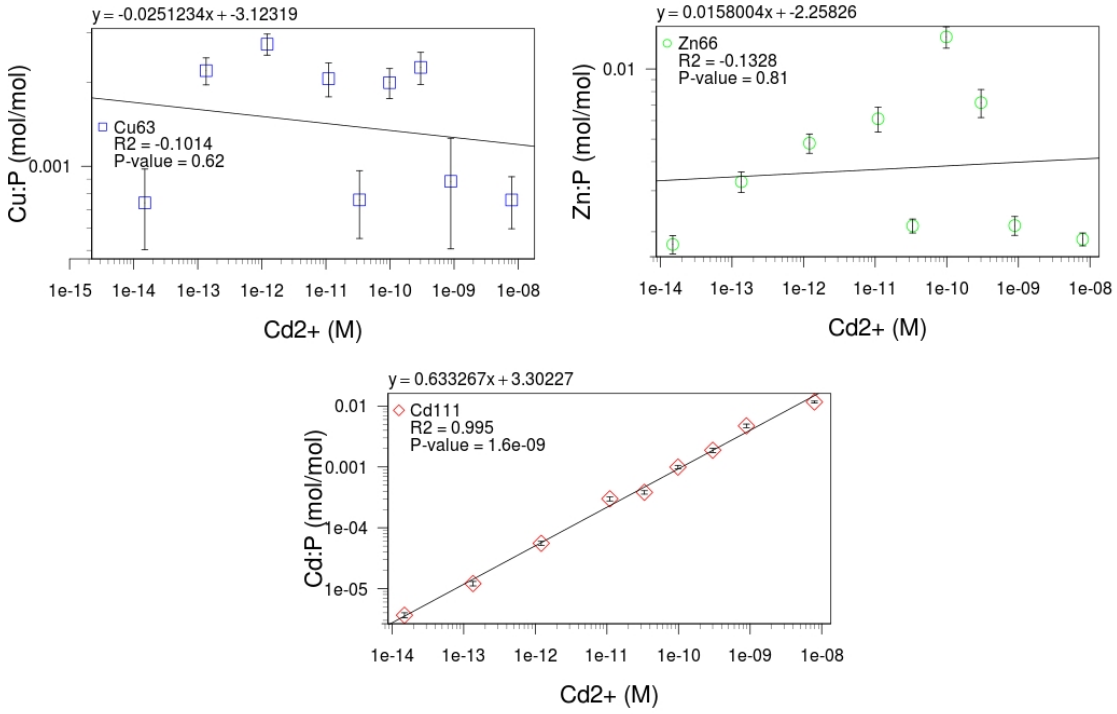

Figure D.5: Intracellular fraction, variable Cd. Expanded view of plots in figure 2.4, bottom left corner with linear fit, equation, R^2, and p-value.

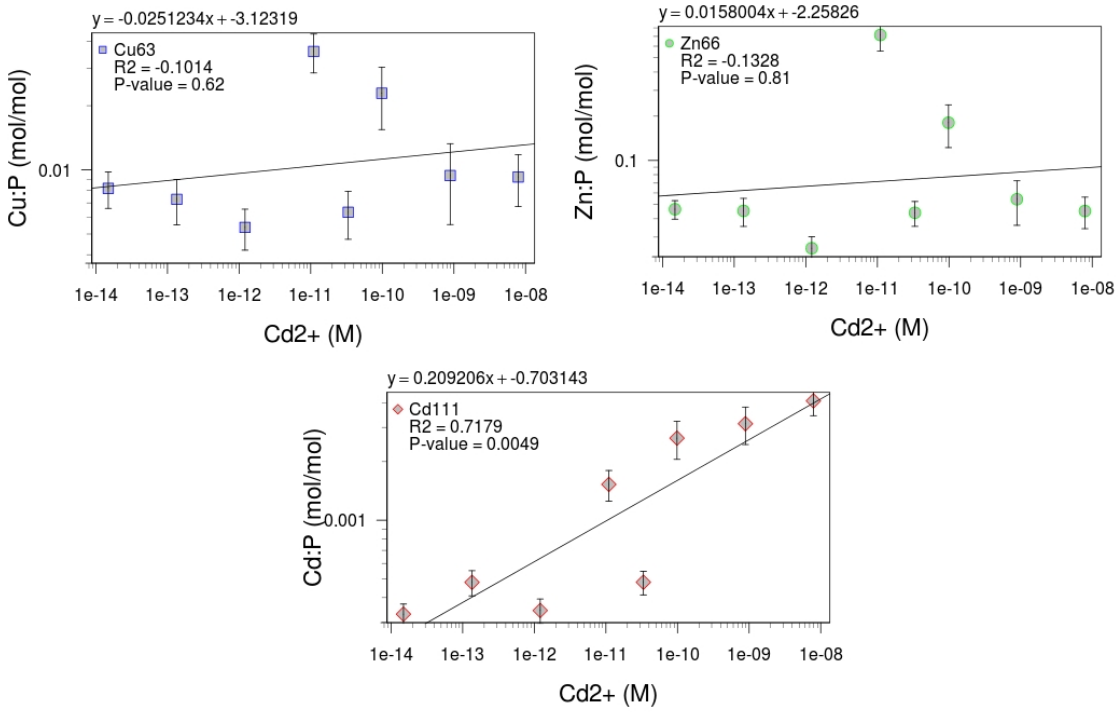

Figure D.6: Frustule fraction, variable Cd. Expanded view of plots in figure 2.4, bottom right corner with linear fit, equation, R^2, and p-value.

Appendix E

Single Element Plots, Me:Zn66

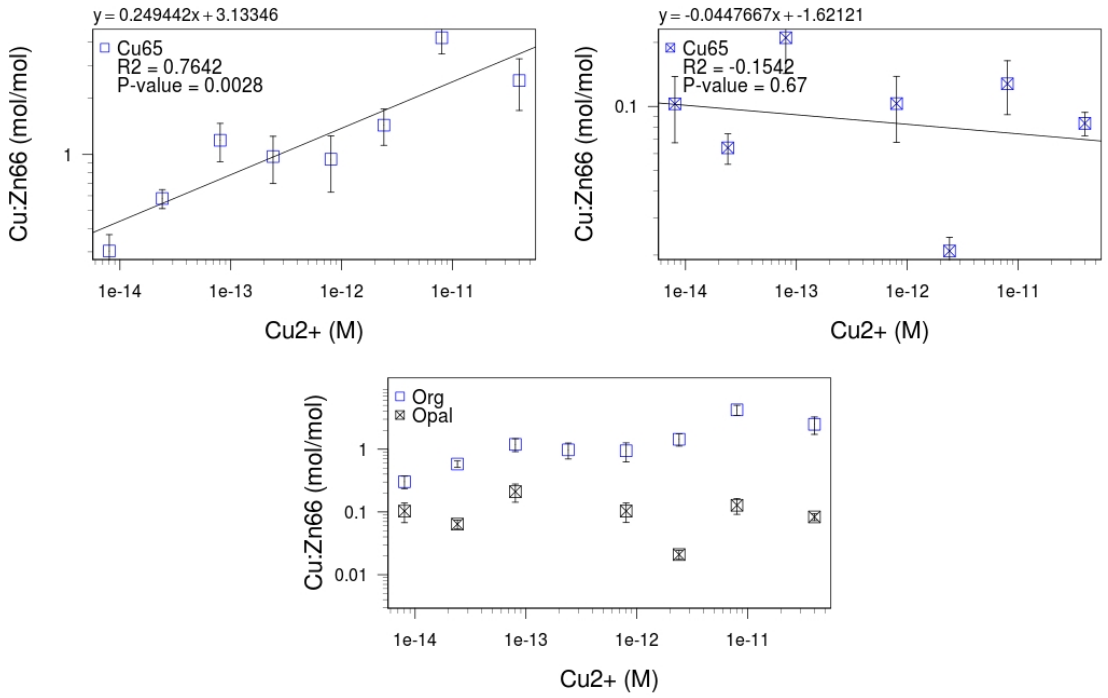

Figure E.1: Variable Cu, intracellular (i.e. "Org") fraction in open squares (top left), opal fraction reprsented by squares with an X (top right), and the two plots combined (bottom).

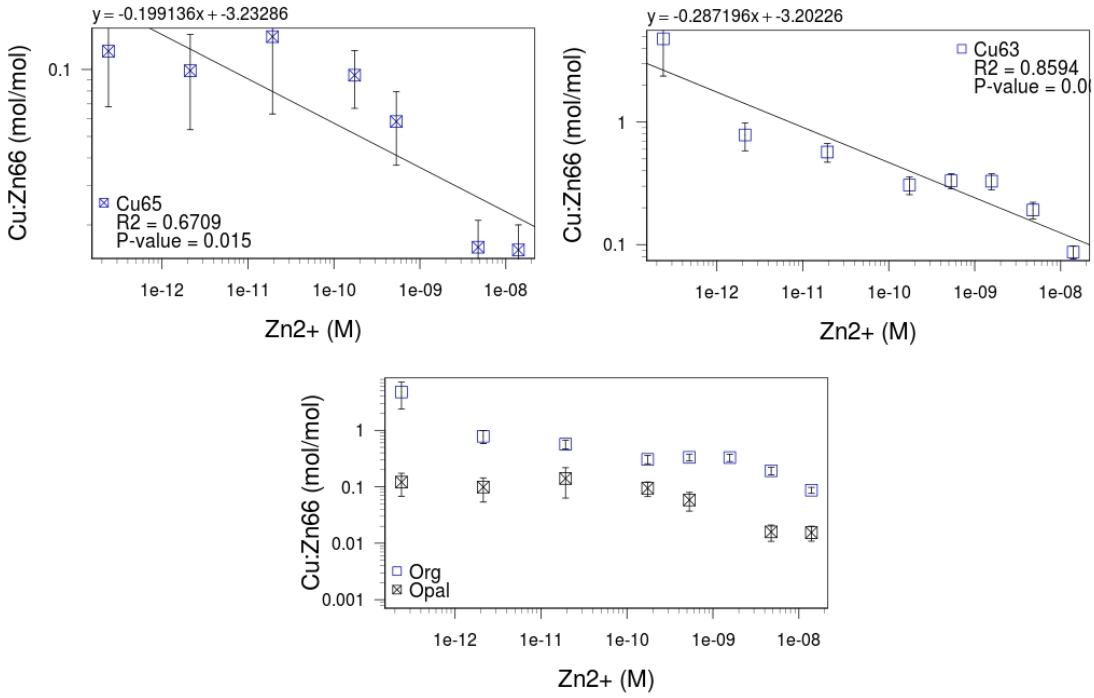

Figure E.2: Variable Zn, intracellular (i.e. "Org") fraction in open squares (top left), opal fraction reprsented by squares with an X (top right), and the two plots combined (bottom).

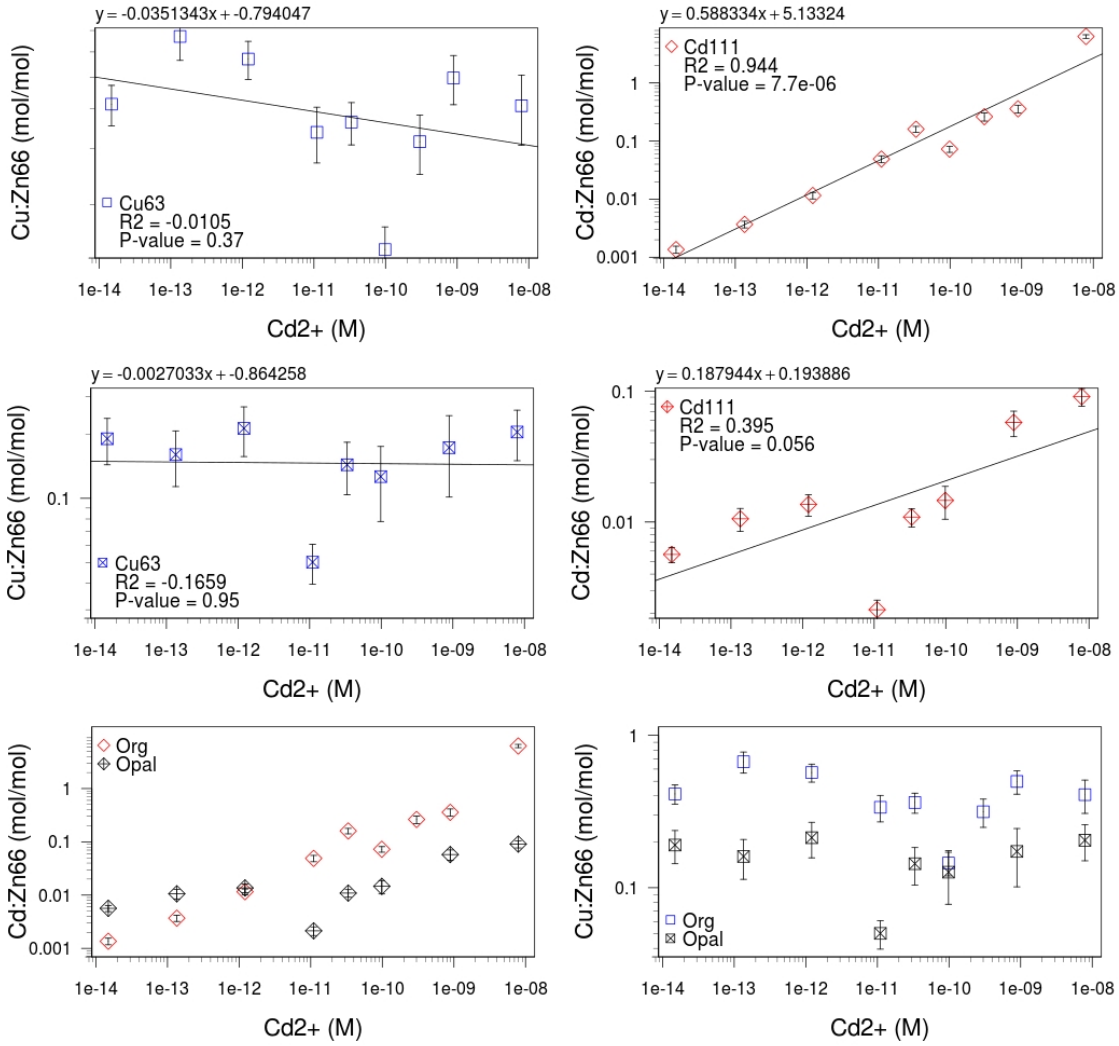

Figure E.3: Variable Cd. Top row: intracellular (i.e. "Org") with open boxes for Cu (left) and Cd (right) relative to Zn66. Middle row: opal fraction reprsented by crossed squares for Cu (left), and crossed diamonds for Cd (right). Bottom row: Intracellular (i.e. "Org") and opal fractions combined, with the opal fraction always represented in black; diamonds and boxes still checked. Cd:Zn66 on left, Cu:Zn66 on right.

Appendix F

Growth Data for *Tp*-f and *Sur*-f

F.1 *Tp*-f (Tables F.1-4) and *Sur*-f (Tables F.5-7) growth data. *To* fluorescence data used to determine the end of expontential growth (Table F.8), and *Tw* Absorbance data used to determine the end of exponential growth (Table F.9).

Note: Counts for Sur are not included since the low number of cells counted each day allowed for too much variability.

Table F.1: Absorbance at 400 nm. Blanked instrument with DI water before and after measuring all 8 samples. "nd" means no data, and "collected" indicates a sample was filtered the day before.

#		1	2	3	4	5	6	7	8	
Cu Conc	blank	1E-8	7E-8	1E-7	7E-7	1E-6	3E-6	7E-6	1E-5	blank
Date	before									after
01/31/11	0.049	0.057	0.055	0.055	0.054	0.053	0.055	0.053	0.052	0.044
02/01/11	0.046	0.096	0.072	0.067	0.072	0.083	0.076	0.072	0.073	0.048
02/02/11	0.047	0.104	0.110	0.111	0.115	0.116	0.106	0.100	0.102	0.047
02/03/11	0.046	0.161	0.180	0.186	0.168	0.174	0.165	0.186	0.182	0.046
02/04/11	0.051	0.293	0.282	0.299	0.283	0.305	0.302	0.294	0.049	0.049
02/05/11	0.048	0.234	0.232	0.235	0.229	0.239	0.241	0.226	0.233	0.047
02/06/11	0.047	0.291	0.291	0.308	0.296	0.307	0.303	0.299	0.300	0.046
02/07/11	0.051	0.283	0.282	0.299	0.283	0.305	0.302	0.294	0.294	0.049
02/08/11	0.046	collected	collected	collected	collected	collected	collected	0.321	0.329	0.046

Table F.2: Fluorescence at 660 nm. Blanked instrument with DI water before and after measuring all 8 samples. "nd" means no data, and "collected" indicates a samplewas filtered the day before.

#		1	2	3	4	5	6	7	8	
Cu Conc	blank	1E-8	7E-8	1E-7	7E-7	1E-6	3E-6	7E-6	1E-5	Blank
Date	before									after
01/31/11	0.13	1.47	1.6	1.42	2.6	2.55	1.66	1.56	1.47	0.03
02/01/11	0.18	1.91	1.78	2.11	2.49	3.02	2.4	2.58	2.16	0.18
02/02/11	0.15	6.01	9.93	10.34	11.36	7.03	6.38	5.26	5.49	0.13
02/03/11	0.03	10.15	11.66	11.35	10.91	13.12	11.26	10.28	10.34	0.12
02/04/11	0.11	18.61	19.85	20.55	17.59	19.49	19.44	18	18.89	0.13
02/05/11	0.14	14.7	16.32	15.71	14.86	15.79	15.71	14.21	15.36	0.12
02/06/11	0.16	18.28	18.1	18.02	16.4	18.33	18.01	17.47	17.56	0.06
02/07/11	0.11	18.61	19.85	20.55	17.59	19.49	19.44	18	18.89	0.13
02/08/11	0.19	collected	collected	collected	collected	collected	collected	16.4	16.48	0.32

Table F.3: pH meter was calibrated daily with a slope > 0.95.

#	1	2	3	4	5	6	7	8
Cu Conc	1E-8	7E-8	1E-7	7E-7	1E-6	3E-6	7E-6	1E-5
Date								
01/31/11	8.09	8.2	8.27	8.28	8.32	8.32	8.35	8.33
02/01/11	8.16	8.18	8.26	8.23	8.22	8.28	8.22	8.31
02/02/11	8.32	8.35	8.39	8.41	8.41	8.38	8.38	8.38
02/03/11	8.39	8.41	8.46	8.46	8.47	8.47	8.46	8.45
02/04/11	8.22	8.25	8.32	8.32	8.28	8.31	8.31	8.32
02/05/11	8.22	8.23	8.26	8.25	8.24	8.26	8.27	8.25
02/06/11	8.28	8.32	8.37	8.36	8.33	8.36	8.39	8.37
02/07/11	8.22	8.25	8.32	8.32	8.28	8.31	8.31	8.32
02/08/11							8.27	8.31

Table F.4: Cell counts by hemocytometer. Counts include the cultures with the highest and lowest RFU. 2 counts were made for each sample, and are vertically stacked. Counts are not included for innoculation day, since all cultures wereinoculated to have the same starting concentration of 1E5 cells/ml. Cells were not counted on 1/31/11.

#	1	2	3	4	5	6	7	8
Cu Conc	1E-8	7E-8	1E-7	7E-7	1E-6	3E-6	7E-6	1E-5
Date								
02/01/11			22		20			
			25		22			
02/02/11				125			109	
				77			91	
02/03/11	138				122			
	128				119			
02/04/11			266	265				
			363	312				
02/05/11		208					177	
		195					217	
02/06/11				209	215			
				211	266			
02/07/11			266	265				
			363	312				
02/08/11							253	229
							241	167

Table F.5: Absorbance at 400 nm. Blanked instrument with DI water before and after measuring all 8 samples. "nd" means no data, and "collected" indicates a sample was filtered the day before.

Date	Cu Conc [M]	Blank before	1 3E-8	2 1E-7	3 3E-7	4 7E-7	5 1E-6	6 3E-6	7 1E-5	8 5E-5	Blank after
05/12/10		0.048	0.052	0.053	0.052	0.051	0.051	0.049	0.049	0.049	0.048
05/14/10		0.044	0.055	0.053	0.053	0.053	0.051	0.052	0.052	0.053	0.043
05/19/10		0.044	0.074	0.079	0.075	0.082	0.075	0.077	0.094	0.076	0.043
05/21/10		0.043	0.131	0.118	0.113	0.095	0.105	0.117	0.128	0.112	0.043
05/24/10		0.044	0.149	0.171	0.162	0.172	0.158	0.138	0.157	0.148	0.043
05/25/10		0.043	0.165	0.217	0.203	0.219	0.189	0.170	0.190	0.188	0.044
05/28/10		0.043	collected	collected	0.217	0.208	0.223	0.178	0.215	0.193	0.047

Table F.6: Fluorescence at 660 nm. Blanked instrument with DI water before and after measuring all 8 samples. "nd" means no data, and "collected" indicates a samplewas filtered the day before.

Date	Cu Conc [M]	Blank before	1 3E-8	2 1E-7	3 3E-7	4 7E-7	5 1E-6	6 3E-6	7 1E-5	8 5E-5	Blank after
05/12/10		0.050	0.130	0.210	0.330	0.370	0.280	0.380	0.570	0.350	0.050
05/14/10		0.070	0.590	0.600	0.500	0.730	0.570	0.950	0.760	0.580	0.150
05/19/10		0.110	1.950	2.770	1.750	2.630	1.620	2.080	2.360	1.650	0.110
05/21/10		0.120	6.320	6.080	5.780	5.470	6.270	5.560	5.850	4.850	0.150
05/24/10		0.070	7.280	8.510	8.660	9.310	8.620	6.860	8.240	6.400	0.130
05/25/10		0.050	8.410	9.720	11.240	10.450	10.540	9.450	10.660	8.550	0.050
05/28/10		0.040	collected	collected	10.300	8.820	9.610	7.480	8.230	7.540	0.140

Table F.7: pH meter was calibrated daily with a slope > 0.95.

Date	1 3E-8	2 1E-7	3 3E-7	4 7E-7	5 1E-6	6 3E-6	7 1E-5	8 5E-5
05/12/10	8.9	9	9	9	9.1	8.9	9	8.9
05/14/10	8.1	8.1	8.1	8.1	8.1	8.1	8.1	8.1
05/19/10	8.1	8.2	8.2	8.2	8.2	8.2	8.3	8.2
05/21/10	8.4	8.5	8.5	8.6	8.4	8.4	8.5	8.3
05/24/10	8.3	8.5	8.6	8.7	8.5	8.4	8.5	8.5
05/25/10	8.6	8.4	8.4	8.5	8.5	8.6	8.5	8.5
05/28/10	collected	collected	8.2	8.2	8.2	8.2	8.2	8.2

Table F.8: Fluorescence at 660 nm for *To*. Blanked instrument with DI water before and after measurements. Numbers represent the average of 8 cultures grown for a separate purpose. These numbers were used to determine the end of exponential growth.

Date	RFU
7/17/09	0.87375
7/18/09	0.9975
7/19/09	1.9025
7/20/09	2.93625
7/21/09	5.9325
7/22/09	10.42375
7/23/09	17.69
7/24/09	20.67875
7/25/09	20.86625
7/26/09	22.65375
7/28/09	25.57875
7/29/09	22.735

Table F.9: Absorbance at 400 nm for *Tw*. Blanked instrument with DI water before and after measurements. Numbers represent the average of 8 cultures grown for a separate purpose. These data were used to determine the end of exponentail growth.

Date	A_{400}
02/22/13	0.012
02/24/13	0.03
02/25/13	0.031
02/26/13	0.05
02/27/13	0.061
02/28/13	0.074
03/01/13	0.077
03/02/13	0.083
03/03/13	0.093
03/04/13	0.098

Appendix G

C:N and C:P Ratios

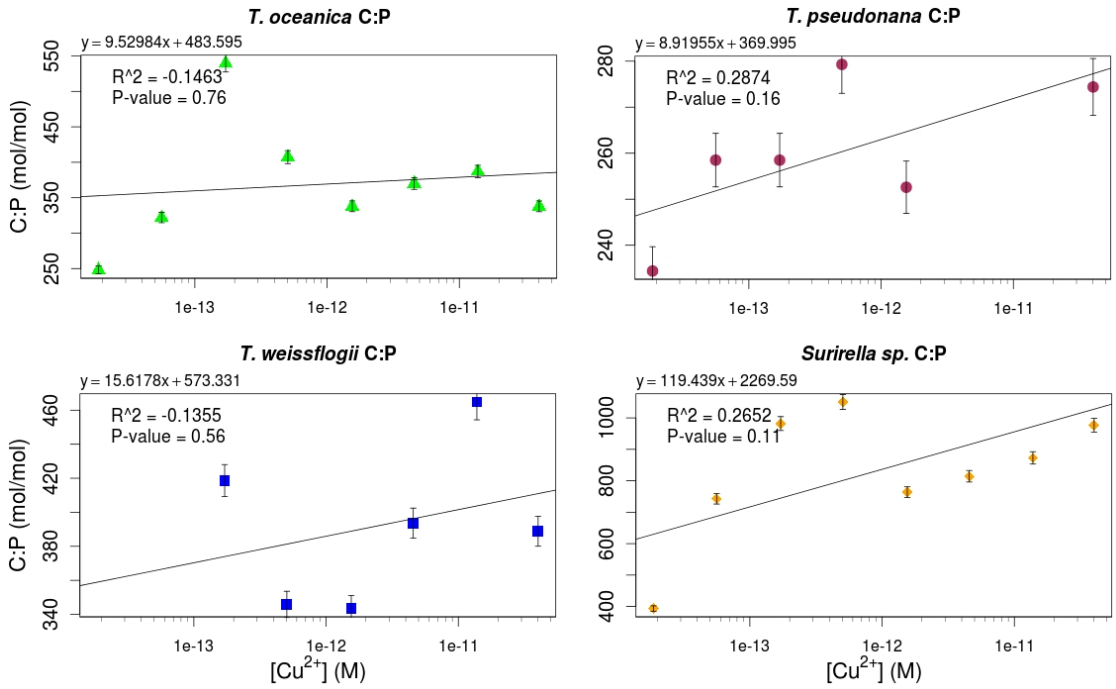

Figure G.1: $[Cu^{2+}]$ vs C:P data. If decreased P really is responsible for the lowered N:P ratio seen at higher e-poly P, C:P data should increase as *e*-poly P increases.

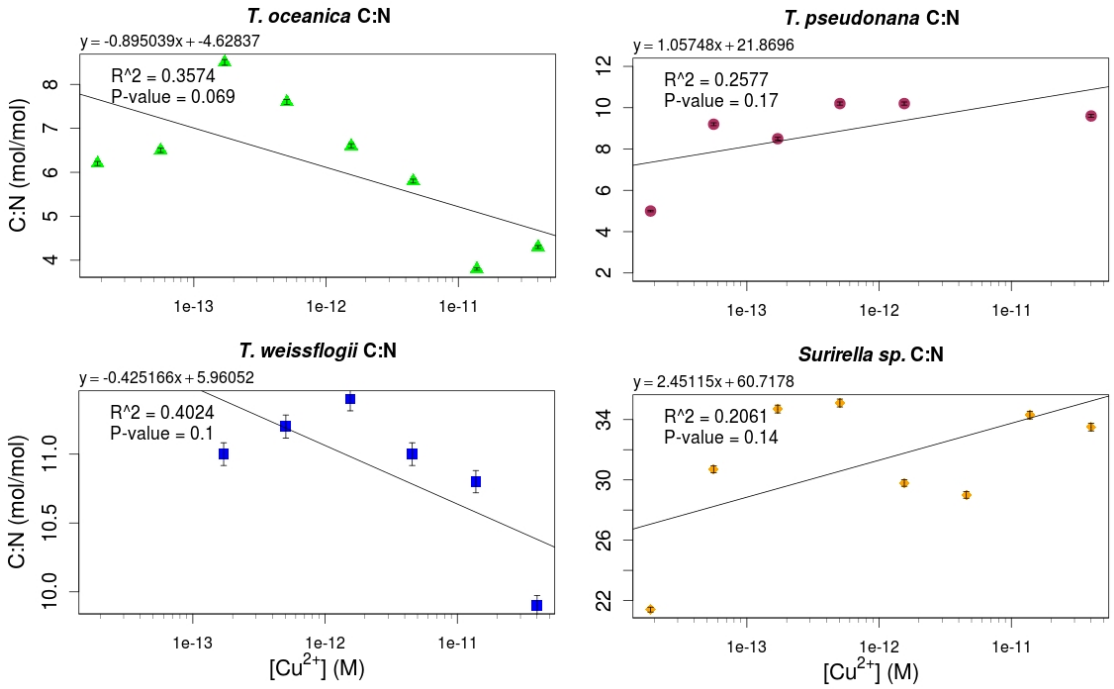

Figure G.2: $[Cu^{2+}]$ vs C:N data. If increased N really is responsible for the lowered N:P ratio seen at higher e-poly P, C:N data should decrease as *e*-poly P increases.

Appendix H

Community composition vs *e*-poly P

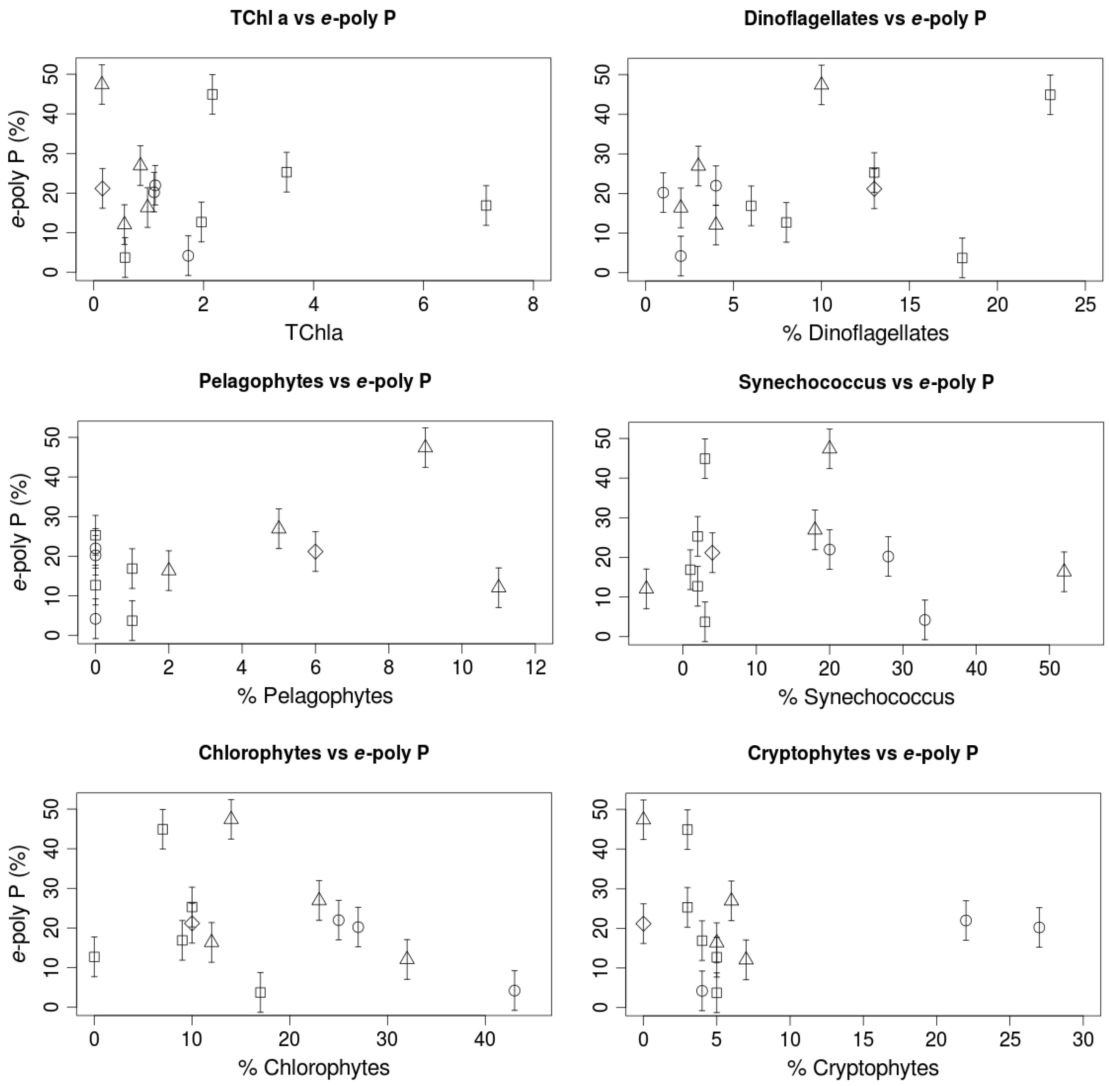

Figure H.1: TChl a and % microalgal community composed of dinoflagellates, pelagophytes, synechococcus, chlorophytes, and cryptophytes vs *e*-poly P; i.e. the taxa not included in figure 4.4. Prochlorococcus was excluded since it composed 0% of the community all but the last 5 sites, where it displayed little variability.

Appendix I

Humboldt and California Current Metal Speciation Data

Table I.1: Speciation data for Chile and California samples. Cu_T = total copper, Fe_T = total iron, stdev = standard deviation of the individual measurement, [SA] = the concentration of salicylaldoxime, a well-characterized ligand. $[L_s]$ = the concentration of the strong ligand, $[L_w]$ = concentration of the weak ligand. Log K_s and log K_w are the conditional stability constants of the strong (K_s) and weak (K_w) ligands, respectively, and reflect measured ligand strength with higher values representing stronger ligands. Log$[Cu^{2+}]$ is the log of the calculated $[Cu^{2+}]$ in M. The values eL_{Cu} and eL_{Fe} represent excess ligand and are calculated by subtracting from the total ligand concentration the total dissolved concentration of Cu or Fe, respectively. E.g. $eL_{Cu} = [L_s] + [L_w]$ $[Cu_T]$

		Total Dissolved				Cu Speciation										Fe Speciation					
Cruise	site	$[Cu_T]$	stdev	$[Fe_T]$	stdev	[SA]	$[L_s]$	stdev	log K_s	stdev	$[L_w]$	stdev	log K_w	stdev	log$[Cu^{2+}]$	eL_{Cu}	SA	$[L_s]$	stdev	log K_s	stdev	eL_{Fe}
		nM		nM		µM	nM				nM				nM	nM	µM	nM				nM
Chile	1	3.80	0.60	2.02	0.02	25	13.79	0.14	15.55	0.01					-15.96	9.93	25	5.78	0.03	11.63	0.04	3.76
Chile	2	1.11	0.06	2.93	0.33	25	4.55	0.13	16.03	0.46					-16.52	3.44	25	6.01	0.05	12.3	0.06	3.08
Chile	3	2.09	0.41	0.23	0.05	25	9.44	0.44	15.43	0.37					-15.98	7.35	25	3.62	0.01	11.25	0.01	3.39
Chile	4	1.09	0.07	0.40	0.03	25	7.94	0.04	15.44	0.05					-16.24	6.85	25	3.68	0.13	11.5	0.15	3.28
Chile	5	0.71	0.05	0.47	0.04	25	7.86	0.12	14.83	0.07					-15.83	7.15	25	3.13	0.25	11.8	0.41	2.66
Chile	6	2.82	0.32	1.09	0.06	2.5					7.78	0.16	13.95	0.02	-14.20	4.96	25	3.3	0.1	11.72	0.34	2.21
Chile	7	1.57	0.44	1.14	0.13	2.5					5.52	0.02	13.97	0.21	-14.37	3.95	25	3.14	0.19	11.16	0.12	2.00
Chile	8	1.65	0.12	2.50	0.44	2.5					7.62	0.34	13.9	0.18	-14.46	5.97	25	5.57	0.03	11.72	0.04	3.07
Chile	9	2.68	0.10	0.91	0.04	25	6.38	0.18	15.35	0.16					-15.49	3.70	25	3.97	0.24	11.97	0.62	3.06
Chile	10	2.24	0.11	0.56	0.04	25	5.09	0.31	15.4	0.3					-15.50	2.85	25	3.81	0.08	11.4	0.15	3.25
Chile	11	1.10	0.11	0.85	0.15	25	6.31	0.19	15.09	0.12					-15.77	5.21	25	2.72	0.09	11.71	0.22	1.87
California	1	2.07	0.32			25	4.39	0.15	16.03	0.05	5.9	0.3	14.84	0.07	-16.19							
		2.07	0.32			2.5					10.62	0.16	13.67	0.05								
California	2	0.72	0.14			25	1.71	0.08	16.45	0.03	0.91	0.2	14.3	0.24	-16.59							
		0.72	0.14			2.5					10.55	0.01	13.48	0.11								
California	3	1.55	0.1																			
California	4	2.166	0.03																			

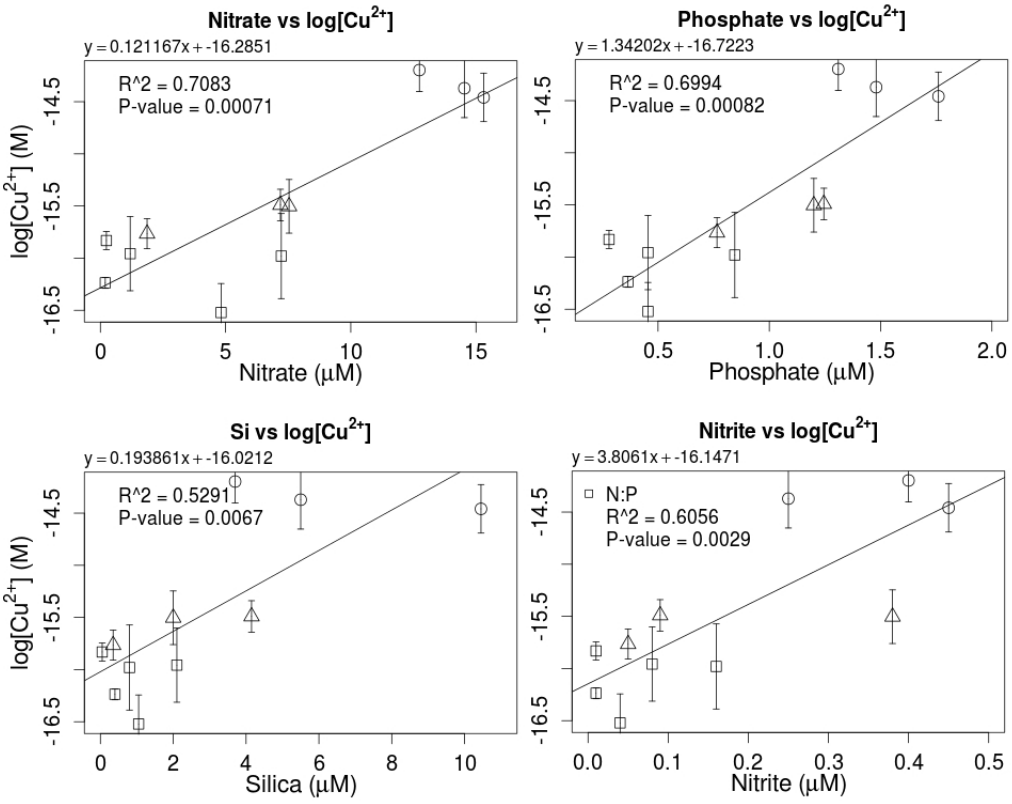

Figure I.1: Strong correlations ($p < .01$) were found between macronutrients and $\log[Cu^{2+}]$. Clockwise from the upper left and in order of strength of correlation, A) nitrate, B) phosphate, C) nitrite, and D) silicic acid vs. the log $[Cu^{2+}]$. Nitrate and phosphate both had $p < .001$, with a slightly stronger correlation for nitrate.

Bibliography

Alheit, J. and Niquen, M. (2004). Regime shifts in the Humboldt Current ecosystem. *Progress in Oceanography*, 60(2-4):201–222.

Allan, R. and Miller, J. J. (1980). Influence of S-adenosylmethionine on DAPI-induced fluorescence of polyphosphate in the yeast vacuole. *Canadian journal of microbiology*, 26(8):912–20.

Alvarez, S. and Jerez, C. (2004). Copper ions stimulate polyphosphate degradation and phosphate efflux in Acidithiobacillus ferrooxidans. *Applied and environmental microbiology*, 70(9):5177–5182.

Andersen, R. (2005). *Algal culturing techniques*. Elsevier Academic Press, Burlington, MA.

Armbrust, E. V. (2009). The life of diatoms in the world's oceans. *Nature*, 459(7244):185–92.

Armstrong, R., Lee, C., and Hedges, J. (2001). A new, mechanistic model for organic carbon fluxes in the ocean based on the quantitative association of POC with ballast minerals. *Deep Sea Research Part II:*, 49:219–236.

Aspila, K. I., Agemian, H., and Chau, a. S. (1976). A semi-automated method for the determination of inorganic, organic and total phosphate in sediments. *The Analyst*, 101(1200):187–97.

Bakun, A. and Nelson, C. (1991). The seasonal cycle of wind-stress curl in subtropical eastern boundary current regions. *Journal of Physical Oceanography*, 21:1815–1834.

Balistrieri, L. and Murray, J. (1984). Marine scavenging: Trace metal adsorption by interfacial sediment from MANOP site H. *Geochimica et Cosmochimica Acta*, 48:921–929.

Barón, M., Arellano, J., and Gorgé, J. (1995). Copper and photosystem II: A controversial relationship. *Physiologia Plantarum*, 94(1):174–180.

Benitez-Nelson, C. R. (2000). The biogeochemical cycling of phosphorus in marine systems. *Earth-Science Reviews*, 51(1-4):109–135.

Bidle, K. D. and Azam, F. (1999). Accelerated dissolution of diatom silica by marine bacterial assemblages. *Nature*, 397:508–512.

Boyd, P., Jickells, T., Law, C., and Blain, S. (2007). Mesoscale iron enrichment experiments 1993-2005: Synthesis and future directions. *Science*, 315:612–617.

Boyle, E. (1977). The distribution of dissolved copper in the Pacific. *Earth and planetary science letters*, 37:38–54.

Boyle, E. A. (1992). Cadmium and δ13C Paleochemical Ocean Distributions during the Stage 2 Glacial Maximum. *Annual Review of Earth and Planetary Sciences*, 20:245–87.

Boyle, E. A., Labeyrie, L., and Duplessy, J.-c. C. (1995). Calcitic foraminiferal data confirmed by cadmium in aragonitic Hoeglundina : Application to the last glacial maximum in the northern Indian Ocean. *Paleoceanography*, 10(5):881–900.

Brand, L. E., Sunda, W. G., and Guillard, R. R. (1986). Reduction of marine phytoplankton reproduction rates by copper and cadmium. *Journal of Experimental Marine Biology and Ecology*, 96(3):225–250.

Brown, M. and Kornberg, A. (2004). Inorganic polyphosphate in the origin and survival of species. *Proceedings of the National Academy of Sciences of the United States of America*, 101(46):16085–16087.

Bruland, K. (1980). Oceanographic distributions of cadmium, zinc, nickel, and copper in the North Pacific. *Earth and Planetary Science Letters*, 47:176–198.

Bruland, K. (1989). Complexation of zinc by natural organic ligands in the central North Pacific. *Limnology and Oceanography*, 34:269–285.

Bruland, K. (1991). Interactive influences of bioactive trace metals on biological production in oceanic waters. *Limnology and Oceanography*, 36(8):1555–1577.

Bruland, K., Rue, E., Smith, G., and DiTullio, G. (2005). Iron, macronutrients and diatom blooms in the Peru upwelling regime: brown and blue waters of Peru. *Marine Chemistry*, 93:81–103.

Buck, K. and Lohan, M. (2007). Dissolved iron speciation in two distinct river plumes and an estuary: Implications for riverine iron supply. *Limnology and ...*, 52:843–855.

Buck, K. N. and Bruland, K. W. (2005). Copper speciation in San Francisco Bay: A novel approach using multiple analytical windows. *Marine Chemistry*, 96(1-2):185–198.

Buesseler, K. (1998). The decoupling of production and particulate export in the surface ocean. *Global Biogeochemical Cycles*, 12:297–310.

Bundy, R. M., Barbeau, K. A., and Buck, K. N. (2012). Sources of strong copper-binding ligands in Antarctic Peninsula surface waters. *Deep Sea Research Part II*, pages 1–13.

Carr, M.-E. and Kearns, E. J. (2003). Production regimes in four Eastern Boundary Current systems. *Deep Sea Research Part II: Topical Studies in Oceanography*, 50(22-26):3199–3221.

Cholli, A. L., Yamane, T., and Jelinski, L. W. (1985). Combining solid-state and solution-state 31p nmr to study in vivo phosphorus metabolism. *Proceedings of the National Academy of Sciences of the United States of America*, 82(2):391–5.

Clark, J. E., Beegen, H., and Wood, H. G. (1986). Isolation of intact chains of polyphosphate from "Propionibacterium shermanii" grown on glucose or lactate. *Journal of bacteriology*, 168(3):1212–9.

Coale, K. and Bruland, K. (1988). Copper complexation in the Northeast Pacific. *Limnology and Oceanography*, 33(5):1084–1101.

Cortese, G. and Gersonde, R. (2004). Opal sedimentation shifts in the World Ocean over the last 15 Myr. *Earth and Planetary Science Letters*, 224:509–527.

Cullen, J. (2001). Determination of trace elements in filtered suspended marine particulate material by sector field HR-ICP-MS. *J. Anal. At. Spectrom.*, 16:1307–1312.

Cullen, J. (2006). The nonlinear relationship between dissolved cadmium and phosphate in the modern global ocean: Could chronic iron limitation of phytoplankton growth cause the kink? *Limnology and oceanography*, 51:1369–1380.

Cullen, J., Lane, T., Morel, F., and Sherrell, R. (1999). Modulation of cadmium uptake in phytoplankton by seawater CO2 concentration. *Nature*, 77:165–167.

Daneri, G., Dellarossa, V., Quiñones, R., Jacob, B., Montero, P., and Ulloa, O. (2000). Primary production and community respiration in the Humboldt Current System off Chile and associated oceanic areas. *Marine Ecology Progress Series*, 197:41–49.

Davis, A. K. and Hildebrand, M. (2008). A self-propagating system for Ge incorporation into nanostructured silica. *Chemical communications (Cambridge, England)*, pages 4495–4497.

de Jonge, M. D., Holzner, C., Baines, S. B., Twining, B. S., Ignatyev, K., Diaz, J., Howard, D. L., Legnini, D., Miceli, A., McNulty, I., Jacobsen, C. J., and Vogt, S. (2010). Quantitative 3D elemental microtomography of Cyclotella meneghiniana at 400-nm resolution. *Proceedings of the National Academy of Sciences of the United States of America*, 107(36):15676–80.

De La Rocha, C., Hutchins, D., Brzezinski, M., and Zhang, Y. (2000). Effects of iron and zinc deficiency on elemental composition and silica production by diatoms. *Marine Ecology Progress Series*, 195:71–79.

Del Amo, Y. and Brzezinski, M. A. (1999). The chemical form of dissolved Si taken up by marine diatoms. *Journal of Phycology*, 35:1162–1170.

Diaz, J., Ingall, E., Benitez-Nelson, C., Paterson, D., de Jonge, M. D., McNulty, I., and Brandes, J. a. (2008). Marine polyphosphate: a key player in geologic phosphorus sequestration. *Science*, 320(5876):652–5.

Docampo, R., de Souza, W., Miranda, K., Rohloff, P., and Moreno, S. N. J. (2005). Acidocalcisomes - conserved from bacteria to man. *Nature reviews. Microbiology*, 3(3):251–61.

Dolezal, J., Povondra, P., Šulcek, Z. (1968). *Decomposition Techniques in Inorganic Analysis*.

Drum, R. W. and Pankratz, H. S. (1964). Pyrenoids, raphes, and other fine structure in diatoms. *American Journal of Botany*, 51:405.

Dyhrman, S. T., Jenkins, B. D., Rynearson, T. a., Saito, M. a., Mercier, M. L., Alexander, H., Whitney, L. P., Drzewianowski, A., Bulygin, V. V., Bertrand, E. M., Wu, Z., Benitez-Nelson, C., and Heithoff, A. (2012). The transcriptome and proteome of the diatom Thalassiosira pseudonana reveal a diverse phosphorus stress response. *PloS one*, 7(3):e33768.

Edmond, J. M., Jacobs, S. S., Gordon, A. L., Mantyla, A. W., and Weiss, R. F. (1979). Water column anomalies in dissolved silica over opaline pelagic sediments and the origin of the deep silica maximum. *Journal of Geophysical Research*, 84(C12):7809–7826.

Eixler, S., Selig, U., and Karsten, U. (2005). Extraction and detection methods for polyphosphate storage in autotrophic planktonic organisms. *Hydrobiologia*, 533(1-3):135–143.

Elderfield, H. and Rickaby, R. E. M. (2000). Oceanic Cd/P ratio and nutrient utilization in the glacial Southern Ocean. *Nature*, 405(6784):305–310.

Ellwood, M. J. and Hunter, K. A. (2000a). The incorporation of zinc and iron into the frustule of the marine diatom Thalassiosira pseudonana. *Limnology and oceanography*, 45(7):1517–1524.

Ellwood, M. J. and Hunter, K. A. (2000b). Variations in the Zn/Si record over the last interglacial glacial transition. *Paleoceanography*, 15(October):506–514.

Faul, K. and Paytan, A. (2005). Phosphorus and Barite Concentrations and Geochemistry in Site 1221 Paleocene/Eocene Boundary Sediments. *Proceedings of teh Ocean Drilling Program, Scientific Results*, 199:1–23.

Filippelli, G. and Delaney, M. (1994). The oceanic phosphorus cycle and continental weathering during the Neogene. *Paleoceanography*, 9(5):643–652.

Filippelli, G. and Delaney, M. (1996). Phosphorus geochemistry of equatorial Pacific sediments. *Geochimica et Cosmochimica Acta*, 60(9):1479–1495.

Fisher, N., Jones, G., and Nelson, D. (1981). Effects of copper and zinc on growth, morphology, and metabolism of Asterionella japonica(Cleve) 1. *Journal of Experimental Marine Biology and Ecology*, 51:37–56.

Fuh, C. B. (2000). Split-Flow Thin Fractionation. *Analytical chemistry*, 72(April):266 A–271 A.

Garcia, H. E., Locarnini, R. A., Boyer, T. P., Antonov, J. I., Zweng, M. M., Baranova, O. K., and Johnson, D. R. (2009). *World Ocean Atlas 2009, Volume 4: Nutrients (phosphate, nitrate, silicate)*. U.S. Government Printing Office, Washington, D.C., noaa atlas edition.

Gehlen, M., Beck, L., and Calas, G. (2002). Unraveling the atomic structure of biogenic silica: evidence of the structural association of Al and Si in diatom frustules. *Geochimica Et Cosmochimica Acta*, 66(9):1601–1609.

Goericke, R. and Montoya, J. (1998). Estimating the contribution of microalgal taxa to chlorophyll a in the field-variations of pigment ratios under nutrient-and light-limited growth. *Marine Ecology Progress Series*, 169:97–112.

Goldhammer, T., Brüchert, V., Ferdelman, T. G., and Zabel, M. (2010). Microbial sequestration of phosphorus in anoxic upwelling sediments. *Nature Geoscience*, 3(8):557–561.

Gruber, N. and Sarmiento, J. (1997). Global patterns of marine nitrogen fixation and denitrification. *Global Biogeochemical Cycles*, 11(2):235–266.

Hashemi, F., Leppard, G., and Kushnert, D. (1994). Copper resistance in Anabaena variabilis: effects of phosphate nutrition and polyphosphate bodies. *Microbial ecology*, 27(2):159–176.

Hendry, K. R., Rickaby, R. E., de Hoog, J. C., Weston, K., and Rehkämper, M. (2008). Cadmium and phosphate in coastal Antarctic seawater: Implications for Southern Ocean nutrient cycling. *Marine Chemistry*, 112(3-4):149–157.

Heppel, L., Harkness, D., and Hilmoe, R. (1962). A study of the substrate specificity and other properties of the alkaline phosphatase of Escherichia coli. *Journal of Biological Chemistry*, 237(3):841–846.

Ingall, E. D. (2010). Biogeochemistry: Phosphorus burial. *Nature Geoscience*, 3(8):521–522.

Jaccard, T., Ariztegui, D., and Wilkinson, K. J. (2009a). Assessing past changes in bioavailable zinc from a terrestrial (Zn/Si)opal record. *Chemical Geology*, 258(3-4):362–367.

Jaccard, T., Ariztegui, D., and Wilkinson, K. J. (2009b). Incorporation of zinc into the frustule of the freshwater diatom Stephanodiscus hantzschii. *Chemical Geology*, 265(3-4):381–386.

Jensen, T., Baxter, M., Rachlin, J., and Jani, V. (1982a). Uptake of heavy metals by Plectonema boryanum(cyanophyceae) into cellular components, especially polyphosphate bodies: An X-ray energy dispersive. *Environmental Pollution Series A*, 27:119–127.

Jensen, T. E., Rachlin, J. W., Jani, V., and Warkentine, B. (1982b). An X-ray energy dispersive study of cellular compartmentalization of lead and zinc in Chlorella saccharophila (Chlorophyta), Navicula incerta and Nitzschia closterium (Bacillariophyta). *Environmental and Experimental Botany*, 22(3):328–328.

John, S., Geis, R., Saito, M., and Boyle, E. (2007). Zinc isotope fractionation during high-affinity and low-affinity zinc transport by the marine diatom Thalassiosira oceanica. *Limnology and Oceanography*, 52(6):2710–2714.

Karl, D. and Björkman, K. (2002). Dynamics of DOP. In Hansell, D. A. and Carlson, C. A., editors, *Biogeochemistry of marine dissolved organic matter*, chapter 6, pages 249–366. Elsevier Science.

Keller, M. D., Bellows, W. K., and Guillard, R. R. (1988). Microwave treatment for sterilization of phytoplankton culture media. *Journal of Experimental Marine Biology and Ecology*, 117:279–283.

King, A. and Barbeau, K. (2007). Evidence for phytoplankton iron limitation in the southern California Current System. *Marine Ecology Progress Series*, 342:91–103.

King, A., Buck, K., and Barbeau, K. (2012). Quasi-Lagrangian drifter studies of iron speciation and cycling off Point Conception, California. *Marine Chemistry*, 128-129:1–12.

King, A. L. and Barbeau, K. A. (2011). Dissolved iron and macronutrient distributions in the southern California Current System. *Journal of Geophysical Research*, 116(January):1–18.

Kohfeld, K., Quéré, C. L., Harrison, S., and Anderson, R. (2005). Role of marine biology in glacial-interglacial CO2 cycles. *Science*, 308(April):74–78.

Koning, E., Gehlen, M., a. M. Flank, Calas, G., and Epping, E. (2007). Rapid post-mortem incorporation of aluminum in diatom frustules: Evidence from chemical and structural analyses. *Marine Chemistry*, 106(1-2):208–222.

Lane, E. S., Jang, K., Cullen, J. T., and Maldonado, M. T. (2008). The interaction between inorganic iron and cadmium uptake in the marine diatom Thalassiosira oceanica. *Limnology and Oceanography*, 53(5):1784–1789.

Lane, T. and Morel, F. (2000). Regulation of carbonic anhydrase expression by zinc, cobalt, and carbon dioxide in the marine diatom Thalassiosira weissflogii. *Plant Physiology*, 123:345–352.

Löscher, B. (1999). Relationships among Ni, Cu, Zn, and major nutrients in the Southern Ocean. *Marine chemistry*, 67:67–102.

Maldonado, M., Carmona, M., Uriz, M., and Cruzado, A. (1999). Decline in Mesozoic reef-building sponges explained by silicon limitation. *Nature*, 401(October):785–788.

Mann, E., Ahlgren, N., Moffett, J., and Chisholm, S. (2002). Copper toxicity and cyanobacteria ecology in the Sargasso Sea. *Limnology and Oceanography*, 47(4):976–988.

Mantoura, R. and Riley, J. (1975). The analytical concentration of humic substances from natural waters. *Analytica chimica acta*, 76(2):97–106.

Martin, J., Gordon, R., and Fitzwater, S. (1990). Iron in Antarctic waters. *Nature*, 345:156–158.

Martin, J. H. and Knauer, G. A. (1973). The elemental composition of plankton. *Geochimica et Cosmochimica Acta*, 37:1639–1653.

Matsumoto, K. (2002). Silicic acid leakage from the Southern Ocean: A possible explanation for glacial atmospheric pCO2. *Global Biogeochemical Cycles*, 16:23.

Matsumoto, K. and Sarmiento, J. L. (2008). A corollary to the silicic acid leakage hypothesis. *Paleoceanography*, 23(2):PA2203.

Milligan, A. J. and Morel, F. M. M. (2002). A proton buffering role for silica in diatoms. *Science*, 297(5588):1848–50.

Mino, T. (2000). Microbial selection of polyphosphate-accumulating bacteria in activated sludge wastewater treatment processes for enhanced biological phosphate removal. *Biochemistry. Biokhimiia*, 65(3):341–8.

Moffett, J. W. and Brand, L. E. (1996). Production of strong, extracellular Cu chelators by marine cyanobacteria in response to Cu stress. *Limnology and Oceanography*, 41(3):388–395.

Monaghan, E. and Ruttenberg, K. (1999). Dissolved organic phosphorus in the coastal ocean: Reassessment of available methods and seasonal phosphorus profiles from the Eel River Shelf. *Limnology and Oceanography*, 44(7):1702–1714.

Monteiro, P. M. S. and Orren, M. J. (1985). Trace metals in the Southern Ocean: on the geochemistry of copper. *Marine Chemistry*, 15:345–355.

Moon, M. H., Yang, S. G., Lee, J. Y., and Lee, S. (2005). Combination of gravitational SPLITT fractionation and field-flow fractionation for size-sorting and characterization of sea sediment. *Analytical and bioanalytical chemistry*, 381(6):1299–304.

Moore, J., Doney, S., Glover, D., and Fung, I. (2002). Iron cycling and nutrient-limitation patterns in surface waters of the World Ocean. *Deep Sea Research Part II*, 49:463–507.

Morel, F. and Reinfelder, J. (1994). Zinc and carbon co-limitation of marine phytoplankton. *Nature*, 369:740–742.

Morin, S., Coste, M., and Hamilton, P. B. (2008). Scanning Electron Microscopy Observations of Deformities in Small Pennate Diatoms Exposed To High Cadmium Concentrations. *Journal of Phycology*, 44(6):1512–1518.

Nathan, Y., Soudry, D., Levy, Y., Shitrit, D., and Dorfman, E. (1997). Geochemistry of cadmium in the Negev phosphorites. *Chemical Geology*, 142(1-2):87–107.

Nelson, D. and Tréguer, P. (1995). Production and dissolution of biogenic silica in the ocean: revised global estimates, comparison with regional data and relationship to biogenic sedimentation. *Global Biogeochemical Cycles*, 9:359–372.

Orchard, E. D., Benitez-Nelson, C. R., Pellechia, P. J., Lomas, M. W., and Dyhrman, S. T. (2010). Polyphosphate in Trichodesmium from the low-phosphorus Sargasso Sea. *Limnology and Oceanography*, 55(5):2161–2169.

Paytan, A., Cade-Menun, B. J., McLaughlin, K., and Faul, K. L. (2003). Selective phosphorus regeneration of sinking marine particles: evidence from 31P-NMR. *Marine Chemistry*, 82(1-2):55–70.

Paytan, A. and McLaughlin, K. (2007). The oceanic phosphorus cycle. *Chemical reviews*, 107(2):563–76.

Perry, C. (2003). Silicification: the processes by which organisms capture and mineralize silica. *Reviews in mineralogy and geochemistry*, 54:291–327.

Perry, M. (1976). Phosphate utilization by an oceanic diatom in phosphorus-limited chemostat culture and in the oligotrophic waters of the central North Pacific. *Limnology and oceanography*, 21(1):88–107.

Pickett-Heaps, J., Schmid, A., and Edgar, L. (1990). The cell biology of diatom valve formation. *Progress in Phycological Research*, 7:1–168.

Price, N., Harrison, G., and Hering, J. (1988). Preparation and chemistry of the artificial algal culture medium Aquil. *Biological Oceanography*, 6:443–462.

Reimers, C. and Ruttenberg, K. (1996). Porewater pH and authigenic phases formed in the uppermost sediments of the Santa Barbara Basin. *Geochimica et Cosmochimica Acta*, 60(21):4037–4057.

Rickaby, R. E. M. and Elderfield, H. (1999). Planktonic foraminiferal Cd/Ca: Paleonutrients or paleotemperature? *Paleoceanography*, 14(3):293–303.

Rings, A., Lücke, A., and Schleser, G. H. (2004). A new method for the quantitative separation of diatom frustules from lake sediments. *Limnology and Oceanography: Methods*, 2:25–34.

Round, F. E., Crawford, R. M., and Mann, D. G. (1990). *The Diatoms*. Cambridge University Press, Bath.

Rue, E. and Bruland, K. (1995). (III) by natural organic ligands in the Central North Pacific as determined by a new competitive ligand equilibration/adsorptive cathodic stripping voltammetric method. *Marine Chemistry*, 50:117–138.

Rueter Jr, J. and Morel, F. (1981). The interaction between zinc deficiency and copper toxicity as it affects the silicic acid uptake mechanisms in Thalassiosira pseudonana. *Limnology and Oceanography*, 26:67–73.

Ruttenberg, K. C. and Berner, R. A. (1993). Authigenic apatite formation and burial in sediments from non-upwelling, continental margin environments. *Geochimica et Cosmochimica Acta*, 57:991–1007.

Ružić, I. (1982). Theoretical aspects of the direct titration of natural waters and its information yield for trace metal speciation. *Analytica Chimica Acta*, 140:99–113.

Saito, M. A., Sigman, D. M., and Morel, F. M. (2003). The bioinorganic chemistry of the ancient ocean: the co-evolution of cyanobacterial metal requirements and biogeochemical cycles at the ArcheanProterozoic boundary? *Inorganica Chimica Acta*, 356:308–318.

Scatchard, G. (1949). The attractions of proteins for small molecules and ions. *Annals of the New York Academy of Sciences*, 51:660–672.

Schröder, H. C., Wang, X., Tremel, W., Ushijima, H., and Müller, W. E. G. (2008). Biofabrication of biosilica-glass by living organisms. *Natural product reports*, 25(3):455–74.

Seufferheld, M. J., Alvarez, H. M., and Farias, M. E. (2008). Role of polyphosphates in microbial adaptation to extreme environments. *Applied and environmental microbiology*, 74(19):5867–74.

Seufferheld, M. J. and Curzi, M. J. (2010). Recent Discoveries on the Roles of Polyphosphates in Plants. *Plant Molecular Biology Reporter*, 28(4):549–559.

Sigman, D. M., Altabet, M. A., McCorkle, D. C., Francois, R., and Fischer, G. (1999). The delta N-15 of nitrate in the Southern Ocean: Consumption of nitrate in surface waters. *Global Biogeochemical Cycles*, 13:1149–1166.

Sinoir, M., Butler, E. C. V., Bowie, A. R., Mongin, M., Nesterenko, P. N., and Hassler, C. S. (2012). Zinc marine biogeochemistry in seawater: a review. *Marine and Freshwater Research*, 63(7):644–657.

Slomp, C. and Epping, E. (1996). A key role for iron-bound phosphorus in authigenic apatite formation in North Atlantic continental platform sediments. *Journal of marine research*, 54(6):1179–1205.

Solorzano, L. and Strickland, J. (1968). Polyphosphate in seawater. *Limnology and Oceanography*, 13(3):515–518.

Spero, H. J., Bijma, J., Lea, D. W., and Bemis, B. E. (1997). Effect of seawater carbonate concentration on foraminiferal carbon and oxygen isotopes. *Letters to Nature*, 390:497–500.

Strickland, J. and Parsons, T. (1965). A Manual of Sea Water Analysis. *Bulletin*.

Sturchio, N., Antonio, M., and Soderholm, L. (1998). Tetravalent uranium in calcite. *Science*, 281(5379):971–973.

Sunda, W. and Huntsman, S. (1992). Feedback interactions between zinc and phytoplankton in seawater. *Limnology and Oceanography*, 37:25–40.

Sunda, W. and Huntsman, S. (1996). Antagonisms between cadmium and zinc toxicity and manganese limitation in a coastal diatom. *Limnology and Oceanography*, 41(3):373–387.

Sunda, W. G. (1988). Trace metal interactions with marine phytoplankton. *Biological Oceanography*, 6(5-6):411–442.

Suzumura, M., Ishikawa, K., and Ogawa, H. (1998). Characterization of dissolved organic phosphorus in coastal seawater using ultrafiltration and phosphohydrolytic enzymes. *Limnology and Oceanography*, 43(7):1553–1564.

Talley, L. (1999). Some aspects of ocean heat transport by the shallow, intermediate and deep overturning circulations. *GEOPHYSICAL MONOGRAPH 112*.

Tang, D. G. and Morel, F. M. M. (2006). Distinguishing between cellular and Fe-oxide-associated trace elements in phytoplankton. *Marine Chemistry*, 98(1):18–30.

Thamatrakoln, K. and Hildebrand, M. (2008). Silicon uptake in diatoms revisited: a model for saturable and nonsaturable uptake kinetics and the role of silicon transporters. *Plant physiology*, 146:1397–1407.

Tijssen, J., Beekes, H., and Steveninck, J. V. (1982). Localization of polyphosphates in Saccharomyces fragilis, as revealed by 4', 6-diamidino-2-phenylindole fluorescence. *Biochimica et Biophysica Acta*, 721:394–398.

Twining, B. S., Baines, S. B., and Fisher, N. S. (2004). Element stoichiometries of individual plankton cells collected during the Southern Element stoichiometries Ocean Iron Experiment (SOFeX). *Limnology and oceanography*, 49(6):2115–2128.

Tyrrell, T. (1999). The relative influences of nitrogen and phosphorus on oceanic primary production. *Nature*, 400:525–531.

van den Berg, C. M. G. (1982). Determination of copper complexation wiht natural organic ligands in seawater by equilibration with MnO2 II. Experimental procedures and application to surface seawater. *Marine Chemistry*, 11:323–342.

Voelz, H., Voelz, U., and Ortigoza, R. O. (1966). The polyphosphate overplus phenomenon in myxococcus xanthus and its influence on the architecture of the cell. *Archiv für Mikrobiologie*, 53(4):371–88.

Walsh, R. S. and Hunter, K. A. (1992). Influence of phosphorus storage on the uptake of cadmium by the marine alga Macrocystis pyrifera. *Limnology and oceanography*, 37(7):1361–1369.

Weiss, M., Abele, U., Weckesser, J., Welte, W., Schiltz, E., and Schulz, G. (1991). Molecular architecture and electrostatic properties of a bacterial porin. *Science*, 254(5038):1627–1630.

Westall, J., Zachary, J., and Morel, F. (1976). MINEQLgeneral algorithm for computation of chemical-equilibrium in aqueous systems. *Abstr. Pap. Am. Chem. Soc*, 172:8–8.

Young, C. L. and Ingall, E. D. (2010). Marine Dissolved Organic Phosphorus Composition: Insights from Samples Recovered Using Combined Electrodialysis/Reverse Osmosis. *Aquatic Geochemistry*, 16(4):563–574.

Yu, R. and Wang, W. (2004). Biological uptake of Cd, Se (IV) and Zn by Chlamydomonas reinhardtii in response to different phosphate and nitrate additions. *Aquatic microbial ecology*, 35:163–173.

Zapata, M., Rodríguez, F., and Garrido, J. (2000). Separation of chlorophylls and carotenoids from marine phytoplankton: a new HPLC method using a reversed phase C8 column and pyridine-containing mobile. *Marine Ecology Progress Series*, 195:29–45.

Zhu, C. and Lee, Y. (1997). Determination of biomass dry weight of marine microalgae. *Journal of applied phycology*, 9:189–194.